A STUDY OF BURIED ORGANICS ON MARS - A COMPUTATIONAL AND EXPERIMENTAL APPROACH

ANKITA DAS

A THESIS SUBMITTED TO

THE FACULTY OF GRADUATE STUDIES

IN PARTIAL FULFILLMENT OF THE REQUIREMENTS

FOR THE DEGREE OF

MASTER OF SCIENCE

GRADUATE PROGRAM IN EARTH AND SPACE SCIENCE

YORK UNIVERSITY

TORONTO, ONTARIO

September 2023

ABSTRACT

This thesis consists of two related projects investigating exogenous organic burial on the surface of Mars and potential detection methods. Mars receives a significant quantity of organic material through exogenous sources such as micrometeorites. This work investigates the preservation of such material within sedimentary structures formed through the gradual airfall of dust particles. The computer model devised indicates rapid burial of organics and presents amount of organic carbon preserved at selected locations on Mars after 10 Martian years (99% preserved). The model is further extended globally to point at sites on Mars which are most favorable for organic preservation and hence possible sites for robotic exploration. The experimental section of this thesis investigates organic detection (Tryptophan) in simulated Martian dust matrix (JSC-1 Mars) through Ultraviolet Light Induced Fluorescence (LIF) spectroscopy. Instrument used was unable to detect Tryptophan in 100 ppm concentrations owing to the UV absorptive nature of JSC-1 Mars.

DEDICATION

To my mothers, baba, and Freddie for their warmth and comfort during tough times.

ACKNOWLEDGMENTS

This endeavor would not have been possible without the support and guidance of my supervisors Dr. John E. Moores and Dr. Haley Sapers who showed great patience and willingness to conduct in-depth discussions on various concepts with me over the duration of my degree which has culminated in this thesis. I would like to express my gratitude and thanks to Dr. Michael Daly for allowing me to conduct experiments in his laboratory. I am extremely grateful to Dr. Elizabeth Lymer for her guidance and presence in the laboratory despite her busy schedule. I'd like to acknowledge my several colleagues around the world who have been part of the research discussion enabling me to complete the work presented here. Special mention to folks at the Centre for Women's and Trans People (York University) for providing a safe space, a sense of community, and encouragement during my degree. Finally, I would like to thank my family and friends for their unwavering support and belief in me over the years.

TABLE OF CONTENTS

ABSTRACT ii
DEDICATION iii
ACKNOWLEDGMENTS iv
TABLE OF CONTENTS v
LIST OF TABLES vii
LIST OF FIGURES viii
Chapter One: Introduction 1
Chapter Two: Background 4
2.1 Martian evolution and changing geological record 5
2.2 Detection of Biosignatures on Mars – Question of Biogenicity 7
2.3 Interplanetary Dust Particles (IDPs) 8
2.3.1 Organic Matter in IDPs and Carbonaceous Meteorites 9
2.4 Radiation Environment on Mars – Degradation of Organics 12
2.5 Martian Dust 14
2.6 Laser Induced Fluorescence Spectroscopy (LIF) for detecting Organics 14
Chapter Three: Research Objectives 16
3.1 Sedimentary Rhythmites 16
3.2 Organic Detection through LIF in Martian Dust Matrix 19
3.3 Relevance of projects and how the two projects fit together 27
Chapter Four: Modeling IDP Burial in Sedimentary Rhythmites 29
4.1 Materials and Methods 29
4.1.1 UV Environment on Mars Model 29
4.1.2 UV Absorption by Martian Dust 31
4.1.3 UV Photolysis of Organic Matter Equation 32
4.1.4 Dust Accumulation on Mars – Mars Climate Database (MCD) 34
4.1.5 Dust Accumulation at Gale Crater – Line of Sight-extinction (LOS-ext) Studies 35
4.1.6 Algorithm Summarized 36
4.2 Results 38
4.2.1 Burial at Gale Crater (seasonal) 43
4.2.2 Global Dust Deposition – Identifying dust sources and sinks from MCD Data 45

4.3 Discussion 50
4.3.1 Sequestration of IDP Organics on Mars – sites of interest for further exploration 50
4.4 Sources of Errors and Assumptions 53
Chapter Five: LIF Spectroscopy of Tryptophan in JSC-1 Mars Matrix 55
5.1 Materials and Methods 55
5.1.1 Experimental Apparatus – 266 nm YU LIF Instrumentation 55
5.1.2 Experimental Matrix 56
5.1.3 Sample Preparation Protocol (Manual Mixing) 62
5.1.4 Summary of Experiment 65
5.1.5 LIF Spectroscopy Measurements – Specifications for Data Collection 66
5.2. Results 70
5.2.1 Comparisons between Blanks 70
5.2.2 LIF Results from Samples 73
5.2.3 Spectrum after Magnetic Stir-bar Mixing 76
5.2.4 Manual vs. Magnetic Mixing 77
5.3 Discussion 78
5.4 Sources of Error and Possible Explanations for Observed Results 87
5.5 Summary - How both projects are related 88
Chapter Six: Conclusions 91
Chapter Seven: Future Work 92
References 94
Appendices 106
Appendix A: Source Code Base for IDP Burial Model 106
Appendix B: Calculation for Depth used in Layered JSC-1 Mars on Tryptophan Measurement 113

LIST OF TABLES

Table 1: Identification of eight protein amino acids @g/g) in the Murchison meteorite 10
Table 2: Mineralogical Composition of JSC-1 Mars Simulant Soil 25
Table 3: Yearly dust deposition rates at chosen investigation sites on Mars (Moore, 2019) 39
Table 4: Concentration of organics preserved in sedimentary rhythmites relative to dust mass 42
Table 5: Experimental Matrix showing sample space along with blanks 59
Table 6: UV LIF spectroscopy instrument specification 67
Table 7: Mineralogical composition of MMS simulant used in Carrier et al. (2019) (Data from Clark et al., 2020) 80
Table 8: Instrument comparisons between three instruments – SHERLOC, MOBIUS, and LIF (266 nm) 81
Table 9: Summary of Quenching in various samples tested in this work using LIF (266 nm) 84
Table 10: Quenching of Tryptophan sample layered with 0.03 cm of JSC-1 Mars – Compared with results presented in Carrier et al. (2019) 85

LIST OF FIGURES

Figure 2.1: Surface activity and characteristics of different time periods on Mars as a function of time on Mars. Figure shows the relative prevalence of different processes (impact cratering, volcanism), the time and relative rates of formation of various features and units (valley networks, Dorsa Argentea Formation), and types and rates of weathering, during different evolutionary periods. The approximate boundaries of the major time periods of Mars history are shown, (recreated from Ehlmann et al. (2011). 6

Figure 2.2: Scanning electron microscope image of an ~11 µm chondritic IDP collected from the Earth's stratosphere by a NASA aircraft. The individual surface features are micron or submicron grains that have aggregated to form this dust particle (image source: NASA, Flynn (2020) 10

Figure 2.3: IDP flux Incident mass along with surviving mass from modeling studies conducted by Flynn (1996) 12

Figure 2.4: Total UV flux (base-10 log) in one Martian year for different optical depth modeled for present day Mars (Moores et al., 2007) 13

Figure 2.5: Jablonski diagram illustrating energy states of a fluorescing molecule – the principle of Laser Induced Fluorescence spectroscopy (Source: https://jascoinc.com/learning-center/theory/spectroscopy/fluorescence-spectroscopy/)15

Figure 3.1: Locations on Mars where quasi-periodic rhythmic sedimentary rocks have been discovered 17

Figure 3.2: Sketch illustrating infalling IDPs on the Martian surface embedded in sedimentary rhythmites upon layering of airfall Martian dust. The orange spheres on this diagram represent IDPs. As time passes, each layer of IDP on the surface has more dust sedimented on top, leading to more robust shielding from UV flux 18

Figure 3.3: Chemical structure of Tryptophan 21

Figure 3.4: Emission and Absorption Spectra of Tryptophan. Tryptophan can be excited in the wavelength range 250 to 300 nm (approximately) and emits a fluorescence spectra over a range of wavelengths starting from 300 nm, peaking at around 340 nm (this depends on the excitation frequency). The SHERLOC laser operates at 248.6 nm (deep UV) and the LIF instrument used in this project operates at 266 nm – both are capable of exciting Tryptophan causing it to fluoresce (Plot recreated from Lakowicz, 2006) 22

Figure 3.5: Deep UV Fluorescence of 24 amino acids excited at 248.6 nm (Source: Razzel Hollis et al., 2023) 24

Figure 4.1: Sample output utilized for UV degradation of IDP organics in this project – plot shows the UV flux received with regard to latitude and time of the year (Solar Longitude) (Source: Smith and Moores, 2020) 30

Figure 4.2: UV extinction by JSC-1 Mars simulant at different particle sizes. This plot depicts the highly UV absorptive nature of JSC-1 Mars simulant and that the absorption coefficient is dependent on the particle size of the simulant soil (Source: Godin et al., 2023) 32

Figure 4.3: Dust deposition at Juventae Chasma throughout the year (time of year represented by solar longitude L_s) computed from MCD data 35
Figure 4.4: Diffusion rate (μm/sol) at Gale crater computed from LOS-ext studies for Mars Years 32 and 33 (Source: Moore, 2019) 36
Figure 4.5: Flow-chart summarizing what IDP organics burial model does 37
Figure 4.6: Organic Carbon remaining at 4 locations on Mars: Arabia Terra, Schiaparelli Crater, Juventae Chasma, and Gale Crater. These plots show rapid burial at sites like Arabia Terra, Schiaparelli Crater, and Juventae Chasma since MCD data indicates a dust deposition of > 20 μm per year. However, the plots show a slower rate of organic sequestration at Gale – this comes as a result of LOS-Ext studies showing us yearly dust deposition at Gale is 3.54 μm. Hence, the plot for Gale looks largely different from the others. 40
Figure 4.7: Model Result of Remaining Organic Carbon at Gale Crater with 3.54 μm /year dust deposition rate up till 50 years. The curve approaches an asymptote after 50 Martian Years showing organic carbon sequestration 41
Figure 4.8: Seasonal Organic Carbon destruction at Gale crater (calculations done using LOS-Ext diffusion rates as a proxy for dust deposition) The orange curve shows the rate at which IDP organic carbon (measured in g/m^2) changes with Solar Longitude (time of year). The curve has some slight variations from a traditional decay curve which is a consequence of periods of dust lifting as opposed to dust deposition. The periods of dust lifting is represented by negative values in the diffusion rate plot in blue (from Moore, 2019) and coincides with the variations in the orange curve 44
Figure 4.9: Global Dust deposition on Mars – calculated from Mars Climate Database (MCD). Dust rich regions are denoted by blue and lighter shades. Apart from dust rich regions near the South Pole, two regions stand out as being dust-rich on this map (circled) 45
Figure 4.10: Topography Map of Mars by Mars Orbiter Laser Altimeter (MOLA) with various landing sites of spacecraft marked. Noticeable regions on this map include the Hellas Basin in the SH and the Tharsis region in the NH in addition to Northern lowland regions and Southern highland regions (Source: http://mola.gsfc.nasa.gov/images.html) 46
Figure 4.11: Normalized Dust Deposition on Mars after manipulating MCD dust deposition data shown in μm. Previously noted regions in the South Polar regions continue to be the richest in dust globally. Most regions have zero to 200 μm dust deposition 47
Figure 4.12: Organics preserved globally using normalized dust deposition plotted in log base 10. The blank regions of the map are regions with negative dust deposition, illogical organic concentrations (an upper limit of 104 ppb was implemented), and extremely low concentrations (100 ppb). This map shows IDP organics preservation (with positive organic carbon concentrations less than 104 ppb) on Mars over the course of 10 Martian years 48
Figure 4.13: Results from figure 4.12 overlayed on a Mars Map showcasing well-known features and regions of Mars (Map from http://planetarymapping.elte.hu/blank-map-of-mars/) 53

Figure 5.1: 266 nm Raman spectrometer instrument diagram (Source: Eshelman et al., 2014) 55
Figure 5.2: Calibration spectrum for Hg-Ar lamp 56
Figure 5.3: JSC-1 Mars unprocessed blank fluorescence spectra excited at 266 nm. The spikes visible are hot pixels or instrument artifacts. A broad spectral signature is faintly visible probably caused by organics present in JSC-1 Mars. 60
Figure 5.4: Crushed JSC-1 Mars measured using 266 nm YU LIF instrument set up. No characteristic organics detected here, only instrument artifacts. Intensity is roughly constant over wavelength. Indicating that spectra obtained in Figure 5.3 could be due to coarse particle sizes. 61
Figure 5.5: Crushed, Sieved, Non-baked JSC-1 Mars prepared with methanol 61
Figure 5.6: Crushed, Sieved, Baked JSC-1 Mars prepared with methanol. No characteristic organic or mineral component is visible. The spikes indicate instrument artifacts. 62
Figure 5.7: Mixed and dried 50 ppm sample (mixed with magnetic stir-bar) (left) and Mixing of 50 % Tryptophan: JSC-1 Mars sample on stirring and heating plate (right) 64
Figure 5.8: Images of magnetic stir-bar with magnetic particles from JSC-1 Mars - 100 ppm sample (left) and 50 ppm sample (right) 65
Figure 5.9: Flowchart summarizing the steps and procedures taken during the experiment starting from sample prep to data collection 66
Figure 5.10: Sketch depicting various instrument specifications. The 266 nm laser enters the detector at a repetition rate of 500 us. An external trigger signal is sent to the detector when the pulse is emitted. The incoming pulse is allowed to enter the detector after a delay time (47.5 ns in our set up). The pulse width used in our measurements were 5 ns and 100 ns. The exposure time is the time instrument CCD is exposed to for one accumulation. We took 200 accumulations. The charge is read out from the detector after each exposure time (0.1 s) and the detector is prepared for the next accumulation. (Sketch adapted for our setup from Eshelman, 2016). 69
Figure 5.11: Fluorescence Spectra comparisons between two blanks (CSBM and CSNBM) excited at 266 nm. One is baked (purple) and the other is unbaked (red), both blanks were prepared with methanol. Both blanks were crushed and sieved and data was averaged over 5 points. 70
Figure 5.12: Fluorescence Spectra comparisons between two blanks (CSBM and NCNSNB) excited at 266 nm. One is baked (purple) and the other is unbaked (red), both blanks were prepared with methanol. One blank was not crushed and neither sieved (unaltered and unprocessed JSC-1 Mars). Both samples were averaged over 5 points. This comparison was made to show that the fluorescence spectra is not drastically different in this particular wavelength range between unprocessed JSC-1 Mars (NCNSNB) and Crushed, Sieved, Baked JSC-1 Mars prepared with Methanol. Although unprocessed JSC-1 Mars has a higher water and organic content in addition to having a coarse particle distribution compared to JSC-1 Mars (CSBM), the instrument gives very similar fluorescence results for both these measurements 71

Figure 5.13: A fluorescence spectra of an empty aluminum cup taken (experiment 1). This spectrum shows a peak around > 340 nm – implying that the sharp peaks observed in the previous (5.11 and 5.12) and following results are in all likelihood instrument artifacts and are not indicative of neither minerals nor organics. 72
Figure 5.14: Background spectra automatically subtracted from spectra obtained 73
Figure 5.15: Fluorescence spectra of pure Tryptophan sample excited at 266 nm. Gain used was 3000 on the YU LIF instrument and averaged over 5 points 74
Figure 5.16: 50% Tryptophan to JSC-1 Mars concentration sample excited at 266 nm during experiment 2 (averaged over 5 points). This observation was made at a higher pulse width (100 ns) than conditions for experiment 1 (pulse width of 5 ns) – here the sample was exposed to a higher number of photons per accumulation. 74
Figure 5.17: Fluorescence signal of pure Tryptophan sample sprinkled with CSB JSC-1 Mars – compared to JSC-1 Blank, 100 ppm and 50 ppm Tryptophan: JSC-1 Mars (excited at 266 nm) 75
Figure 5.18: Fluorescence signal of re-mixed 100 ppm and 50 ppm sample – no organic signature detected (excited at 266 nm) 77
Figure 5.19: Fluorescence signal of re-mixed 100 ppm and 50 ppm sample compared to blank JSC-1 Mars (excited at 266 nm) 77
Figure 5.20: Fluorescence spectra of two 100 ppm samples (excited at 266 nm) - A 78
Figure 5.21: Fluorescence spectra of two 100 ppm samples (excited at 266 nm) - B 78
Figure 5.22: Preliminary results from Carrier et al (2019) studying fluorescence spectroscopy of Phenylalanine under MMS simulant (0.168 cm) The peak in the pure Phenylalanine sample is read to be 60000 counts and that of the sample under MMS is read to be 2700 82
Figure 5.23: Schematic depiction of laser interactions with samples for YU LIF instrument (266 nm) (this work) and work presented in Carrier et al. (2019) The top panel shows (left to right) a) 266 nm laser interacting with pure Tryptophan sample using YU LIF instrument, b) 266 nm interacting with Tryptophan sample layered with JSC-1 Mars (CSB) where UV laser experiences quenching on its journey through the JSC-1 layer to the sample and the emitted fluorescence signal which is also in UV experiences additional quenching before reaching the detector, c) laser-sample interactions of work presented in Carrier et al. (2019) which uses transmittance, Phenyl alanine as fluorescing organic material, and MMS simulant soil. Bottom panel shows 266 nm laser interaction with pure Tryptophan sample compared to Tryptophan sample doped with 50% JSC-1 Mars 83
Figure 5.24: Incident intensity Io interacts with JSC-1 layer resulting in intensity I1 to interact with pure Tryptophan (shaded region). A fluorescence signal which is kI_1 in intensity is emitted. This beam undergoes absorption by the JSC-1 layer and a final intensity of I_2 is detected by the detector. 85

Chapter One: Introduction

The detection of organic material and as an extension, detecting the presence of extinct or extant life on Mars has been a subject of active research and debate. Organic material detection is relevant to the context of life detection since it indicates the possibility of present or previous biological activity (Summons et al., 2007; Westall et al., 2015). Over the last few decades several missions such as the Viking landers, Curiosity, and Perseverance rovers have been sent to Mars primarily to aid in this search.

The Viking landers carried four experiments: Gas Chromatograph – Mass Spectrometer (GCMS), Gas Exchange (GEX), Labeled Release (LR), and Pyrolytic Release (PR). Initial analysis of the GCMS data did not indicate detectable quantities of organic material within the Martian soil. The chlorinated organics detected by GCMS were attributed to contamination from cleaning agents in the instrument. Apart from this, results from the life detection experiments (LR, PR, and GEX) were considered incompatible with biology and were in disagreement with the results of the GCMS experiment.

The GEX experiment measured composition of gases over Martian surface material samples in different modes (Klein, 1978). The experiment concluded that the CO_2 release being measured was not from a biological source. Although the LR and PR experiments gave positive results, the data from all Viking experiments considered together pointed toward nonbiological explanations. Results from the LR experiments garnered a lot of attention and debate since they indicated the Martian soil consisted of metabolizing organisms. However, the experiment assumed that any extant life on Mars would metabolize simple carbon compounds and release waste gases. This understanding was flawed since we now know that it is highly unlikely that extant life on Mars would follow this metabolism pathway. If any extant life on Mars is present, they are more likely to be extremophiles which have different mechanisms for their metabolism. Additionally, this was in contradiction to the results obtained by the GCMS and some characteristics of the LR results did not concur with the understanding of any putative Martian biology. Although no similar life detection experiments were conducted by any following spacecraft sent to Mars, the current general consensus within the scientific community is that the Viking life detection experiments were inconclusive. To explain the GEX and LR experiment results, researchers hinted that it could be due to the presence of strong oxidizing agents present on Mars.

The inconclusive results from biological experiments on Viking landers 1 and 2 in 1976 set the premise for exploration of organic matter on Mars (Biemann et al., 1976). The results from the Viking landers initially puzzled scientists back then since Mars was thought to have been habitable in the past (Mukhopadhyay, 2007). Additionally, it was also well established that organic material is transported to the Martian surface in the form of meteorites and micrometeorites (Flynn, 1996; Flynn et al., 2000). Hence, Viking's results further challenged the understanding researchers had in the 1970s. An important distinction that needs to be made is between the presence of organics and the evidence of extinct or extant life. Organic matter and compounds can be produced abiotically – organic matter does not necessarily indicate biogenicity. However, biological activity in all likelihood will result in organic matter being produced as a result of metabolism and life related processes such as production of waste. Thus, life as we know it will be characterized by presence of organic matter but not all organic matter is a result of biological processes.

Since 1976, the presence of oxidizing compounds indigenous to the Martian soil was hypothesized by Navarro-Gonzalez et al. (2010) and was later confirmed by the results from experiments (Wet Chemistry Laboratory) on the Phoenix lander (Hecht et al., 2009) and was later also corroborated by results from the Curiosity rover (Glavin et al., 2013). Both these independent findings indicate that perchlorate (ClO_4^-) might be a commonly occurring substance in the Martian soil. Perchlorate being a strong oxidizing salt hinted at the possibility of organics being oxidized into chlorinated organics (Yen et al., 2000). This paved the path to reanalyzing the Viking results in search for chlorinated organics which were earlier dismissed as terrestrial contamination from the instruments. Subsequently, chlorinated organics have also been discovered by the Sample Analysis at Mars (SAM) instrument on board the Mars Science Laboratory, Curiosity (Glavin et al., 2013; Freissinet et al., 2015).

In addition to perchlorates, the Martian surface is exposed to a harsh radiation environment. This is primarily due to Mars' ozone layer being typically 3000 times thinner than that of Earth with significant seasonal variation (Montmessin and Lefévre, 2013). Due to a lack of ozone in the Martian atmosphere, UV radiation arrives at the surface is unattenuated. In addition to this, the absence of a magnetic field exposes the surface of Mars to high energy ionizing radiation in the form of Solar Energetic Particles (SEPs) and Galactic Cosmic Rays (GCRs) which further impact

the survivability of organic molecules on the surface (Cockell and Raven, 2004; Dartnell et al., 2007; Dartnell, 2011; Pavlov et al., 2012). It is thought that Mars lost its magnetic field approximately 4 billion years ago. As a consequence, Mars lost a significant amount of its atmosphere and surface water became sparse as time progressed and Mars evolved as a planet. Due to the high radiation environment on Mars, if one were to conduct a search for organics on Mars, they will have to narrow down their search to potential ecological niches where organic matter is preserved and shielded from degradation and photolysis.

This project explores the preservation of exogenous organic material on the Martian surface through sedimentary burial methods in present-day Mars and discusses the detectability of these organics in a Martian dust matrix by instruments on board potential future robotic missions. This work is not only relevant to detection of abiotic organic compounds on Mars, but can also be applied to search for biosignatures on the planet. The following chapter (Chapter Two) focuses on the background material and sets the premise for the rest of the thesis.

Chapter Two: Background

Mars differs from Earth in significant ways despite being a terrestrial planet. Specifically, Mars is only a fraction of Earth's mass with Earth almost 9 times the mass of Mars and the equatorial radius of Mars is approximately half of Earth's. This difference in size most likely resulted in the loss of Mars' geo-dynamo responsible for the planet's magnetic field relatively early in its planetary evolution. The exact point in time when this happened is unknown and debatable but from impact analysis, it is generally thought that Mars did not have a magnetic field when the Hellas, Isidis, and Argyre basins formed around 3.9 billion years ago. Subsequently, as a result Mars also lost a significant amount of its atmosphere and surface water became sparse and during later periods, non-existent. These planetary characteristics along with Mars' location in the solar system (~1.5 AU semimajor axis) and smaller planetary radius have resulted in a divergent evolution of the planet compared to Earth. While there has been plenty of evidence indicating that Mars had a warmer, wetter climate in the past, present-day Mars is very much a hostile environment for the evolution and survival of many forms of Earth-based life.

Despite these environmental challenges, the search for life, biosignatures, and organic molecules on present-day Mars is not as futile an exercise as one might initially think. Extremophiles are a class of microorganisms on Earth that have been found to thrive in environments that are otherwise thought of as hostile. For example, a class of extremophiles such as Xerophiles and Hypoliths, organisms that can survive in cold, dry settings – much like present-day Mars. Other extreme environments where such organisms have been discovered on Earth include highly acidic or alkaline environments, environments of high radiation intensity, and environments of extreme pressure just to name a few. Thus, despite low surface pressure, lack of significant quantities of ozone in the atmosphere, and extreme temperature day-night temperature which makes Mars a challenging environment, finding ecological niches where microorganisms, bacteria, and organic molecules can survive or be preserved should be and rightfully is a realm of active research. It is for these reasons that understanding the Martian evolutionary history and how it has shaped the geology of present-day Mars is important. This chapter briefly touches upon:

- Mars' evolutionary history
- Biosignature detection on present day Mars

- Interplanetary Dust Particles (IDPs) being a source of present-day organics on Mars
- Challenges that are presented to the survivability of organics due to harsh UV and ionizing radiation environment along with the presence of oxidants in the soil
- The role Martian dust has to play in preservation and detection of organics on the Martian surface.

2.1 Martian evolution and changing geological record

Mars formed in a manner similar to other terrestrial planets – through accretion followed by differentiation. Mars' evolutionary history is divided into three main periods (Figure 2.1):

a) the Noachian period
b) the Hesperian period
c) the Amazonian period

These periods have been determined mainly through crater density studies and reflect the environment change through time (Scott and Carr, 1978; Tanaka, 1986). Figure 2.1 below (adapted from Ehlmann et al., 2014) shows an illustration summarizing the major time periods of Mars and the activities during each of these periods. The formation of the Hellas basin (a giant impact basin located in Mars' southern hemisphere) between 4.1 – 3.8 Gyr ago has been adopted and generally accepted to be the beginning of the Noachian period. Mars is thought to have lost its magnetic field at some point before the Noachian period (pre-Noachian). The Noachian period during which Mars had a warmer and wetter climate also saw high cratering rates, erosion, and valley formation. Mars' largest volcanic region – known as the Tharsis also formed during this period. Mineralogically, hydrous weathering products such as phyllosillicates were produced as a result of the conditions present during the Noachian (Carr and Head III, 2010; Carter et al., 2013; Ehlmann and Edwards, 2014).

The end of the Noachian period saw a sharp decline in impact rates, valley formation, weathering, and erosion except for volcanism which continued well into the Hesperian period. The Hesperian era saw episodic floods which were subsequently filled by large bodies of surface water. The Hesperian period which ended around 3 Gyr ago was characterized by canyon formation and reduced water activity on the surface compared to the Noachian. The activity from

this period resulted in sulfate rich deposits (Carr and Head III, 2010; Ehlmann and Edwards, 2014).

The end of the Hesperian era saw a further decline in geologic activity leading into the current period – the Amazonian period. The Amazonian period is characterized by negligible water activity and more noticeable ice transport. This ice accumulation and transport is in the form of polar layered deposits, glacial deposits, mid and high latitude ice-rich veneers (Carr and Head III, 2010).

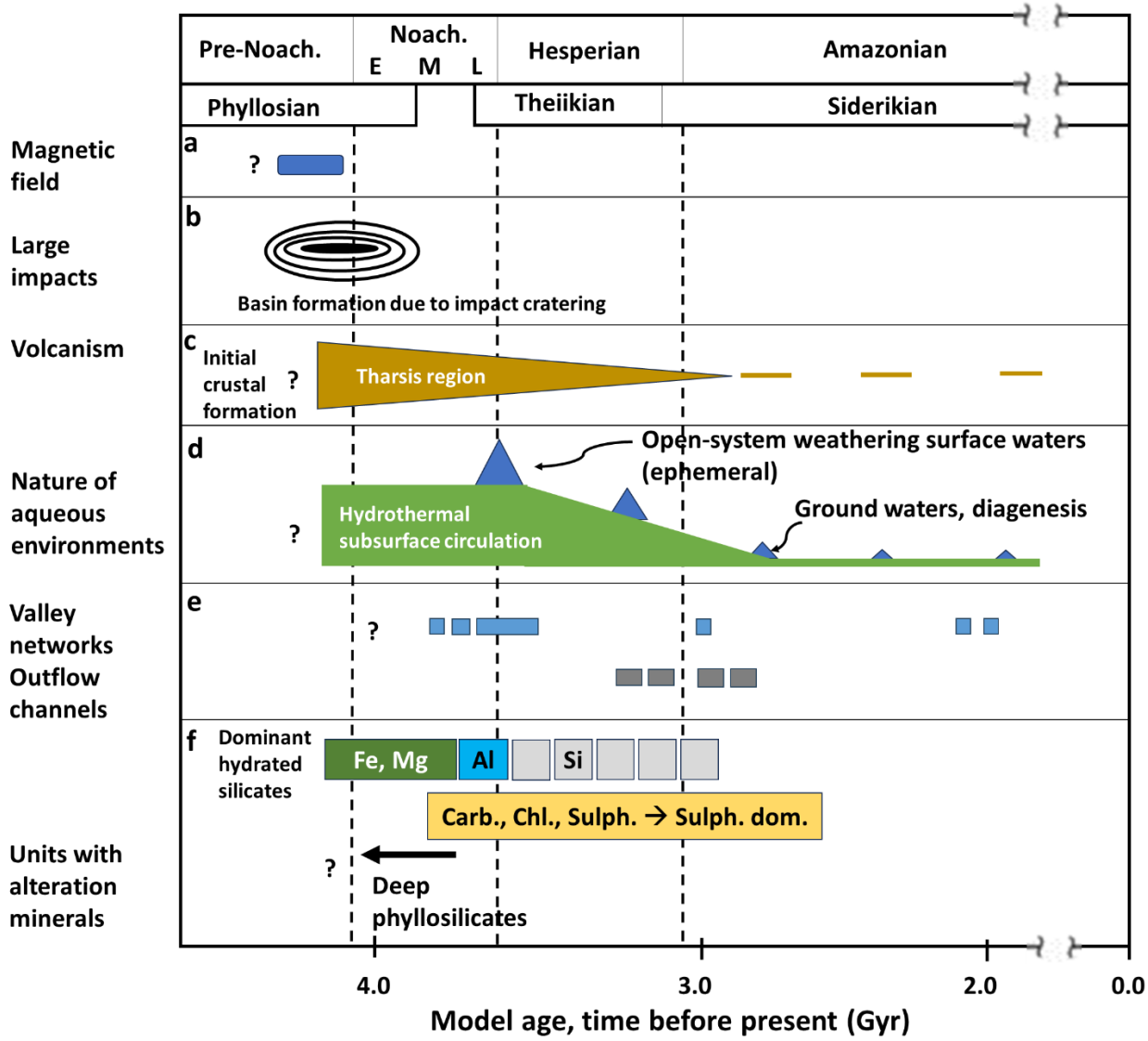

Figure 2.1: Surface activity and characteristics of different time periods on Mars as a function of time on Mars. Figure shows the relative prevalence of different processes

(impact cratering, volcanism), the time and relative rates of formation of various features and units (valley networks, Dorsa Argentea Formation), and types and rates of weathering, during different evolutionary periods. The approximate boundaries of the major time periods of Mars history are shown, (recreated from Ehlmann et al. (2011).

From this summary, it is evident that the environmental conditions have changed drastically from the pre-Noachian to present-day Amazonian. The record of these activities and environmental conditions are preserved in the geological record of Mars often in the form of outcrops or exposed rock surfaces. Today the Martian regolith mostly consists of basaltic minerals with variable quantities of plagioclase ($NaAlSi_3O_8$ – $CaAl_2Si_2O_8$), pyroxene ($XYSi_2O_6$, X, Y = Ca, Fe, Mg or Na, Li, or Al, Fe), and olivine (Mg,Fe) $_2SiO_4$). Regions around large basins like Hellas and Isidis planitia are rich in olivine, most likely originating from late Noachian – early Hesperian volcanic activity. Clay minerals in addition to carbonates, sulfates, and chlorides are more localized and are a result of paleo lake deposits during Noachian and Hesperian eras (Ehlmann and Edwards, 2014).

2.2 Detection of Biosignatures on Mars – Question of Biogenicity

In the field of astrobiology, biosignatures are defined as the detection of objects, substances, or patterns which definitively originated from biological processes indicating the presence of extinct or extant life. Westall et al. (2011) defined biosignatures as morphological, chemical, and isotopic remnants of organisms preserved in lithologic records. These traces can be actual organisms or signs of dormant or past metabolic activities (Mustard et al., 2011). Microbial traces and fossils can also be found in the form of etchings and mineral deposits left in the rocks where microbial colonies were present. Since Earth-based life is the only known example of life available to us, our understanding of biosignatures primarily stems from research conducted on Earth-based microbial colonies and how they interact with their surface environments. This knowledge is later applied in context to the data collected by in-situ spacecrafts on Mars.

Microbial life can leave the following traces: biofilms or colonies, biogenic sedimentary structures, microbial constructions, and stromatolites. In addition to this, organic compounds originating as byproducts of microbial activities are also considered biosignatures, provided they are preserved in the right manner. Biosignatures can range from being more potential to more definitive – more definitive biosignatures indicating that the detection observed is more likely

produced by biological activity. Technically a majority of the biosignatures discussed could be produced through non-biogenic methods, rendering the concept of an absolute definitive biosignature hard to define. As mentioned earlier, organic compounds can be formed through non-biogenic methods. Polycyclic aromatic hydrocarbons (PAHs) have been found to be present in carbonaceous meteorites which can transport these compounds to the surface of Mars (Sephton, 2002; Eigenbrode et al., 2018). This work primarily focuses on the burial of non-Martian organic matter and its detectability in a Martian dust matrix and does not directly explore the detectability of biosignatures. However, provided the background of biosignatures, the results can be applied to potentially biogenic organics and the detection of biosignatures on Mars and in the design of future robotic missions to Mars.

2.3 Interplanetary Dust Particles (IDPs)

Interplanetary Dust Particles (IDPs) also known as micrometeorites and cosmic spherules in the literature, are typically micron-sized extraterrestrial particles that originate from smaller objects in the solar system such as comets and asteroids. IDPs ranging from 5 μm to 50 μm in diameter have been collected by NASA aircrafts flown in the Earth's stratosphere (Brownlee, 1985). However, it is likely that IDPs have a larger size range (up to 2700 μm) and most of the larger sized particles melt and vaporize upon atmospheric entry on Earth (Flynn, 1996). Due to properties of the Martian atmosphere, many of these larger particles are likely to survive decent into the Martian surface without melting (Flynn, 1996).

Laboratory analyses have shown IDPs to contain organic molecules (Clemett et al., 1993; Flynn et al., 2000). These particles find their way through planetary atmospheres and hence these bodies have been analyzed through spectroscopy, electron images, and other laboratory studies – they have been collected in the ice sheets of Greenland and Antarctica and more recently samples of primitive IDPs have been collected from cometary tails by NASA's Stardust mission. Additionally, IDPs that were collected in the stratosphere and analyzed showed characteristics pertaining to comets and bodies in the asteroid belt (Brownlee et al., 1995; Bradley, 2003; Busemann et al., 2009). Organic material found in IDPs is similar to that found in carbonaceous meteorites except that IDP organics are low-ordered similar to terrestrial kerogen (Chan et al., 2017; Chan et al., 2020; Busemann et al., 2009; Clemett et al., 1993; Flynn et al., 2004; Matrajt et al., 2004).

2.3.1 Organic Matter in IDPs and Carbonaceous Meteorites

IDPs like meteorites can be chondritic (non-modified and undifferentiated) according to their petrology. Chondritic IDPs have a composition similar to carbonaceous chondrites in elemental composition, however, they can differ from known carbonaceous chondrites in relative carbon content – with chondritic IDPs being more enriched in carbon compared to carbon-rich CI carbonaceous chondrites (Krot et al., 2014, Rietmeijer, 1992, 1998, 2002; Thomas et al., 1996). This work focuses on carbonaceous IDP and hence the literature review in this section focuses on the same. About 90% of chondritic IDP are comprised of aggregate particles which vary in their level of porosity from being highly porous to being compact particles with a rough surface (Mackinnon and Reitmeijer, 1987; Reitmeijer and Warren, 1994; Reitmeijer, 1998, 2002; Krot et al., 2014). Organic matter such as amino acids have been found in certain carbonaceous chondrite meteorites (e.g., Murchison meteorite) (Cronin et al., 1988). Carbonaceous chondritic meteorites were responsible for delivering organic matter throughout our solar system. A high percentage (90%) of the organic matter found in these primitive hydrated carbonaceous chondrites are insoluble and hence cannot be extracted as easily as its soluble contents (Kerridge 1999).

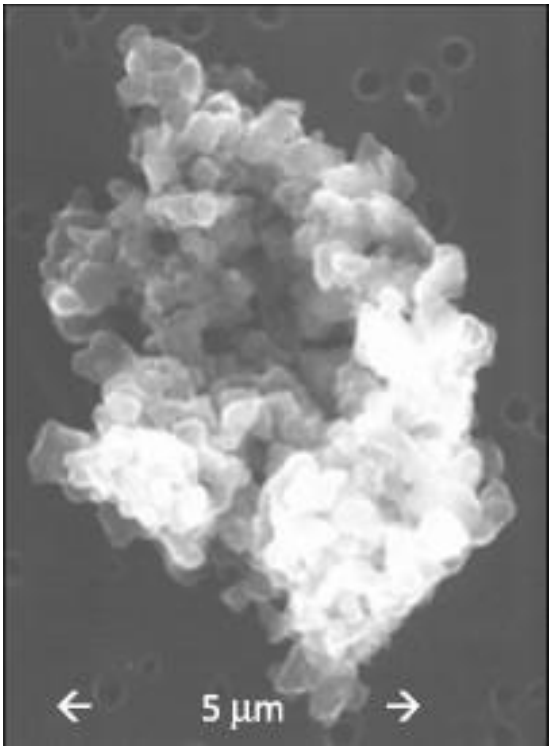

Figure 2.2: Scanning electron microscope image of an ~11 µm chondritic IDP collected from the Earth's stratosphere by a NASA aircraft. The individual surface features are micron or submicron grains that have aggregated to form this dust particle (image source: NASA, Flynn (2020)

Keller er al. (1994) reported a bulk amount of carbon ranging from 4% to 45% in Carbonaceous Porous (CP) IDPs. In addition to elemental carbon, spectroscopic analysis have established the presence of aliphatic compounds and polyaromatic hydrocarbons (PAHs). The textural, isotopic characteristics along with the disordered organic matter present in IDPs links their origin to primitive solar grains.

Organic matter in IDPs compare differently to different carbonaceous chondrites. Flynn et al., 2000 reported a higher C=C/C=O ratio in a sample in the Murchison meteorite (CM2 type) as compared to hydrated IDPs (Flynn et al., 2000). According to studies reported in Busemann et al. (2000), the organic matter in IDPs is very similar to primitive meteorites likely as a result of material transport during the evolutionary stages of the early solar system. Table 1 lists some of the organic compounds identified in the Murchison meteorite through laboratory studies. For a more complete list the reader is directed to Glavin et al. (2020). This implies that similar to meteorites, the organic compounds in IDPs are expected to be diverse.

Table 1: Identification of eight protein amino acids @g/g) in the Murchison meteorite [Source: Pereira et al., 1975]

Amino acid	Nonhydrolyzed Murchison meteorite extract analyzed by mass fragmentography	Nonhydrolyzed Murchison meteorite extract	Hydrolyzed Murchison meteorite
Alanine	2.1	2.1	3.5
Valine	1.2	0.8	1.6
Glycine	3.1	3.4	6.1
Isoleucine	0.3	-	-
Leucine	0.2	-	-
Proline	0.7	0.4	1.3

Amino acid	Nonhydrolyzed Murchison meteorite extract analyzed by mass fragmentography	Nonhydrolyzed Murchison meteorite extract	Hydrolyzed Murchison meteorite
Aspartic Acid	0.3	0.4	1.7
Glutamic Acid	3.3	0.6	3.1

Given the diversity of meteorite classes and IDP classes with each possibly having varying levels of organic matter, an accurate inventory of IDP organics and their percentages relative to various meteorite classes is difficult to report. Additionally, the extent to which organics in IDPs are altered as they travel through a planet's atmosphere depends on various factors ranging from the porosity of the IDP, IDP origin (cometary or asteroid) which determines the entry velocity and angle, and the properties of the planetary atmosphere. At the time of writing, adequate literature was not found on an inventory of organic compounds detected in IDPs. This could be owing to difficulty in analyzing IDPs due to their small size and the chances of terrestrial organics contamination before analysis in laboratories. For this reason, we will be assuming the organic inventory and organic carbon content of standard carbonaceous chondritic meteorites which have been analyzed in the laboratories by independent researchers is essentially similar to the organic inventory of IDPs. There is existing literature and research studying the interactions between crushed and sieved Murchison meteorite irradiated by UV radiation under simulated Mars conditions (Schuerger et al., 2012). Since this thesis focuses on IDP survival on Martian surface despite the UV radiation environment on the surface, we will be using results from experiments conducted with the Murchison meteorite as a proxy for IDPs.

Like Earth, Mars receives a constant flux of organic matter in the form of IDPs, and according to early modeling studies, this value amounts to 8.6×10^6 kg/year of unmelted organic material (Flynn 1996). Similar modeling studies have shown that a large fraction of the IDPs incident on the Martian surface are unaltered and unmelted (shown in Figure 2.3) – put another way, the organic carbon content intrinsic to the IDPs are mostly preserved despite heating from friction

during atmospheric entry through the Martian atmosphere (Flynn, 1996). This implies a surface reservoir of organics on the Martian surface which is constantly being replenished.

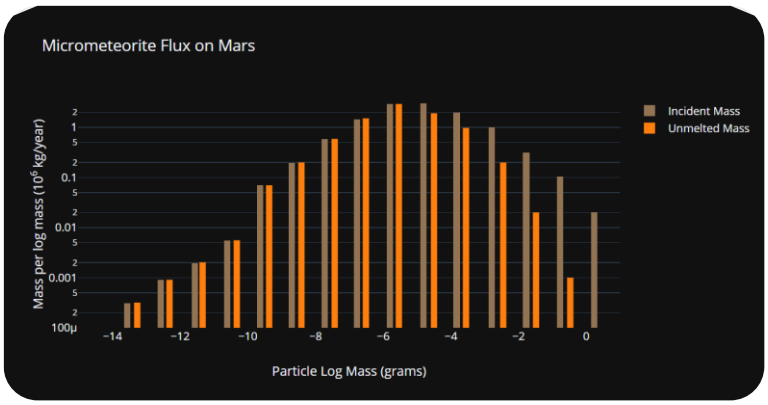

Figure 2.3: IDP flux Incident mass along with surviving mass from modeling studies conducted by Flynn (1996)

2.4 Radiation Environment on Mars – Degradation of Organics

The harsh radiation environment on the surface of Mars needs to be taken into account while devising strategies for detecting organic material on Mars. This is because UV radiation which is mostly unattenuated by the Martian atmosphere degrades the structures of organic molecules that might be present on the surface causing damage to their structural integrity. As mentioned in the introduction, UV radiation is not the only source of degradation – GCRs and SEPs also contribute to radiation-related damage done to organic molecules and bacterial cells. Ionizing radiation from these sources has a greater penetration depth compared to UV radiation and hence can cause damage to microorganisms and organics present at the subsurface level (Baumstark-Khan & Facius 2001; Dartnell 2011). Organics in the soil are also altered by oxidants present in the soil (perchlorates). These factors combined initially seem to indicate that survival of organic matter and bacterial colonies would be difficult in the recent Amazonian period of Mars. According to Cockell et al. (2000), unshielded parts of Mars' surface receive 9.5 times more biologically effective radiation per day between the wavelengths 200 nm and 320 nm.

Unlike Earth's atmosphere, due to a lack of ozone in the Martian atmosphere, high energy UV radiation specifically UVB (280–315 nm) and UVC (200-280nm) are not absorbed effectively. UV radiation with wavelength as small as 190 nm is capable of reaching the surface with shorter

wavelengths being absorbed by the abundant CO_2 in the atmosphere. UV radiation reaching the surface further depends on the time of the year (characterized by solar longitude L_s), the amount of dust in the atmosphere which is often linked to the seasons, and latitude. This implies that although Mars is farther away from the Sun than Earth is, it receives a higher flux of UV radiation on the surface.

Modeling studies have been carried out in order to characterize the radiation environment at different regions on Mars. Optical depth data from landers and rovers have facilitated in the development of these models (Kuhn and Atreya, 1979; Cockell et al., 2000; Patel et al., 2002; Moores et al., 2007; Vicente-Retortillo et al., 2015). An example of such modeling studies undertaken in Moores et al. (2007) showing the total UV flux received on the Martian surface each year assuming flat horizontal surfaces with unobstructed line of sight between horizon to zenith (Figure 2.4).

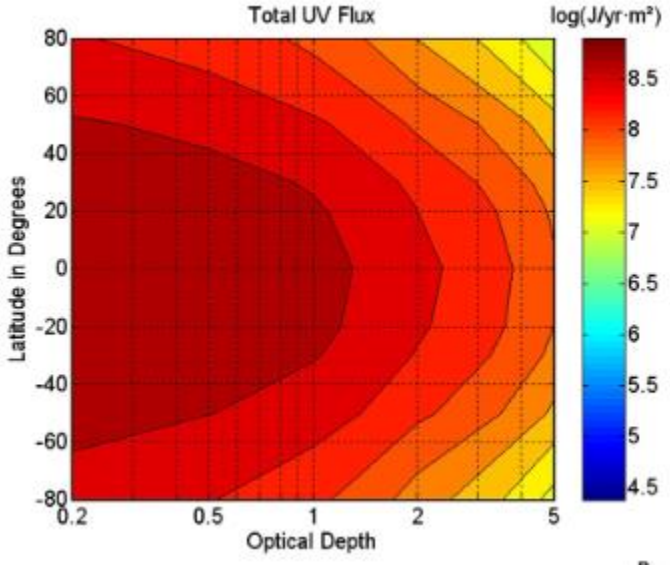

Figure 2.4: Total UV flux (base-10 log) in one Martian year for different optical depth modeled for present day Mars (Moores et al., 2007)

Relatively recently the Rover Environmental Monitoring Station (REMS) instrument on board the Curiosity rover provided measurements of the maximum UV flux present at Gale crater. This amount was approximately 20 W/m^2 which is lower than modeling predictions, but is still significant to cause serious damage to structures of organic compounds present at the surface level (Gomez-Elvira et al., 2014).

2.5 Martian Dust

In-situ investigations by spacecrafts such as Viking landers, Pathfinder, Mars Exploration Rovers (MER), MSL (Curiosity), and most recently the Mars 2020 Perseverance rover has come up with inventory of Martian dust and regolith composition in these sites. A more global understanding of the mineralogy of Mars at different locations is provided by infrared spectroscopic measurements and chemical measurements from instruments on orbiters. Mars' distinctive reddish hue comes from the presence of ferric oxides and oxyhydroxides present in the dust (Singer, 1982). Martian dust is fine-grained – with effective particle radius in the micron range (< 5 μm) (Lemmon et al., 2019).

Data from Very Near Infra-Red spectroscopy (VNIR) have shown strong Fe 3+ absorption by Martian dust and indicated a lack of well-crystalline oxides (Morris et al., 2000). Some data from the VNIR and TIR instruments hint at the presence of hydrated silicates such as Zeolite (Ruff 2004). Thermal Emission Spectroscopy (TES) of dust suspended in the atmosphere insinuates the presence of plagioclase and hydrated silicates and spare quantities of olivine, pyroxenes, and sulfates (Hamilton et al., 2005). Banfield et al. (2003) have also reported Magnesium carbonate in the dust (<4% wt). Data from rovers has pointed out that Martian dust has magnetic properties while being enriched in nanophase Fe 3+ and a lack of olivine relative to the soils (Goetz et al., 2005; Morris et al., 2006). The abundance of amorphous ferric bearing particles in the Martian soil gives rise to its highly UV absorptive properties, making Martian surface material and regolith a good candidate to shield organics from UV photolysis.

2.6 Laser Induced Fluorescence Spectroscopy (LIF) for detecting Organics

This experimental section of this thesis focuses on detecting organics mixed with Martian simulant soil using Laser Induced UV Fluorescence (LIF) spectroscopy. LIF spectroscopy is a relatively non-destructive mechanism to detect the presence of organic material in a sample even in small concentrations. LIF spectroscopy relies on studying the interactions between visible or UV lasers and a sample. An incident photon having sufficient energy can be absorbed by the molecule (an organic molecule in our case), exciting an electron to a higher energy state within the molecule. The electron later returns to its ground energy level – resulting in the emission of a

photon. The instrument used for LIF is detailed in the Materials and Methodologies chapter of this thesis.

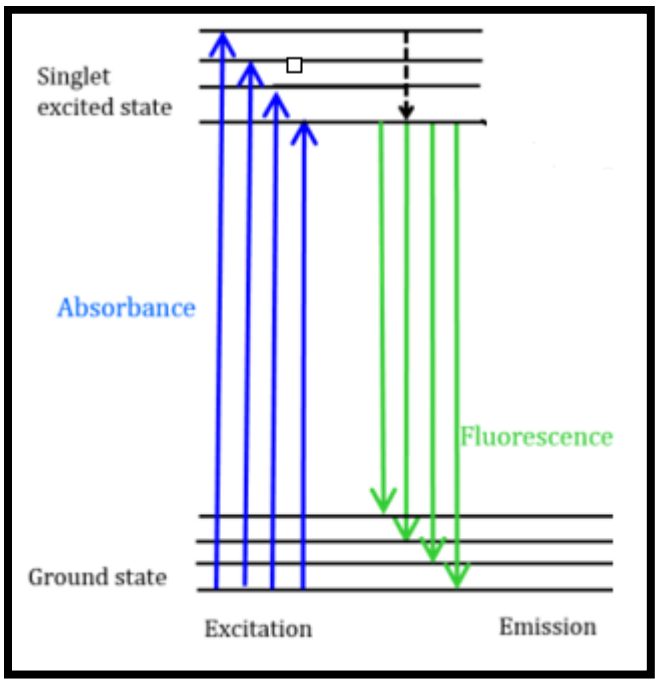

Figure 2.5: Jablonski diagram illustrating energy states of a fluorescing molecule – the principle of Laser Induced Fluorescence spectroscopy (Source: https://jascoinc.com/learning-center/theory/spectroscopy/fluorescence-spectroscopy/)

As mentioned, Martian dust and subsequently most Martian simulant soils are highly absorptive of UV radiation. This characteristic serves well as a preservation mechanism, shielding organics from incoming solar UV radiation on the surface. However, this property also hampers our ability to detect organics mixed with Martian soil using instruments dependent on UV lasers. This part of the project looks at LIF signals from samples of the organic Tryptophan mixed with JSC-1 Mars simulant soil at different concentrations.

Chapter Three: Research Objectives

3.1 Sedimentary Rhythmites

Although Martian rocks are largely volcanic in origin, orbiters and spacecrafts (Mars Express and Mars Reconnaissance Orbiter) have discovered sedimentary layered rock structures exposed on the surface (Malin and Edgett, 2000). Sedimentary rocks are rocks formed from continuous deposits of sediment in the form of particulate matter and precipitated minerals. A majority of these sedimentary structures on Mars are thought to have been formed during the pre-Noachian to the Hesperian era as a result of sediment transported via water flowing on the surface or through glacial activity. Rich deposits of clays and sulfates have been reported in these sedimentary structures (Grotzinger and Milliken, 2012). Despite Mars having a completely different climate compared to Earth (today) with a lack of a present-day hydrological cycle, the sedimentary deposits mentioned are nevertheless subjected to rapid erosion caused by wind-related processes. This implies that only in certain geometric settings, the stratigraphic record of sedimentary rocks will be preserved for further investigations. Sedimentary rocks are also essential in preserving traces of previous environments that existed on the Martian surface – providing the perfect mechanism to study Mars' past and evolution.

Topographic data from HiRISE instrument on board the MRO have indicated the presence of rhythmic sedimentary rocks with quasi-periodic bedding mainly in several locations at Arabia Terra in addition to other regions on the planet, shown in Figure 3.1 below (Lewis and Aharonson, 2014; Kite et al., 2016). These features however are hypothesized to be a result of dust deposition through gradual airfall of dust particles - taking place during the present Amazonian period. Through dust deposition through the years, after some point, the layers of dust undergo cementation, resulting in lithification from the weight of sediments and dust particles stacked on top of each other. The same imagery data has also indicated that the bedding of these sites are quasiperiodic, linking these formations to periodic changes in the orbital parameters of Mars (Laskar, 2004). Changing orbital parameters such as the obliquity of the planet changes the solar insolation received which in turn impacts the amount of dust suspended in the atmosphere, leading to changing thickness of dust deposition in what we will be calling sedimentary rhythmites in this work.

Some of the sites where sedimentary rhythmites with quasiperiodic bedding have been reported by Lewis and Aharonson (2014) are shown in the map presented in Figure 3.1. These sites were selected specifically since the sedimentary rhythmites at these locations exhibit quasiperiodic bedding.

Figure 3.1: Locations on Mars where quasi-periodic rhythmic sedimentary rocks have been discovered

[Source: https://github.com/PietPtr/MarsMap, MOLA, NASA]

Since sedimentary rhythmites are a result of the gradual settling of Martian dust suspended in the atmosphere, due to its small particle size and composition, they could be a potential niche environment for preserving organic material from incoming IDPs being delivered on Mars constantly. A schematic diagram presented in Figure 3.2 shows a concept of how IDPs can be embedded within layers of airfall sediment. Keeping in mind that UV radiation is a major concern for effectively preserving surface organics on Mars due to its ability to damage carbon bonds and their molecular structures, layers of Martian dust present in these rocks can potentially shield organics from being subjected to UV alteration and degradation.

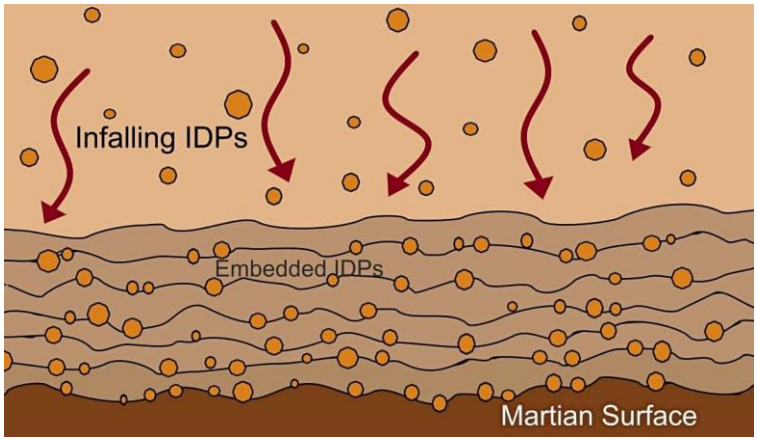

Figure 3.2: Sketch illustrating infalling IDPs on the Martian surface embedded in sedimentary rhythmites upon layering of airfall Martian dust. The orange spheres on this diagram represent IDPs. As time passes, each layer of IDP on the surface has more dust sedimented on top, leading to more robust shielding from UV flux

In such a scenario, the spectral properties of Martian dust play an important role in shielding organics from being exposed to high UV radiation fluxes. Since at the time of writing no sample of Martian dust or regolith was present on Earth for laboratory analysis, our only available material for analysis were the use of Martian simulant soil retrieved from specific environments on Earth. Simulant soils have been crafted to match our understanding of spectral, grain size distribution, density and porosity properties of Martian soil. Several studies have looked at the UV absorptive nature of Martian simulant soil (e.g., Carrier et al., 2019). For the purposes of this modeling the concept shown in Figure 3.2, we consider the results of a study undertaken by Godin et al. (2023) using JSC-1 Mars simulant soil. Godin et al. (2023) shows that JSC-1 Mars is highly absorptive in the UV range and can hence effectively shield IDP organics.

From Figure 3.2, assuming the UV absorptive characteristics of JSC-1 Mars simulant soil reported in Godin et al. (2023), over time, sedimentary rhythmites can, in principle provide UV shielding to layered deposits of organics in IDPs. The schematic diagram illustrates a possible burial mechanism for the preservation of IDP organics within sedimentary rhythmic rocks. This work aims to generate numerical simulations for the sequestration of organic carbon from IDPs in rhythmites as a consequence of UV absorption by layers of Martian dust sediment.

Reiterating, UV radiation, radiation from galactic and solar energetic particles (GCRs and SCRs) are other potential destructive mechanisms for organics on Mars. SCRs are capable of destroying

organic molecules in the first 2 cm of Martian regolith and GCRs penetrate further (Pavlov et al., 2012). The discovery of perchlorate at the Phoenix landing site implies possible oxidization of organics by oxychlorine species (Hecht et al., 2009). The decomposition of perchlorates produces reactive species which degrade organic material (Quinn et al., 2013). This work focuses only on UV photolysis as a pathway of organic degradation and doesn't consider additional sources like GCRs, SEPs, and perchlorates. GCR and SEP flux is negligible compared to the UV flux received, and hence this thesis focuses on the dominant UV radiation on the surface. The results obtained here would serve only as an upper bound for organic material preservation expected at the sites we will explore.

This thesis details the work and calculations employed in simulating the preservation and sequestration of organic carbon in sedimentary rhythmites, drawing conclusions on whether or not sedimentary rhythmites are a good candidate to preserve organic matter being delivered to Mars through IDPs. Further comments are made on what regions of Mars are best suited for preserving this type of organics through this mechanism.

3.2 Organic Detection through LIF in Martian Dust Matrix

There are different methods to detect organic materials in the Martian context. Until 2020, Gas Chromatography Mass Spectroscopy (GCMS) was the only experiment that was sent to Mars on three different spacecrafts – Viking 1, Viking 2, and Curiosity. As mentioned in the introductory chapters, the GCMS analysis results from the Viking landers were ambiguous, leading to the suggestion of superoxides present in the Martian soil. Notable results have been obtained from the GCMS on the Curiosity rover (Freissinet et al., 2015; Eigenbrode et al., 2018).

Recently, the Perseverance rover carried the Scanning Habitable Environments with Raman and Luminescence of Organics and Chemicals (SHERLOC) instrument which is equipped with a compact deep ultraviolet Raman spectrometer (248 nm) along with a fluorescence spectrometer and context imager (Wide Angle Topographic Sensor for Operations and eNgineering – WATSON). SHERLOC is tasked with the detection of organic compounds and characterizing the mineralogy at Jezero crater (landing site of Perseverance rover). While the GCMS involves heating soil samples to a high temperature (pyrolysis) which can alter the organics present in the sample. In contrast to GCMS, DUV Raman spectroscopy and Fluorescence spectroscopy are newly emerging techniques being employed for organic detection on Mars.

LIF (Light Induced Fluorescence) spectroscopy works on the principle of using a laser to excite a molecule to a higher energy state and a detection is characterized by the emission of photons as the molecule returns to its ground state (refer Figure 2.5 from Section 2.6). LIF typically uses visible or UV light to excite the molecule present in a sample. Specifically, lasers in Deep UV (DUV) wavelengths (100 – 280 nm) are befitting for the detection of fluorescence from organic molecules present in a sample (Bhartia et al., 2008, 2010; Beegle et al., 2015, 2016). The advantages of employing this technique compared to traditional methods like GCMS for our investigations on detecting small concentrations of organic material mixed with Martian simulant soil are the following:

- LIF is non-invasive and doesn't involve processing the sample to a large extent (heating for example). This ensures that the organic content within the sample is not altered and thus the results of the detection are easily decipherable and clear.
- LIF is also capable of detecting small concentrations (single ppm) of organic material in a sample mixture.
- Observations can be obtained within a few seconds -It is time efficient compared to GCMS
- Can also detect mineral fluorescence – enabling the identification of minerals and organics in a sample matrix

In the experimental section of this thesis, we will be employing LIF spectroscopy to detect organics mixed in a Martian simulant soil matrix. Taking note of LIF's sensitivity, LIF among other UV spectroscopy methods is an efficient tool to detect organics present in small concentrations (possibly IDP concentrations) within sedimentary rhythmic rocks. We will be focusing on a single organic molecule for our experimental work – Tryptophan. The next section details the LIF signature of Tryptophan and why the detection of Tryptophan in an experimental setup like ours is important to contextualize organic material detection in Martian soil.

3.2.1 LIF Signature of Tryptophan

L-Tryptophan is an organic compound (aromatic amino acid) with a molecular formula of $C_{11}H_{12}N_2O_2$ and is an essential amino acid - Tryptophan plays an important role in protein

synthesis in the human body. More importantly, Tryptophan is one of the 20 amino acids crucial for synthesizing proteins in all life that we know of. Its chemical structure is shown in Figure 3.3.

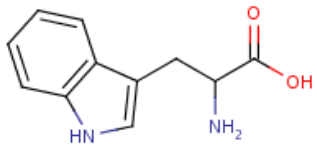

Figure 3.3: Chemical structure of Tryptophan

[Source: https://sielc.com/compound-trypthophan]

Tryptophan (Trp), Phenylalanine (Phe), and Tyrosine (Tyr) are three fluorescent amino acids, due to their conjugated aromatic ring side chains (shown in Figure 3.3 for Tryptophan).

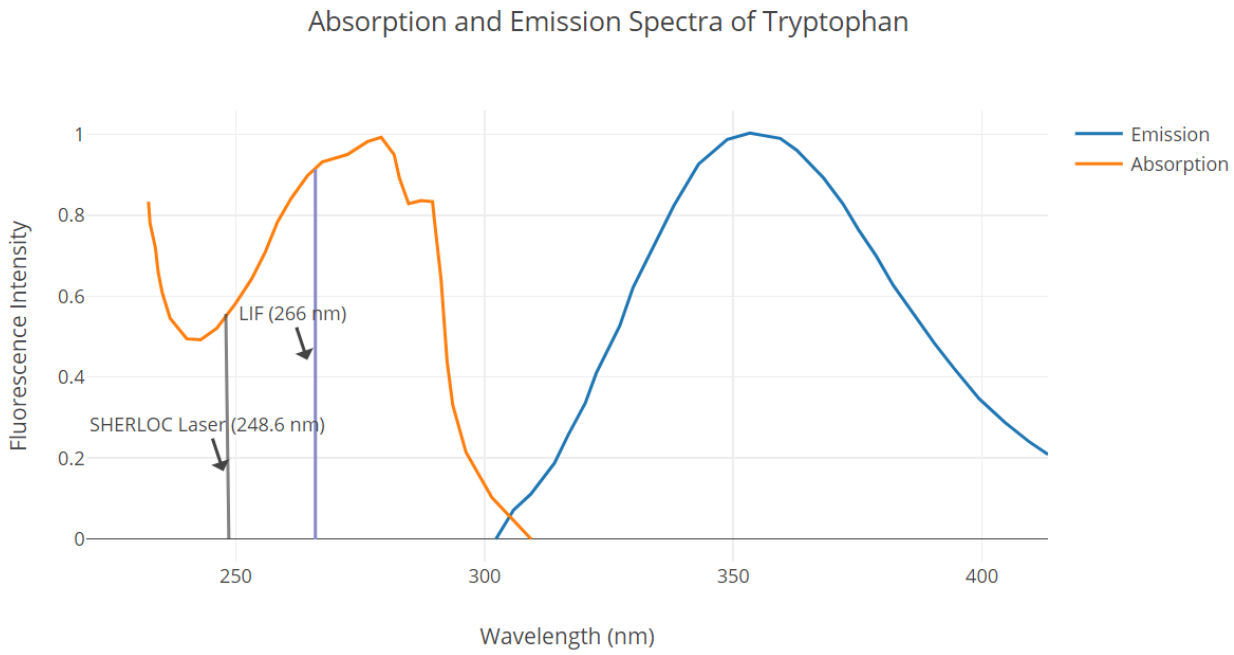

Figure 3.4: Emission and Absorption Spectra of Tryptophan. Tryptophan can be excited in the wavelength range 250 to 300 nm (approximately) and emits a fluorescence spectra over a range of wavelengths starting from 300 nm, peaking at around 340 nm (this depends on the excitation frequency). The SHERLOC laser operates at 248.6 nm (deep UV) and the LIF instrument used in this project operates at 266 nm – both are capable of exciting Tryptophan causing it to fluoresce (Plot recreated from Lakowicz, 2006)

Among them, Tryptophan dominantly absorbs UV radiation around 280 nm to re-emit a characteristic fluorescence signal between 300 – 400 nm. Studies have shown that in a mixture of proteins, the fluorescence mainly originates from Tryptophan, primarily due to the presence of an indole group which is responsible for the dominant absorption and remission within the molecule (Yang et al., 2017). Tryptophan's fluorescence is characterized by a broad peak (333 nm according to Razzel Hollis et al., 2023). From Figure 3.5, comparing the DUV fluorescence of 24 amino acids, one can note the following:

1. Strong fluorescence signal of Tryptophan at around 333 nm
2. Most other amino acids listed have their peaks in the range of 200 nm
3. The 300-340 nm wavelength region is dominated by the Tryptophan signal over a larger wavelength range compared to Lysine - making it more identifiable

These observations indicate that Tryptophan's strong fluorescence signal at 300-400 nm allows for easy detection of the amino acid, even when mixed with other organic compounds. L-Tryptophan will be used as a representation of any organic material that might be present in sedimentary rhythmites. Given Tryptophan's strong fluorescence signal, the detection of Tryptophan using LIF in the Martian context would serve as a lower bound for the detectability of organics mixed with Martian soil or dust. In other words, if a LIF instrument is unable to detect Tryptophan in a Martian dust/soil matrix at a certain concentration, it will be unable to detect any other organics or a mixture of organics at the same concentration that might be present. Additionally, aromatic compounds have been discovered by the SAM instrument on Curiosity, and more recently the SHERLOC instrument on the Perseverance rover has reported fluorescence results that are consistent with aromatic organics from samples analyzing the bottom of Jezero crater. The fluorescence maps resulting from the sample analysis point to a bulk concentration of organics of 0.1 – 10 ppm (Scheller et al., 2022). Although from the literature review conducted for this thesis, we couldn't find literature indicating that Tryptophan has been explicitly reported in IDP material analyzed on Earth laboratories, a recent study analyzing mid-IR spectral data from the Spitzer Space Telescope has pointed to the presence of Tryptophan in a molecular cloud (IC 348) thus strongly suggesting that even relatively complex organic molecules such as Tryptophan can be forged through abiotic processes which may later be transported (Iglesias-Groth, 2023). Hence, we argue that Tryptophan is a good candidate for our experimental study.

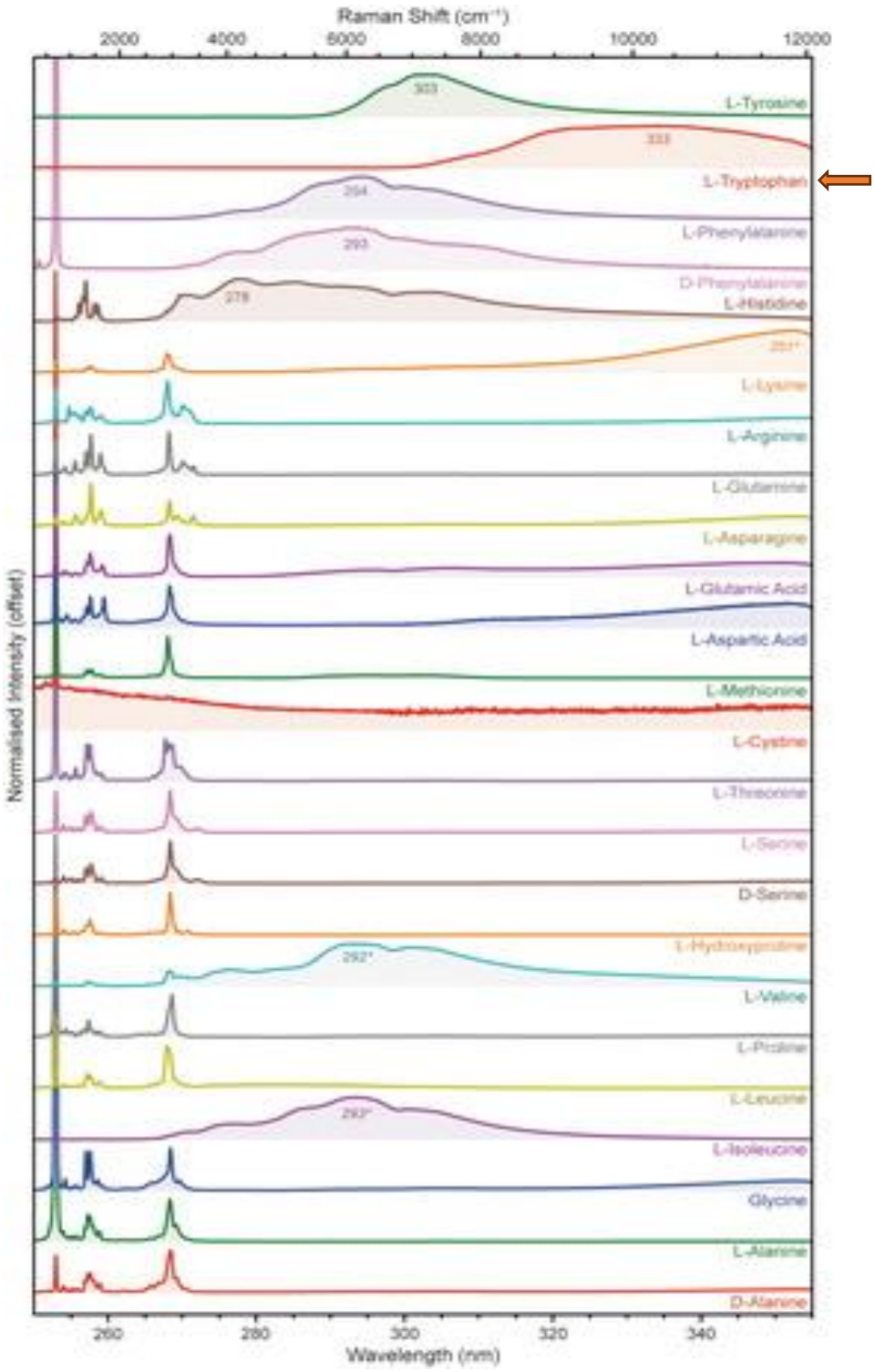

Figure 3.5: Deep UV Fluorescence of 24 amino acids excited at 248.6 nm (Source: Razzel Hollis et al., 2023)

3.2.2 End-member cases explored

Our experiment consists of detecting Tryptophan in a JSC-1 Mars matrix. JSC-1 is a Martian simulant soil sourced from weathered volcanic ash from Pu'u Nene cinder cone in Hawaii. JSC-1 is spectrally similar to the bright regions of Mars (Allen et al., 1998). Table 2 shows the mineralogical composition of JSC-1 Mars measured using Rietveld refinement (Stalport et al., 2012).

Table 2: Mineralogical Composition of JSC-1 Mars Simulant Soil

(data from Stalport et al., 2012))

	JSC Mars-1	
Mineral	**Chemical Formula**	**Wt%**
Anorthite	$CaAl_2Si_2O_8$	62.1
Augite	$(Ca,Mg,Fe)_2(Si,Al)_2O_6$	27.3
Forsterite	$MgSiO_4$	8.8
Chromite	$FeCrO_4$	1.0
Ilmenite	$FeTiO_3$	0.9

JSC-1 Mars has a high magnetic component consisting mainly of feldspar ($KAlSi_3O_8$ – $NaAlSi_3O_8$ – $CaAl_2Si_2O_8$) and Ti-magnetite in addition to minor olivine, pyroxene, and glass. The magnetic and ferric component of JSC-1 Mars is majorly responsible for UV quenching (relevant in the results chapter). It should also be noted that JSC-1 Mars is poor in clays and is rich in basaltic minerals. Data presented in Table 2 does not report the amorphous content of JSC-1 Mars (64 %) which contain iron bearing particles (nanophase iron) and contribute to absorption of UV rays resulting in quenching of the probing laser beam in addition to any resulting fluorescence signal produced in UV wavelengths (such as that of Tryptophan). It should be noted that JSC-1 Mars also contains trace quantities of clays which are not mentioned in Table 2.

The chemical and mineralogical composition of Martian soil and how it varies globally are relatively unknown – particularly due to the limited number of landers and rovers sent to the

surface and the limited ability to sample Martian soil globally. Although most of the Martian soil is expected to be basaltic in nature, one needs to keep in mind that clay particles (phyllosilicates) also constitute surface matter in some areas of Mars – especially the regions where exposed rock from the Noachian is present. Minerals like phyllosilicates ($(Mg,Fe)3Si_2O_5(OH)_4$), often referred to as clays and iron hydroxyoxides have been shown to play a key role in preserving organic matter by providing their large surface areas for adsorption mechanisms, protecting organics from the external environment (Eigenbrode et al., 2018; Biondi et al., 2007; Scappini et al., 2004).

Given the prevalence of global dust storms on Mars, one could argue that the dust and topsoil settled over rocks and bedrocks at different locations on the planet will be almost homogenous. Additionally, a study shows that a large quantity of dust on the planet is sourced from the Medusae Fossae Formation (MFF) region on Mars (Ojha et al., 2018). The MFF region is also home to discontinuous, thick sedimentary deposits. As of now, we don't have spectral data of material from this region and hence cannot accurately assign any mineralogical signatures (Grotzinger and Milliken 2012). It is hypothesized that the material deposited at MFF consists of volcanic airfall and other igneous rock-like material (Bradley et al., 2002; Mandt et al., 2008; Kerber and Head, 2010). Although JSC-1 Mars is primarily basaltic, with traces of plagioclase, making it not the best candidate for preserving organic matter, it is however an accurate enough representation of what generic Martian dust might consist of. Moreover, JSC-1 Mars mimics the spectral features of Martian soil, making it a good candidate for this study. Thus, we argue that using a basaltic JSC-1 Mars as a representation of dust and soil on the Martian surface is sufficient to study and to further draw conclusions on the detectability of organics in a Martian dust matrix. Our modeling work for IDP organics burial in sedimentary rhythmic rocks is also based on the spectral properties of JSC-1 Mars. Thus, choosing JSC-1 Mars for the dust component of our Tryptophan + dust matrix in this experimental project will allow us to compare results and draw relevant conclusions.

To summarize, we will be devising an experiment to detect Tryptophan in a JSC-1 Mars simulant soil mix using LIF spectroscopy. Reiterating, Tryptophan is an organic compound with a strong fluorescence signal making it the strongest candidate for organic matter detectability in conjunction with JSC-1 Mars simulant soil which due to its basaltic composition is not the best

type of soil to preserve organic compounds. In other words, we are investigating whether or not the most detectable organic compound through fluorescence spectroscopy can be detected in a basaltic soil environment, which is the primary composition of Mars today. This work also aims to provide insights into operating and optimizing the use of future UV spectroscopic instruments on Mars.

3.3 Relevance of projects and how the two projects fit together

Preservation of organic material on Mars is a major theme in the field of astrobiology. Organics can be preserved through adsorption in phyllosilicate mineral deposits like that of the Sheepbed mudstone discovered by Curiosity. However, due to the highly UV absorptive features of the basaltic component in Martian dust and surface material, we argue that the burial of diverse IDP organics underneath a basaltic layer of dust which over years of deposition gives rise to sedimentary rhythmites (after lithification) should be an effective mechanism in burying complex organics. During the burial process, these complex organics will be subject to some amount of UV degradation which will result in the breaking of bonds and the creation of less complex organic matter. The computational part of this thesis aims at answering how much quantity of organic carbon can be sequestered through this mechanism and if these rocks would be a good target for future missions to Mars in search of organic signatures.

The shielding nature of Martian dust which arises from ferric-bearing compounds present in the mineralogy can also unfortunately hamper and negatively interfere with the detection of the biotic or abiotic organics mixed with the Martian dust while employing UV fluorescence techniques. Thus, the nature of Martian dust has its pros when it comes to shielding organics from destructive UV and ionizing radiation, but becomes a disadvantage to efficient detection when one tries detecting the same organics using methods like UV spectroscopy.

This thesis looks at both sides – first modeling UV shielding by layers of lithified Martian dust and then trying to detect ppm level concentrations of organics mixed with Martian simulant soil through UV LIF spectroscopy. The thesis goes on to make observations and draw conclusions on what strategies need to be employed when it comes to in-situ detection of organics on Mars using UV spectroscopy instruments.

3.3.1 Objectives of IDP – Sedimentary Rhythmite Burial Project

The first part of the thesis details a project carried out through computer modeling where IDPs being buried in sedimentary rhythmites were considered. The objectives of this project were the following:

1. Model IDP organic preservation in sedimentary rhythmites at Gale crater where we have in-situ data measured by the Curiosity rover.
2. Similarly model IDP organic preservation in sedimentary rhythmites at other places where quasiperiodic sedimentary rhythmites have been reported by Lewis and Aharonson (2014) - Arabia Terra, Schiaparelli crater, and Juventae Chasma
3. Further predict IDP organic preservation potential globally on Mars and identify regions which favor IDP organic preservation

3.3.2 Objectives of Organic Detection through LIF Project

The latter half of this thesis details a project on the detection of organics mixed with Martian simulant soil (JSC-1 Mars) through UV LIF method. The objectives of this project were the following:

1. To measure UV fluorescence of L- Tryptophan mixed with JSC-1 Mars at the following concentrations: 100 ppm, 50 ppm, and 50% Tryptophan: JSC-1 Mars using LIF instrument available at York University
2. To characterize attenuation of UV signal caused by a layer of JSC-1 Mars over a layer of pure Tryptophan
3. Compare results obtained with similar experiments documented in literature

Chapter Four: Modeling IDP Burial in Sedimentary Rhythmites

4.1 Materials and Methods

The numerical model devised takes into account several components of the Martian environment which have a role to play in the preservation and degradation of buried organics. The reader is reminded that organic degradation resulting from GCRs and SEPs is not considered in this model and is out of scope of this project. The model considers the following for calculating the mass of organics remaining after UV degradation and shielding of the same by Martian dust:

1. The UV radiation on the surface over the year – data taken from a radiative transfer model of the Martian atmosphere
2. Yearly Dust Deposition at different regions – informed from Mars Climate Database, and Line of Sight Extinction studies (LOS-ext) for Gale crater specifically
3. Organic carbon photolysis reactions from Schuerger et al., 2012
4. UV extinction caused by Martian dust (taken from Godin et al., 2023).

The following sections first briefly discuss the background work and relations from existing literature which are later used to build the computer code in this project.

4.1.1 UV Environment on Mars Model

We utilize the results (UV radiation incident on the surface) produced by a 1.5-dimension Mars Doubling and Adding Radiative Transfer (RT) model (Moores et al., 2007; Moores et al., 2017; Smith & Moores, 2020). The model is similar in functionality to the one developed by Griffith et al. (2012) for Titan and has been adapted for Martian conditions (Griffith et al., 2012). The reader should note that the following discussion on the Doubling and Adding Radiative Transfer model (henceforth referred to as the RT model) is not the work of the author. The working of this model is discussed briefly to give the reader an idea of the calculations involved in arriving at the surface UV flux on Mars which is later used for arriving at the results presented in this thesis.

The RT model covers a wavelength range between 200 – 2000 nm since the solar spectrum makes a negligible contribution to UV flux below 200 nm and CO_2 absorption is also high, leading to not much UV flux reaching the surface below 200 nm. The model considers the surface of Mars to be a Hapke surface with the radiative response being informed by the observations by the Rover Environmental Monitoring Station (REMS) instrument on Mars

Science Laboratory (Smith et al., 2016). The RT code models the atmosphere as consisting of two levels of the atmosphere and takes into account gaseous and aerosol absorption, Mie scattering by aerosols, and Rayleigh scattering for the species found in the Martian atmosphere (Moores et al., 2017). Specifically, the model treats the upper level to contain Rayleigh scattering (majorly by CO_2, N_2, Ar, and O_2) and gaseous absorption and Mie scattering is only prevalent in the lower level.

An example of an output from the RT model that was used to compute the UV degradation of IDP organics in this thesis is shown in Figure 4.1 below. The figure depicts the energy received per sol (Martian day) at different latitude points and solar longitude. This is the output generated while assuming that the planet's surface is flat and smooth – it doesn't take into account geographies of the planet.

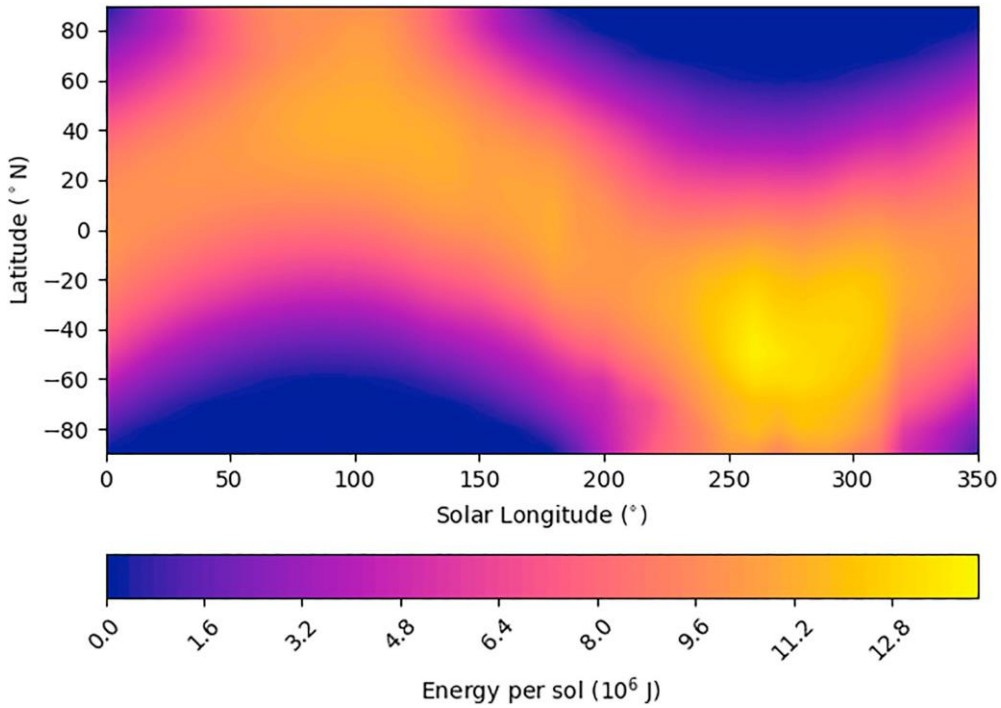

Figure 4.1: Sample output utilized for UV degradation of IDP organics in this project – plot shows the UV flux received with regard to latitude and time of the year (Solar Longitude) (Source: Smith and Moores, 2020)

4.1.2 UV Absorption by Martian Dust

In order to calculate how well Martian dust can shield the IDP organics on the surface, we need to parameterize the UV absorption coefficient of Martian dust for our calculations. Martian dust particle size is typically in the micron range with radius (< 5 μm) (Lemmon et al., 2019).

The absorption coefficient relates to how much of the UV radiation is absorbed by one unit length of layered particulate matter of a certain particle size (150 μm, 250 μm, 350 μm, etc.).

Figure 4.2 shows the zenith extinction spectra indicative of the high UV absorption characteristics of JSC-1 Mars (taken from Godin et al., 2023) at different dust particle sizes (ranging from 150 μm to 850 μm). The absorption coefficient follows from Beer- Lambert's law.

$$I(\lambda) = I_0(\lambda)e^{-L\sigma(\lambda)}$$

The absorption coefficient in the equation is given by $\sigma(\lambda)$, $I(\lambda)$ and $I_0(\lambda)$ are the radiance after and before interacting with the sample respectively, and L is the depth (thickness) of the sample. The work of Godin et al., 2023 measured UV radiance interacting with crushed and sieved JSC-1 Mars simulant soil at different particle sizes as seen in Figure 4.2. Further interpreting this plot, one can note that the radiance of UV light after interacting with the sample is almost e^{-30} times lower than the incident radiation for 1 mm of 150 μm dust sample – meaning JSC-1 Mars is highly absorptive and just a few millimeters of this dust can attenuate the UV flux by a significant value.

Referring to Godin et al. (2023), the absorption coefficient is inversely proportional to the size of the simulant particle. Looking at Figure 4.2, the absorption coefficient corresponding to 150 μm particle size (smallest particle size reported on) is - 30.49, 29.54, 29.35 mm^{-1} for UVC, UVB, and UVA respectively These values were used as input for our computational model. It should be noted that 150 μm particle size is quite large compared to Martian dust. However, since UV absorption increases with a decrease in particle size, the absorption coefficient used and subsequently the UV shielding computed by our model would underestimate UV shielding in the context of the project. In actuality, provided Martian dust is a few μm in radius, these particles are likely to attenuate UV flux to a greater extent.

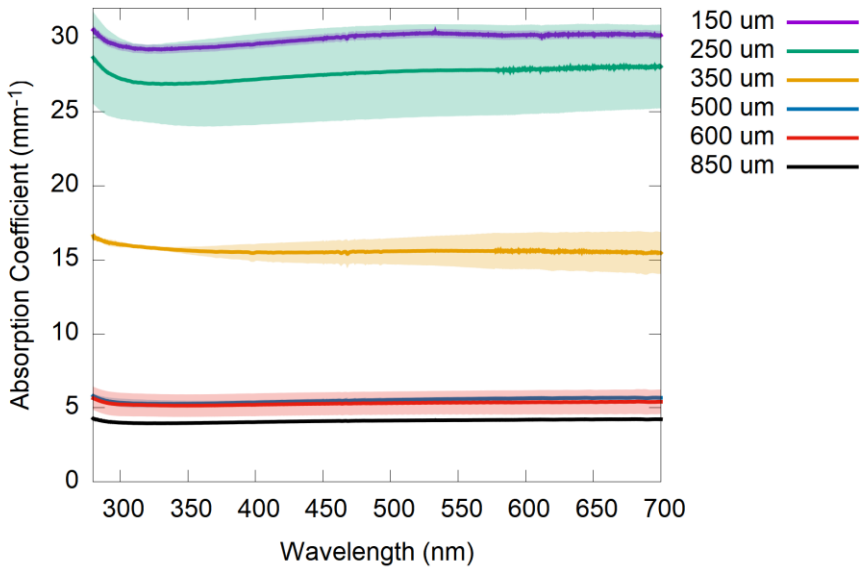

Figure 4.2: UV extinction by JSC-1 Mars simulant at different particle sizes. This plot depicts the highly UV absorptive nature of JSC-1 Mars simulant and that the absorption coefficient is dependent on the particle size of the simulant soil (Source: Godin et al., 2023)

4.1.3 UV Photolysis of Organic Matter Equation

It was established in the introductory chapters that IDPs contain a complex and diverse cocktail of organics. Several studies have looked into degradation mechanisms. Given how diverse the organics are, it is hard to model and consider all the different mechanisms that have been proposed by researchers. Experimental analysis carried out previously by Keppler et al. (2012), Scherger et al. (2011), and Stoker and Bullock (1997) have reported the release of methane from UV-exposed organics in Martian conditions. The mechanism considered in this work for UV degradation of Carbon is the UV/Methane mechanism where Methane is produced from UV-irradiated carbonaceous chondrites – Murchison specifically since it has been widely analyzed by multiple groups of researchers (Schuerger et al., 2012). Equations representing meteoritic organic matter interactions with UV radiation have been reported by Schuerger et al. (2012) from laboratory studies conducted in simulated Martian conditions of 6.7 mbar pressure. These equations have been incorporated in our model calculations.

The efficiency at which carbon is converted to methane per joule of incoming radiation is given by *Quantum Efficiency (QE)*. Schuerger et al. (2012) found this to be a function of *surface temperature (T), mass fraction of carbon (x)* - taken to be 0.0169 for a sample of the Murchison

meteorite, and carbon content in a sample (10% by weight). The final expression utilized from Moores et al. (2017) for QE is given as:

$$QE(x,T) = 4.87 \times 10^{-14}T - 2.73 \times 10^{-12}$$

where QE has units of mol/J.

Using this, the time taken to convert the carbon in each IDP size bin can be calculated (IDP lifetime) given in the equation below. IDP lifetime (L_n) is defined as the amount of time it will take in seconds to completely destroy the organic carbon content of a single IDP particle. It can be computed using the equation provided (taken from Moores et al., 2017)

$$L_n = \frac{2\chi D_n \rho f}{3M_w F_{UV,\,AVG} QE}$$

where χ is the carbon mass fraction in IDPs (0.0169), ρ is the density of IDPs, and f is the fraction of unmelted and unaltered carbon present. $F_{UV,\,AVG}$ is the yearly averaged UV flux received at Gale Crater.

Thus, using these equations, we take inputs of UV flux and temperature (data from Thermal Emission Spectra (TES)) at different times of the year to calculate QE followed by L_n. QE is calculated for different points of the year and integrated. Both these quantities are calculated for the size range of IDPs. The particle size range with surviving carbon considered is from Flynn (1996) and ranges from 910 μm to 0.2 μm (radius). IDPs can be larger than 910 μm in diameter but these are melted during its ascent through the Martian atmosphere (Flynn, 2996).

These calculations are modeled for a specified length of Martian years. For each year, the total mass of carbon is summed up over particle size. The carbon remaining after each year was calculated using the following expression in our model:

$$C_{ij} = C_{i-1\,j} - \frac{C_{i-1\,j}}{L_{ij}}$$

i being the year number and j being particle size bin. The total carbon in one IDP layer is obtained from summing over particle size (*j*). Thus, each year, more carbon is subtracted from the previous year. However, since IDP lifetime keeps increasing with the deposition of multiple layers of Martian dust obstructing UV flux from reaching a layer of IDPs, the subtraction term

ought to approach zero after enough layers of Martian dust have been deposited. This implies that our Carbon decay curve plotted over a time axis will reach an asymptote once enough Martian dust has settled over the IDP particles.

4.1.4 Dust Accumulation on Mars – Mars Climate Database (MCD)

The yearly dust deposition for different locations (Lat, Long) on Mars was computed from data obtained from the Mars Climate Database (MCD) v6.1 web interface using the default settings.. The MCD (developed by LATMOS and LMD among other collaborators) employs a Global Circulation Model (GCM) to compute a multitude of geophysical and meteorological quantities relevant to understanding the atmosphere and surface interactions on the planet (Forget et al., 1999; Madeleine et al. 2011; Milllour et al., 2018). The Mars GCM takes into account various processes occurring on Mars such as different cycles (CO_2, dust, water, and HDO cycle), climate variations, photochemistry. Specifically relevant to this project is the MCD's dust model which computes dust lifting, mixing, transport, and deposition.

Since we don't have spacecraft stationed at many locations on Mars, we need to rely heavily on models such as the MCD to provide inputs to our model on yearly dust deposition rates at a given region.

Python scripts were used to retrieve dust deposition data over the year at specific locations where sedimentary rhythmites have been discovered. A similar script was used to download the dust deposition data on a global scale. The dust deposition provided by the MCD was in units of $kg/m^2/s$. Calculations were made to integrate this dust deposition over the day and subsequently through the year. The quantity obtained was converted to an approximate dust layer depth for one Martian year, assuming Martian dust settled on the surface has a packing density similar to JSC-1 Mars - 870 kg/m^3 (Allen et al., 1998). An example of dust deposition during the year at Juventae Chasma is provided in Figure 4.3. It can be noted that dust deposition is highest between solar longitudes (L_s) 200 and 250, and minimum between 50 and 100 L_s.

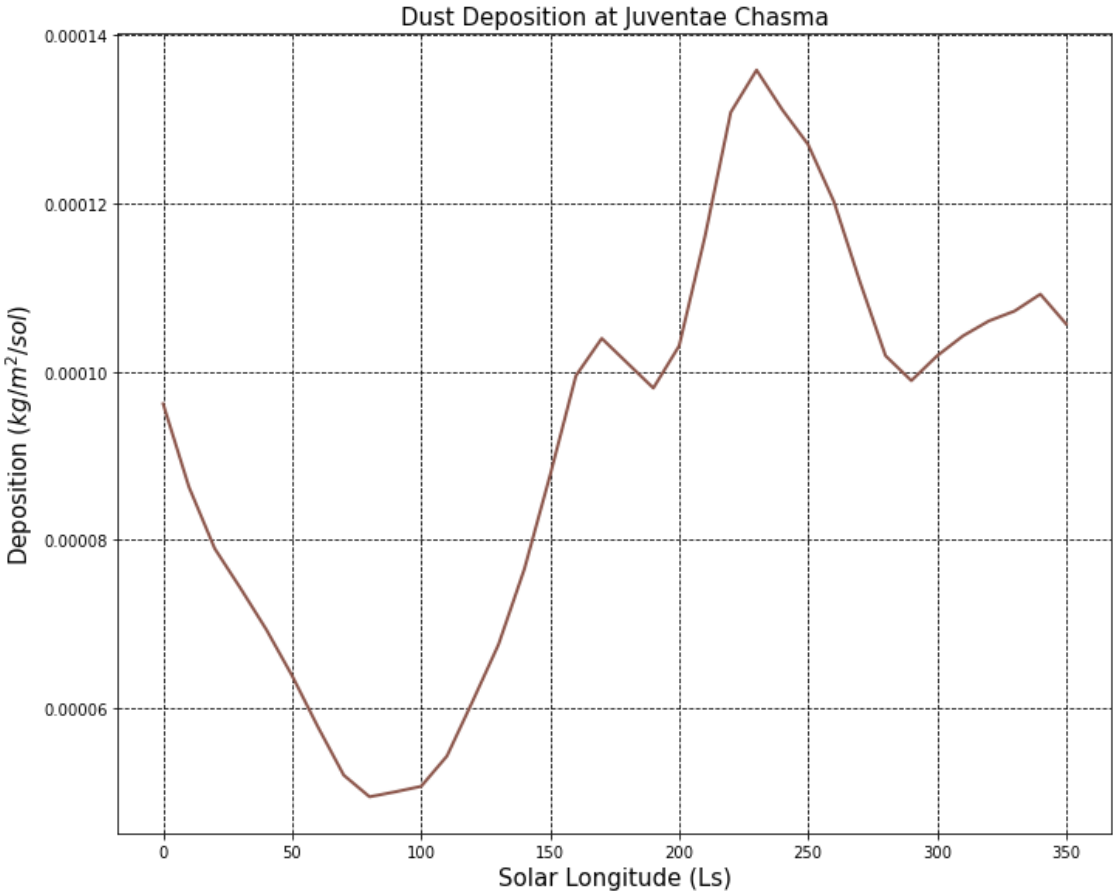

Figure 4.3: Dust deposition at Juventae Chasma throughout the year (time of year represented by solar longitude L_s) computed from MCD data

4.1.5 Dust Accumulation at Gale Crater – Line of Sight-extinction (LOS-ext) Studies

The Curiosity rover, stationed at Gale crater has been monitoring the dust diffusion at Gale crater since 2012. Studies have utilized Navcam images to calculate Line of Sight – extinction (LOS-ext) which further relates to dust settling at Gale crater. Taking advantage of a spacecraft presence at Gale, the yearly and seasonal dust deposition for our model at the Gale crater was informed by LOS-ext studies previously undertaken by fellow researchers.

To give the reader a high-level understanding of how LOS-ext values can provide an understanding on dust settling, the work from Moore (2019) is summarized. LOS-ext can be calculated from rover images that have been radiometrically calibrated. These images consist of the foreground, the distant crater rim, and the sky above the crater rim. The visibility of the images (provided we know the distances between the rover and the crater rim) will allow one to

calculate the dust diffusion locally at Gale. The amount of dust suspended in the air above the crater impacts visibility within the crater and calculations can be made to arrive at the extinction coefficient in (km^{-1}). Furthermore, analyses can be made with Fick's law which calculates diffusion flux from the Eddy diffusivity coefficient and change in dust concentration of the Planetary Boundary Layer (PBL) (Moore, 2019).

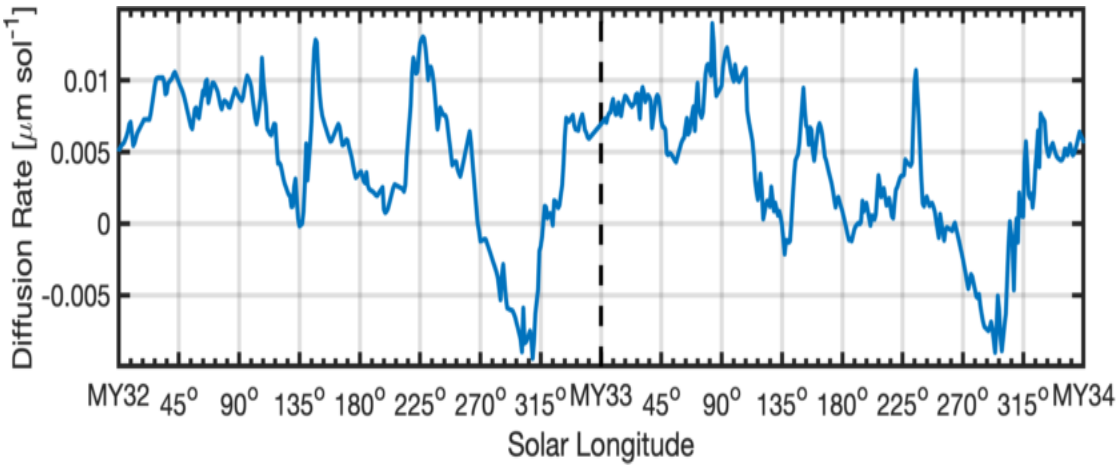

Figure 4.4: Diffusion rate (µm/sol) at Gale crater computed from LOS-ext studies for Mars Years 32 and 33 (Source: Moore, 2019)

The LOS-ext analysis performed by Moore (2019) was considered to arrive at the yearly dust deposition at Gale crater which was used as an input for the IDP organics burial model. Furthermore, a one-year IDP organics decay scenario at Gale crater was also explored with the code using data from Figure 4.4. One can observe that the diffusion rate dips below 0 at certain times of the year – this represents dust being lifted from the crater rather than being deposited.

4.1.6 Algorithm Summarized

Figure 4.5 provides a flowchart of the algorithm used for this analysis.

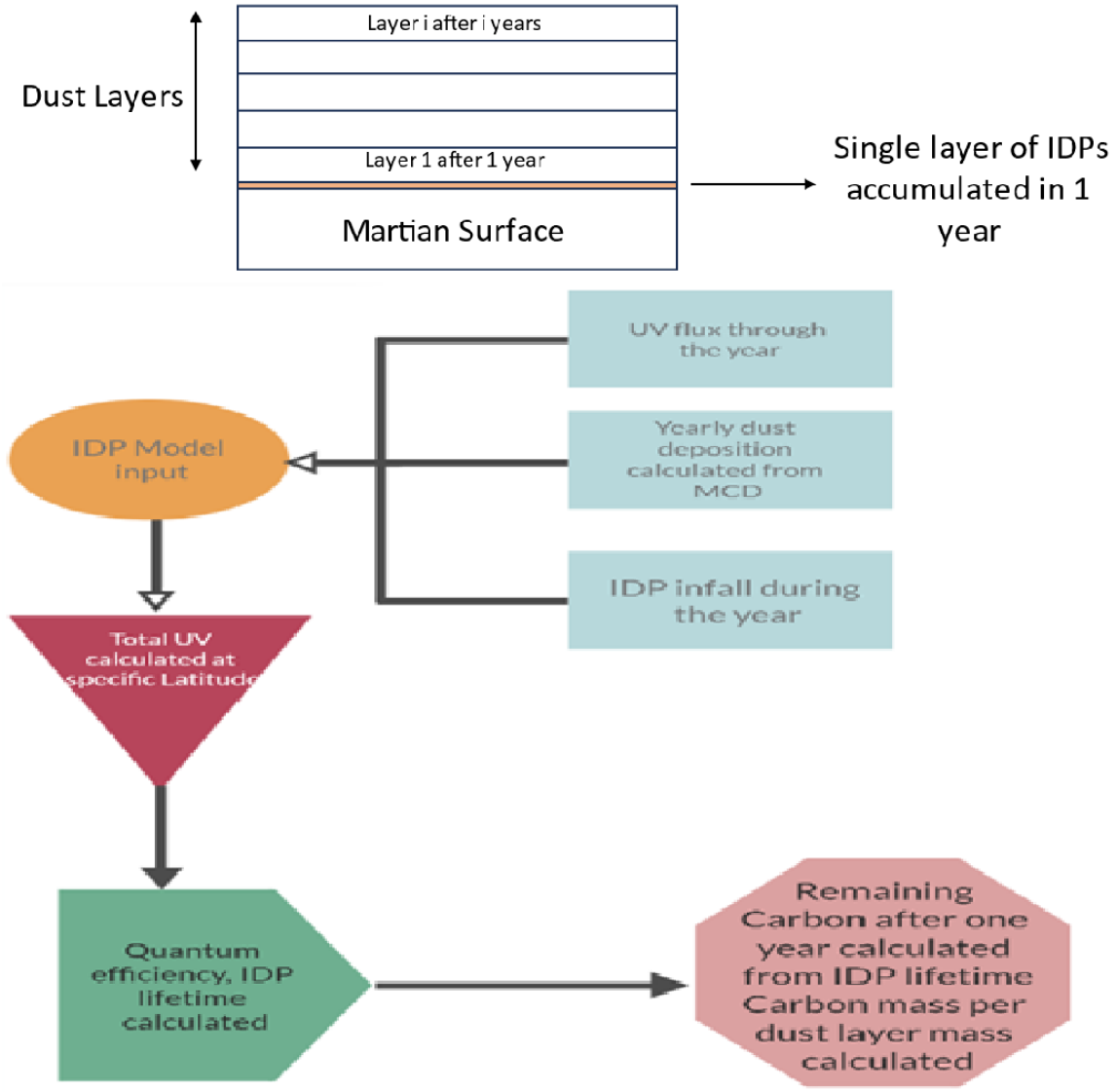

Figure 4.5: Flow-chart summarizing what IDP organics burial model does

The computer model devised takes results and inputs from various sources which were detailed in this section earlier, namely:

- UV radiation environment at a specific latitude and solar longitude (time of the year)
- The depth of dust deposited each year was computed from MCD data for Arabia Terra, Juventae Chasma, and Schiaparelli crater (locations where sedimentary rhythmites with quasiperiodic bedding have been reported)

- Depth of dust deposited in each sol for Mars Year 32 at Gale crater was taken from LOS-Ext studies carried out by Moore, 2019.
- Amount of UV flux reaching IDP organics after yearly dust deposition on top depends on the absorption coefficient of Martian dust. This was assumed to be equal to that reported by Godin et al. (2023) for JSC-1 Mars at particle size 150 μm.
- The input IDP flux was taken to be that reported in Flynn (1996).
- Equations detailed in Schuerger et al. (2012) were used to model the efficiency with which UV flux degrades organic carbon present in. From the quantum efficiency, the IDP lifetime was calculated. IDP lifetime denotes the number of years it would take to completely destroy the carbon content in a single IDP particle – allowing us to compute the amount of carbon remaining after each year. This is done for a range of IDP particle sizes. The fraction of IDP mass that has been altered and melted during its travel through the Martian atmosphere is taken into account in this step (also reported by Flynn (1996)).
- Finally, the carbon content in a layer of IDPs was summed over particle sizes, and the carbon concentration embedded in each dust layer is computed.

4.2 Results

The IDP organics burial model detailed in the Materials and Methods section uses yearly IDP influx, yearly dust deposition, and day temperature at the location as inputs. It is assumed that IDP flux is evenly distributed across the surface area of Mars. Our computer code was run for four primary locations on Mars (Figure 3.1 and Table 3). The yearly dust deposition rate for Arabia Terra, Schiaparelli crater, and Juventae Chasma were calculated from daily dust deposition MCD data. However, the dust deposition at Gale crater was calculated from LOS-Ext diffusion rates mentioned in Moore (2019) for the model input. Table 3 summarizes the yearly dust deposition rates for each of these locations.

Table 3: Yearly dust deposition rates at chosen investigation sites on Mars (Moore, 2019)

(Green represents the value used in our calculations/code)

Location on Mars	Latitude and Longitude	Yearly dust deposition (µm) from MCD	Yearly dust deposition (µm) from LOS-Ext
Arabia Terra	21 N 6 E	22.92	-
Schiaparelli crater	2.7 S 16 E	22.33	-
Juventae Chasma	3.5 S 61.4 W	18.32	-
Gale crater	5.4 S 137.8 E	31.8	3.54

From the values listed in Table 3, it is evident that there is a significant difference between the deposition rate retrieved from MCD data and that from LOS-Ext studies (Moore, 2019) at Gale crater. The two methods of calculating dust deposition values give us varied outcomes and results. The effects of this disparity can be seen in results presented in Figure 4.6.

The results shown in Figure 4.6 were obtained from the algorithm detailed in the Materials and Methods section. The nature of the plots in the figure resembles each other – it is an exponentially decaying curve. This can be expected since the degradation of organic carbon occurs at a higher rate when there is a smaller depth of dust deposited. As the dust depth increases over the years, the UV flux reaching the layer of IDP organics decreases due to UV absorption by the layers of Martian dust.

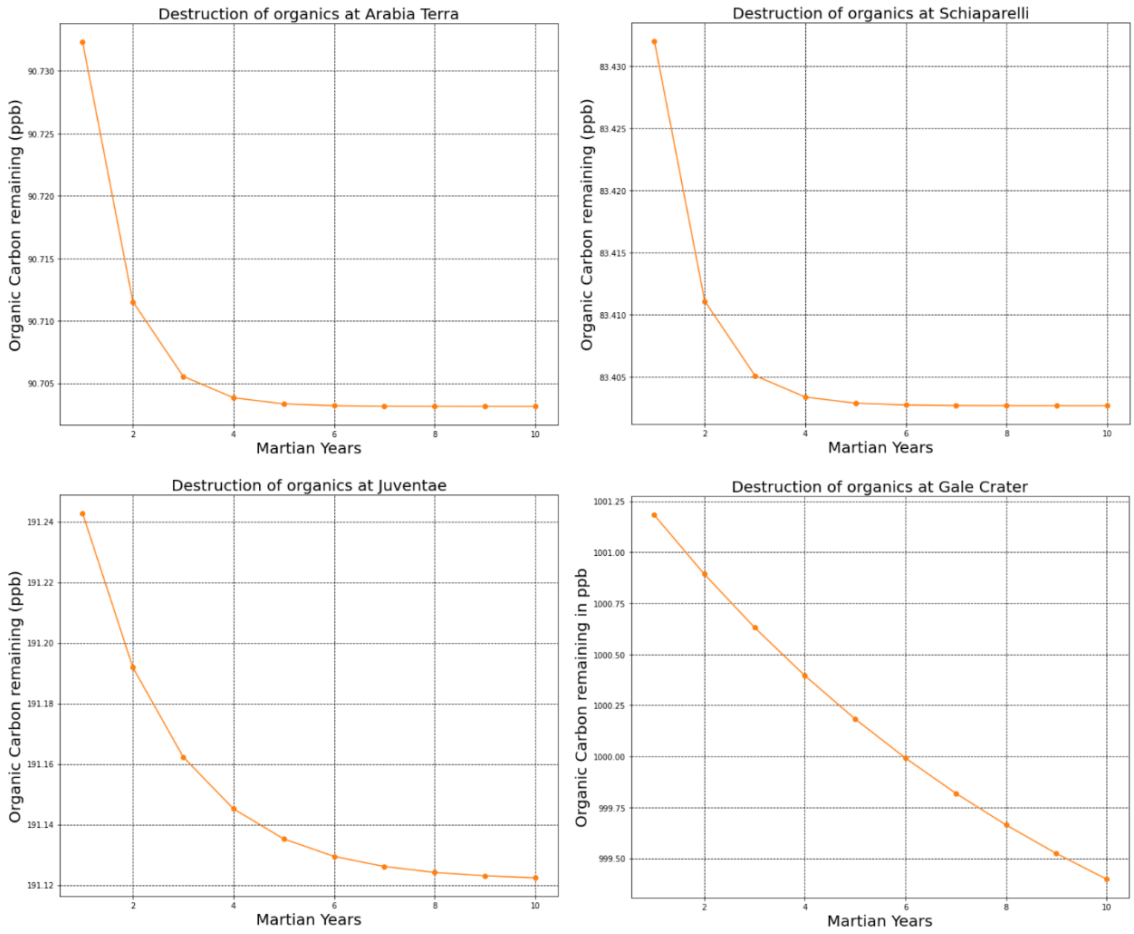

Figure 4.6: Organic Carbon remaining at 4 locations on Mars: Arabia Terra, Schiaparelli Crater, Juventae Chasma, and Gale Crater. These plots show rapid burial at sites like Arabia Terra, Schiaparelli Crater, and Juventae Chasma since MCD data indicates a dust deposition of > 20 µm per year. However, the plots show a slower rate of organic sequestration at Gale – this comes as a result of LOS-Ext studies showing us yearly dust deposition at Gale is 3.54 µm. Hence, the plot for Gale looks largely different from the others.

The organic carbon remaining value in the first three locations quickly asymptotes within 10 years – yielding ppb level concentrations of buried organic carbon (by mass). The yearly dust depositions at the sites retrieved from MCD data are very similar – greater than 15 µm. However, since our model used dust deposition from ground observation-based LOS-Ext studies to run the calculation for Gale crater, the results between Gale and the other sites appear to be vastly

different. The MCD data points to a yearly dust deposition rate of 31.8 µm which significantly disagrees with the values provided by LOS-Ext studies (3.54 µm).

Although considering a dust deposition rate of 3.54 µm / year if we run our model up to 50 Martian years, we get the result shown in Figure 4.7 which indicates burial of organic carbon can be achieved in a span of more than 50 Martian years.

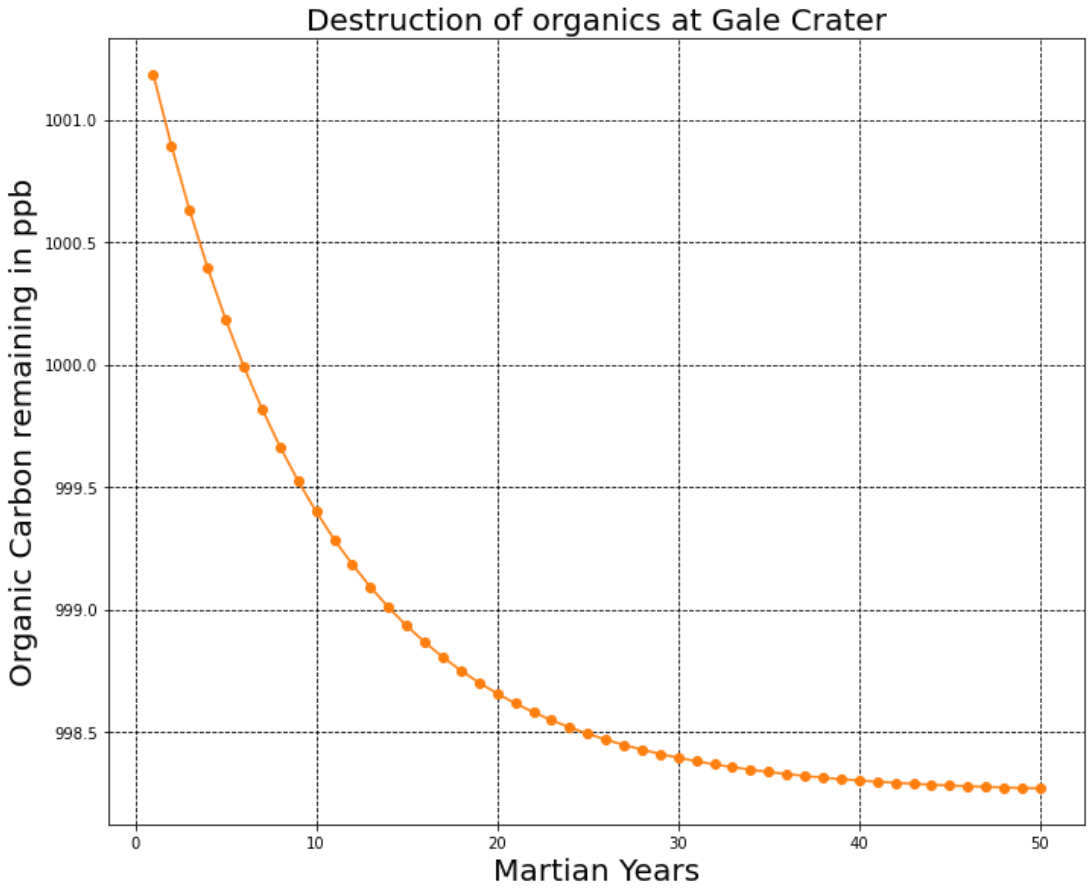

Figure 4.7: Model Result of Remaining Organic Carbon at Gale Crater with 3.54 µm /year dust deposition rate up till 50 years. The curve approaches an asymptote after 50 Martian Years showing organic carbon sequestration

The concentration of organics preserved in sedimentary rhythmites relative to dust mass was also calculated. The results of the same are presented in Table 4. Our calculations show that this is in the ppb range with Gale crater having a higher concentration of preserved organics in these rocks. The higher concentration of organics obtained at Gale can be explained by considering that lower amounts of dust deposition results in more organics per g of dust deposited. Whereas

for the other sites investigated using the much higher values of MCD dust deposition, and since we consider an even distribution of IDP organics across the globe, there is a higher amount of dust per layer, yielding a smaller organic to dust ratio.

Table 4: Concentration of organics preserved in sedimentary rhythmites relative to dust mass

Location	Dust Deposition (μm /year)	Initial Organics (10^{-6} g/m^2)	Initial Organics Concentration (ppb)	Final Organics Concentration (ppb)	Organics Concentration destroyed (ppb)	Organic Percentage (final to initial)
Arabia Terra	22.92 (MCD)	1.5243	83.432	83.405	0.026	99.96
Schiaparelli Crater	22.33 (MCD)	1.5243	83.432	83.402	0.029	99.96
Juventae Chasma	18.32 (MCD)	1.5243	191.24	191.12	0.12	99.93
Gale Crater	3.54 (LOS-Ext)	1.5243	1001.18	998.27	2.91	99.71

Our calculations also show that a significant fraction of the organics can be preserved in sedimentary rhythmic structures (approximately 99%). If we consider the data from the MCD to be valid, sites like Arabia Terra will sequester organic carbon at a faster rate due to the high dust deposition rate. However, the high dust deposition rate will also lower the total organic matter to dust ratio. Hence our results for these sites show a lower ppb concentration. A concentration of this ppb range might not be detectable by current methods of organic detection. In contrast, Gale crater does efficiently bury IDP organics within 50 Martian years despite having a low dust deposition rate of 3.54 μm per year (Figure 4.7).

In our model's UV photolysis calculations, we have considered the UV/CH_4 model detailed in Schuerger et al. (2012) where organic matter is converted to methane upon being irradiated by

UV. From the results obtained shown in Figures 4.6, 4.7, and Table 4, showing the rapid burial of IDP organics within sedimentary rhythmites, it can be concluded that a high fraction of the carbon in these IDPs get sequestered before they get a chance to convert to methane from effective UV interactions. If this is indeed the case, it can be further concluded that IDP organics are an unlikely source of methane on Mars.

It should also be noted that the absorption coefficient used in our calculations serves as a lower bound (for 150 μm) for UV shielding possible by Martian dust. In reality, Martian dust has a much smaller particle size which will absorb UV radiation more effectively than the numbers we have used. This might result in a significant difference in the rate of organic burial. Although our model gives us a lower bound for the dust shielding properties, we have not considered perchlorate salts which are known to further alter and degrade organic material mixed in the Martian soil.

4.2.1 Burial at Gale Crater (seasonal)

A seasonal degradation of organics at Gale crater was also calculated using the data from Moore (2019) for Mars Year (MY) 32. Figure 4.8 shows how organic degradation occurs during the year. It can be noted from Figure 4.8 that the destruction plot is not a straight line – this is due to brief periods of dust lifting as opposed to dust deposition during certain periods of the year. The degradation calculated is presented along with the diffusion rate calculated by LOS-ext studies (Moore, 2019) in Figure 4.8.

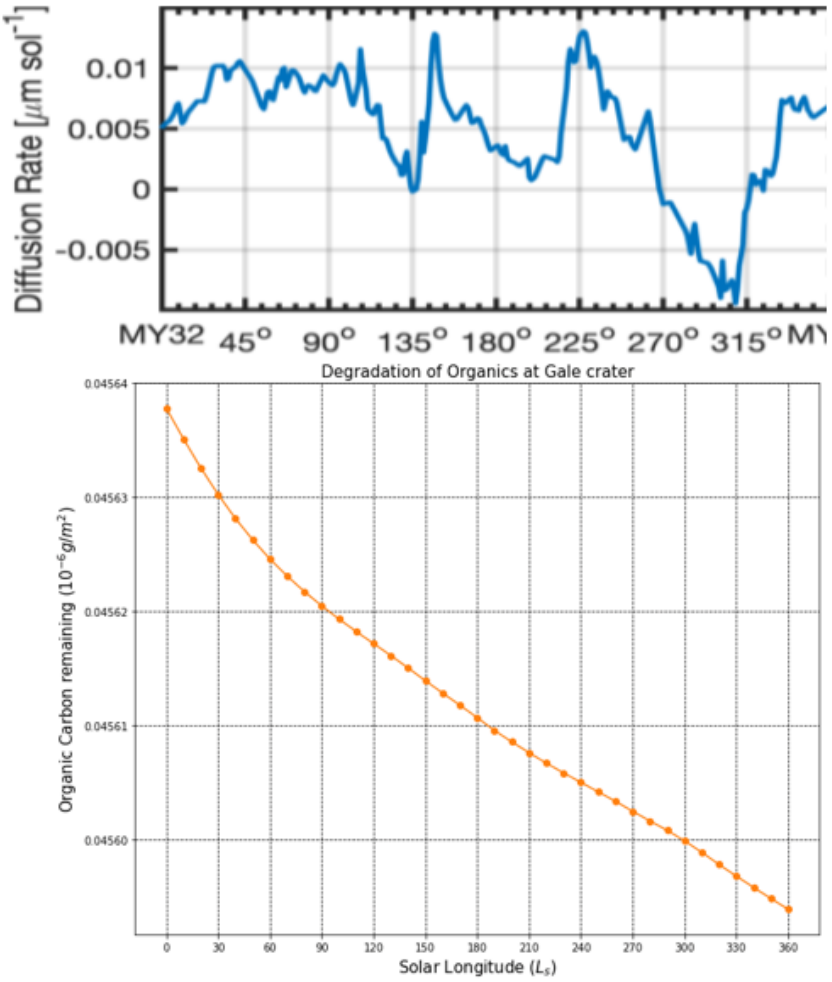

Figure 4.8: Seasonal Organic Carbon destruction at Gale crater (calculations done using LOS-Ext diffusion rates as a proxy for dust deposition) The orange curve shows the rate at which IDP organic carbon (measured in g/m^2) changes with Solar Longitude (time of year). The curve has some slight variations from a traditional decay curve which is a consequence of periods of dust lifting as opposed to dust deposition. The periods of dust lifting is represented by negative values in the diffusion rate plot in blue (from Moore, 2019) and coincides with the variations in the orange curve

From Figure 4.7 and Figure 4.8, one can conclude that although there is no IDP carbon burial happening throughout the year and the decay curve does not reach an asymptote, the cumulative effects of dust deposition over years lead to efficient preservation of IDP carbon.

4.2.2 Global Dust Deposition – Identifying dust sources and sinks from MCD Data

To gain a global understanding of dust deposition and dust transport on Mars, we undertook the exercise of calculating yearly dust deposition on a global scale. The plot presented in Figure 4.9 depicts regions on Mars that are relatively dustier compared to the rest of the planet. Dust deposition is high around the southernmost latitudes, close to the polar caps. This is in contrast to lower amounts of dust deposited in the northern most latitudes. Apart from this, there are two major regions of dust deposition noticeable from Figure 4.9 in the Northern and Southern hemispheres (marked by circles).

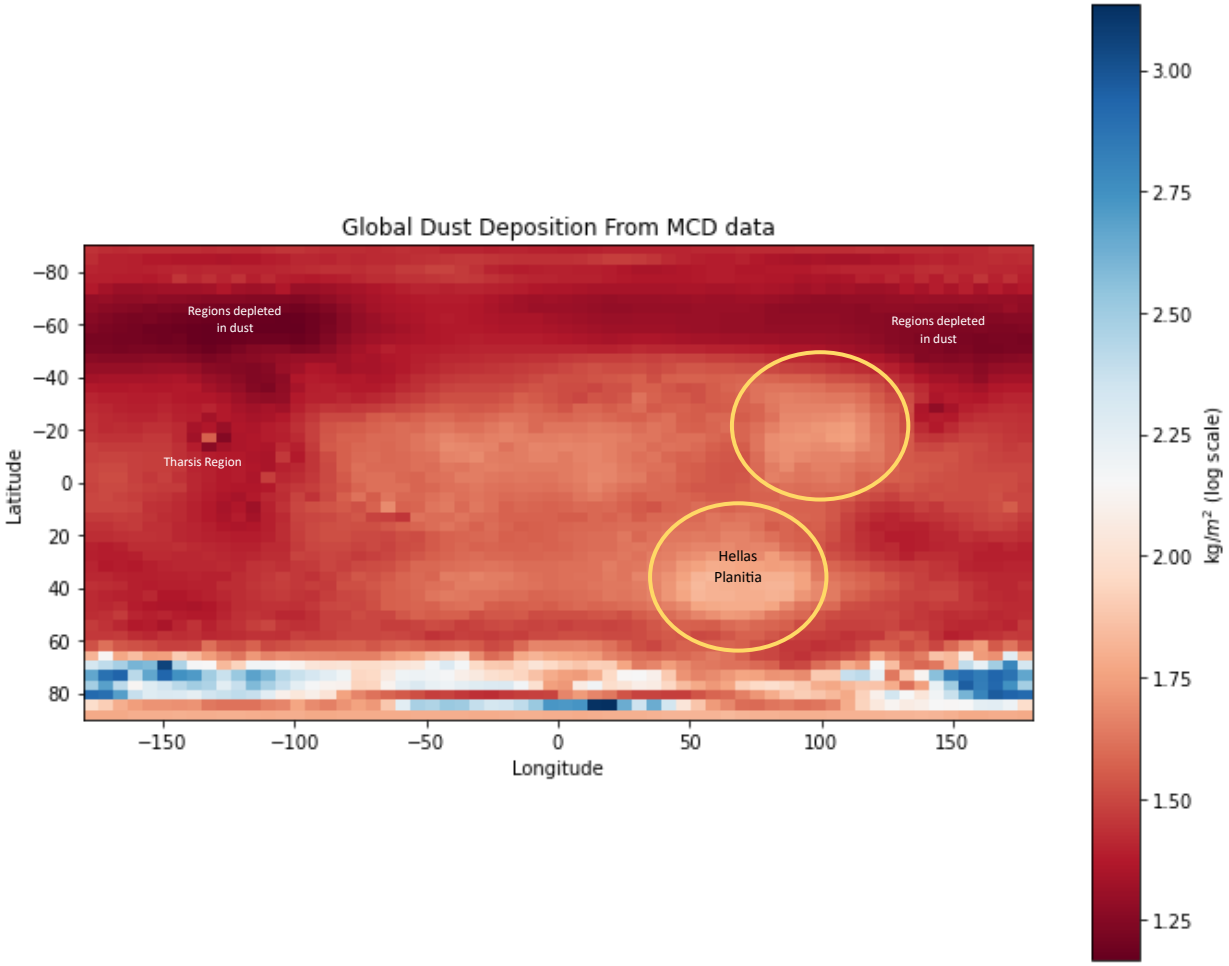

Figure 4.9: Global Dust deposition on Mars – calculated from Mars Climate Database (MCD). Dust rich regions are denoted by blue and lighter shades. Apart from dust rich regions near the South Pole, two regions stand out as being dust-rich on this map (circled)

The two circled equatorial to mid-latitude regions have a considerable dust deposition compared to the rest of the planet – one of them is a notable impact basin, Hellas Planitia which is approximately 7000 m deep. From the data in Figure 4.9, one can also notice a bright spot-on top of Olympus Mons, indicating reasonable amounts of dust accumulating at the caldera. The darkest regions of the map are present in the Northern Lowlands occurring between longitudes 70 W and 120 E approximately and around 60 - 70 degrees N where not much dust seems to get accumulated over the year.

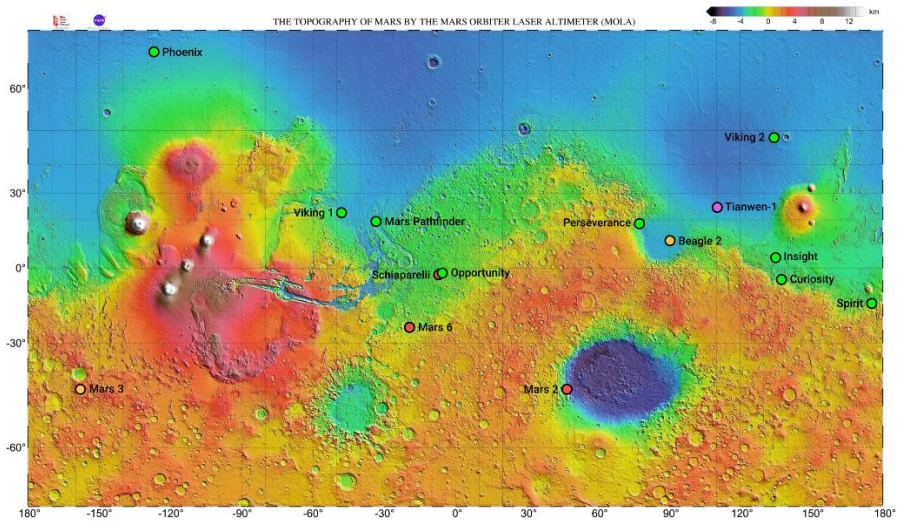

Figure 4.10: Topography Map of Mars by Mars Orbiter Laser Altimeter (MOLA) with various landing sites of spacecraft marked. Noticeable regions on this map include the Hellas Basin in the SH and the Tharsis region in the NH in addition to Northern lowland regions and Southern highland regions (Source: http://mola.gsfc.nasa.gov/images.html)

Figure 4.10 shows the landing sites of various spacecraft that have been sent to Mars over the years. Comparing Curiosity's landing site (Gale Crater) from Figure 4.10 to the map in Figure 4.9, one can infer that Gale is one of the reasonably dustier regions of Mars according to MCD dust deposition data.

It is interesting to note that the data provided by the MCD shows that all regions on Mars have a net positive dust deposition throughout the year. Reading the data presented in Figure 4.9, over the course of one Martian year, the net positive dust deposition globally also indicates that according to the MCD data, no sources of dust on the planet exist and all points are sinks for dust which contradicts mass conservation. This can only hold true if that massive amounts of dust are

being generated every year which is highly unlikely given our present understanding of the planet. The data represented in Figure 4.9 seemingly exaggerates the total dust deposition globally across Mars but gives an idea of the relatively dusty and less dusty regions of Mars.

To investigate further, we manipulated the MCD data to ensure the mass conversion of dust over one Martian year. This was done by multiplying each grid cell by the corresponding amount of dust per unit area according to MCD. These values were then summed up over all grid-cells. Finally, the value of each grid-cell was manipulated to ensure the total dust (globally) sums to a zero. This gave us a grid-space containing both positive and negative dust deposition values. The results of this exercise are shown in Figure 4.11.

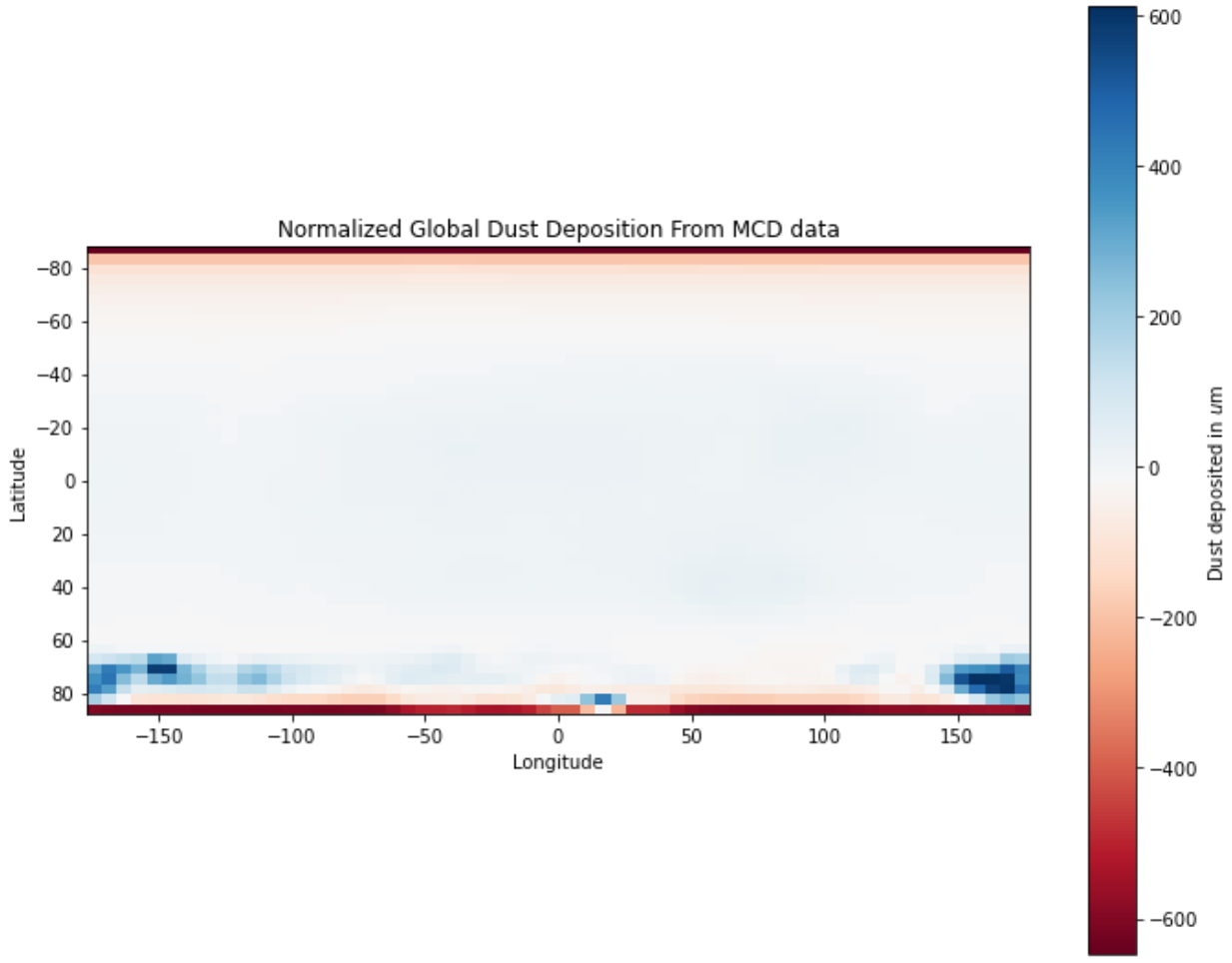

Figure 4.11: Normalized Dust Deposition on Mars after manipulating MCD dust deposition data shown in µm. Previously noted regions in the South Polar regions continue to be the richest in dust globally. Most regions have zero to 200 µm dust deposition

Figure 4.11 shows that after normalization, most of Mars has a dust deposition in the range of approximately 0 to 200 µm. The north polar regions are noted to be dust sources and there is significant dust deposition at latitudes 60 to 80 in the south polar region. It should be noted that Figure 24 shows dust deposition in µm and is not a log plot like that shown in Figure 4.9 and hence, these two heatmaps should not be directly compared.

This modified data was then applied to the IDP organics burial model and a global map of buried organics was obtained. Since negative dust deposition will not result in organic burial, only regions having positive dust deposition were considered in this exercise. Average ground temperatures derived from TES were used for calculating the organic burial similar to the individual cases presented earlier. Computations were made for a time period of 10 Martian years to indicate regions where IDP organics are more effectively buried (Figure 4.12).

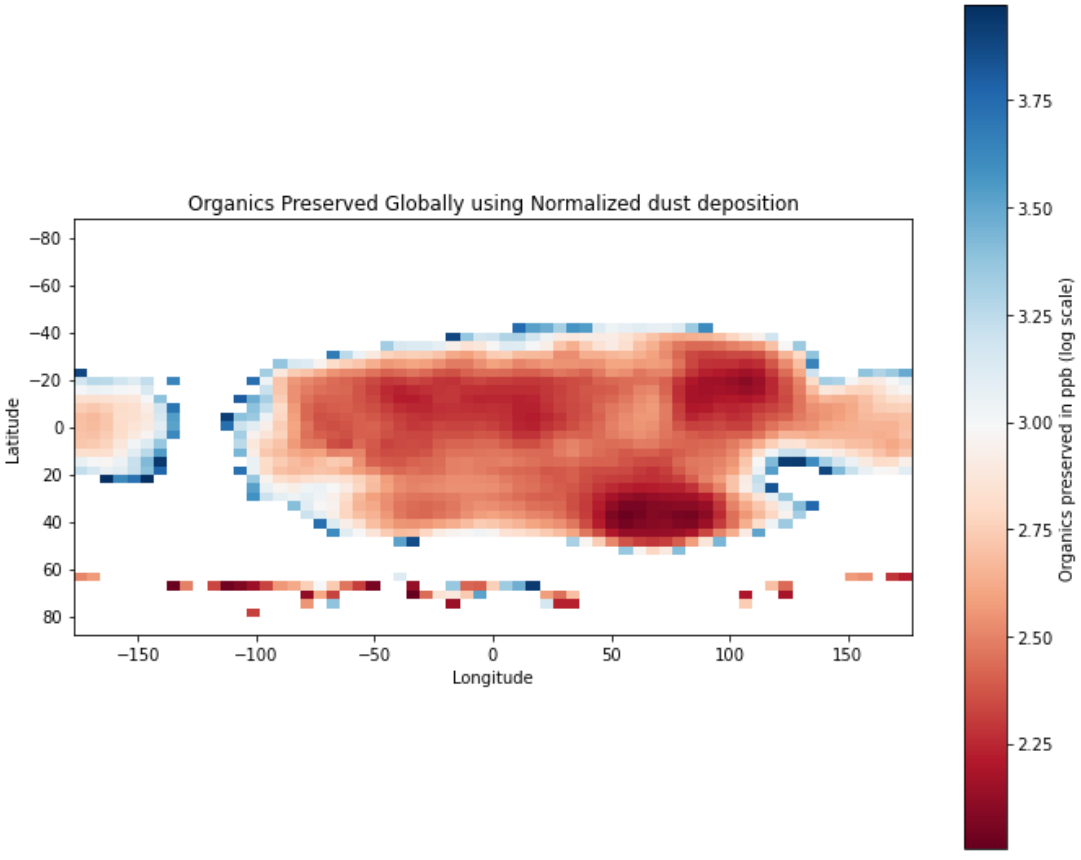

Figure 4.12: Organics preserved globally using normalized dust deposition plotted in log base 10. The blank regions of the map are regions with negative dust deposition, illogical organic concentrations (an upper limit of 104 ppb was implemented), and extremely low

concentrations (100 ppb). This map shows IDP organics preservation (with positive organic carbon concentrations less than 104 ppb) on Mars over the course of 10 Martian years

The map presented in Figure 4.12 indicates regions effective in burying IDP organics across Mars. Data presented does not show regions with absurdly high amounts preserved IDP organics since this is most likely a consequence of gaps in UV and temperature data at these regions (mostly in northern and southern polar regions), the model calculations hence result in large IDP lifetimes and subsequently organic concentrations greater than 10^4 ppb range. These high concentrations calculated by our model could also arise from regions with miniscule dust deposition and hence enormous values for organic concentration. In order to align the model results with our present understanding of the dust-rich environments on Mars and to draw more lucid, detailed conclusions from the calculated results, extremely high and low concentrations have not been plotted on the map. Comparing Figure 4.12 with Figure 4.9, it is interesting to note that the two mid-latitude regions circled as dust rich in Figure 4.9 have some of the lowest concentration of buried IDP organics in Figure 4.12. This again can be explained in a manner similar to the individual site results where Gale crater had a higher organic to dust ratio owing to lower amounts of dust deposition considered at Gale and our model produced significantly lower organic concentration values at relatively dustier places like Arabia Terra. It should be noted that all the sites studied individually in the previous section are part of the data presented in Figure 4.12 allowing us to conclude that these sites are indeed good candidates compared to other places on Mars for studying organics buried in rhythmic sedimentary rocks.

From Figure 4.12, Medusae Fossae region (MFF) (centered around 3.2 S and 163.0 W) is another good candidate for preserving IDP organics within rhythmites. Lewis and Aharonson (2014) have also listed MFF as regions showcasing rhythmic sedimentary rocks. The geologic origins of deposits have been a subject of debate within the scientific community with pyroclastic deposition being one of the leading theories. Given our modeling results, we can conclude that the stratigraphy observed at MFF could be partially attributed to aeolian dust deposition.

4.3 Discussion

4.3.1 Sequestration of IDP Organics on Mars – sites of interest for further exploration

The individual sites selected for our analysis – Arabia Terra, Schiaparelli Crater, Juventae Chasma, and Gale crater effectively preserve organic matter delivered on the surface through IDPs in sedimentary rhythmites within a span of approximately 50 Martian years.

Our results for Gale crater show the highest concentration of organic carbon to dust (approximately 998 ppb). This is a direct result of thinner dust deposition (from LOS-ext studies) compared to the other locations explored. Although sedimentary rhythmites have been discovered at Gale crater where Curiosity is stationed, Curiosity is yet to analyze such rock types for organic content. However, parallels between our result and chlorinated organics discovered in mudstones by Curiosity at Gale crater can be drawn. Chlorinated organics in the form of di-chloro alkanes and chlorobenzene have been discovered in the Sheepbed mudstone (at Gale crater) by the Sample Analysis on Mars (SAM) instrument using GCMS and Evolved Gas Analyzer (EGA) in 150 to 300 ppb concentrations by weight (Freissinet et al., 2015). Although this reported concentration is in agreement with the order of magnitude of our calculated concentrations, mudstones are compositionally and structurally different from sedimentary rhythmites. Mudstones at Gale crater formed in lacustrine (lake) environments and analysis of these samples showed a 20% wt of smectite clays (structured as 2:1 tetrahedral and octahedral layers). Hence, these organics at Sheepbed mudstone were preserved during a period on Mars when lakes were present (Noachian or Hesperian). The sedimentary rhythmites in our investigation are hypothesized to have formed from the gradual airfall of dust particles suspended in the Martian atmosphere in the Amazonian period (Lewis and Aharonson, 2014). Martian dust on average is not enriched in clays and primarily consists of basaltic minerals. Owing to different mineralogical compositions and periods of formation, the method of preservation of both these organics are expected to be different. There is no detectable evidence that the organics discovered in the Sheepbed mudstone are indigenous to Mars – these organics could very much be IDP organics delivered on Mars in the Noachian and Hesperian periods. Thus, given the context of this in-situ discovery of organics, we can say it should be possible to detect IDP organics in similar concentrations embedded within sedimentary rhythmites.

In the future, if one were to design a mission capable of detecting organic compounds in sedimentary rhythmites, what specific terrains are most likely to have preserved IDP organics effectively? From our results, it is easy to be misled into thinking that all terrains present in these regions will contain a stratigraphic section of sedimentary rhythmites. This is not true given the diversity of terrains present on Mars which was not considered in our modeling. In addition to the diverse terrain present across Mars, extreme wind processes such as dust devils are known to lift dust from the surface – it is highly likely that this process also lifts IDP particles containing organics with it. One can further argue that this will eventually result in an uneven surface load of initial IDP organics at different regions on Mars. Moreover, the denser IDPs are less likely to be lifted and aeolian processes will result in IDPs getting concentrated into specific sites. Studies at Mars analog sites on Earth have identified settings where dense micrometeorites can be concentrated and fossilized (Tomkins et al., 2019):

1) at the base of dune sequences

2) at gravel-enriched layers resulting from wind-related processes,

3) inside cracks of hard surfaces

Analog studies carried out by Tomkins et al. (2019) ascertained that sand dune bases have a better potential to preserve micrometeorites on Mars. Thus, we can conclude that only select terrain structures such as sand dune bases present at the regions investigated will be rich in IDPs and hence a higher concentration of preserved organics.

Another inference one can draw from the results presented in Figures 4.6, 4.7 and Table 4 is the rapid burial of organic carbon at these sites resulting in ineffective organic carbon to methane conversions. In other words, the organic content in surface IDPs is buried within sedimentary rhythmites before all their carbon content is converted into methane. This can further imply that surface IDPs do not contribute to the methane budget on Mars. The Moores-Schuerger model which assumes 100% IDP carbon to methane conversion reported a methane production of 2.2×10^{-9} kg m^{-2} yr^{-1} (Moores and Schuerger, 2012) and is consistent with observations of a 11 ppb background level of methane (Atreya et al., 2007; Schuerger et al., 2012). Our model indicates that 99% of the carbon can be preserved in sedimentary rhythmites. Thus, adding both these model results, we predict that IDPs in fact contribute 0.1 % of 2.2×10^{-9} kg m^{-2} yr^{-1} methane to

the Martian atmosphere. We further predict that this should be consistent with a methane background of 0.011 ppb on Mars which is below the detection limits of TGO. Furthermore, following the results of this work, IDP organics interactions with UV radiation cannot explain the seasonal varying level of methane in the Martian atmosphere reported previously by (Geminale et al., 2011; Webster et al., 2018).

Global dust deposition maps generated from the MCD data show a net positive deposition across all latitudes and longitudes on Mars. South polar regions in addition to some equatorial and mid-latitude regions depicted in Figure 4.9 are dust rich on Mars. The high dust index in the southern polar regions is in stark contrast with that observed in the northern polar regions. At the point of writing no possible explanation can be provided for this dichotomy. From Figure 4.9, we note that the dust deposition data retrieved from the MCD is greatly exaggerated. MCD data fails to point toward sources of dust on Mars. Despite this caveat, since there are no other available data for global dust deposition, a normalized dust deposition was used to further calculate global preservation of organics on Mars. Normalizing the dust deposition to ensure a total dust mass of zero yearly is most likely an approximation for the global dust deposition which in all likelihood depends complex dust cycles and processes that might be at play. In other words, further analysis and calculations might be required to more accurately predict a global dust deposition index on Mars from the MCD data. The modeling results hence obtained are yet once again presented in Figure 4.13 this time overlayed with a Mars map featuring key regions of discussion (e.g., Hellas and Isidis Planitia) on Mars. The regions favoring IDP organics preservation on Mars include but is not limited to Arabia Terra, Isidis and Chryse Planitia. However, it should be noted that this overlaying was done manually and hence is only presented to gain a general insight into the broad regions favoring the IDP organics burial mechanism modeled in our studies.

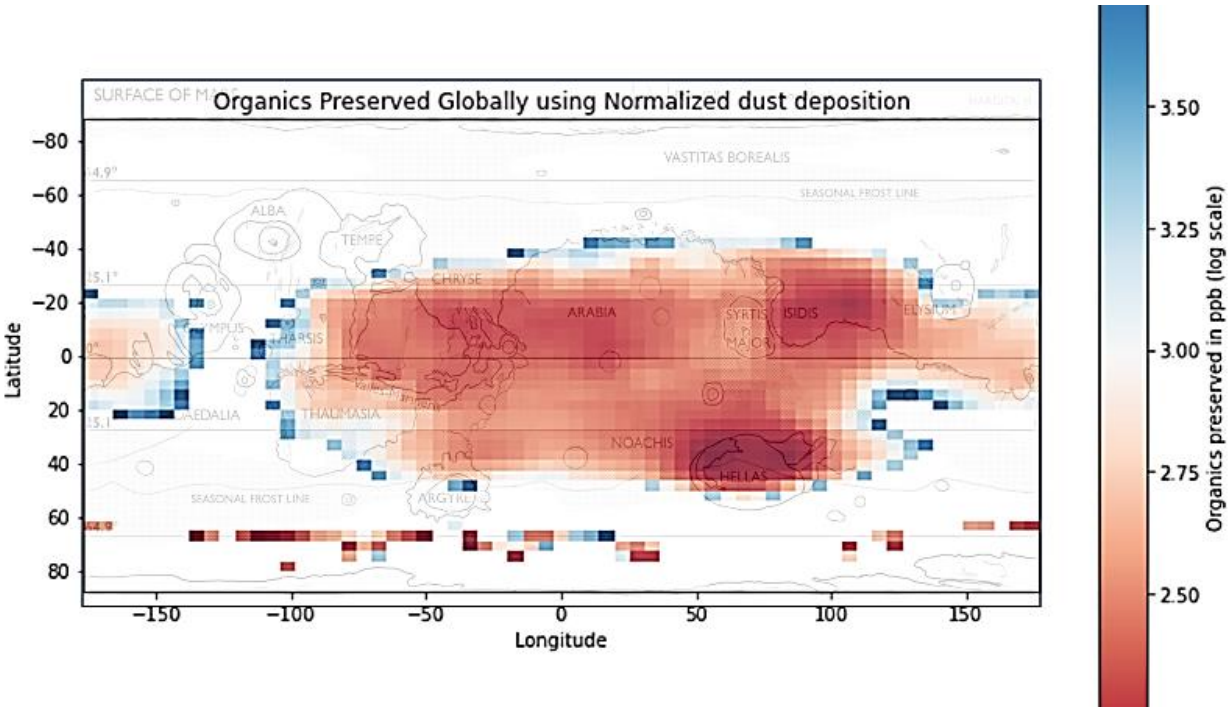

Figure 4.13: Results from figure 4.12 overlayed on a Mars Map showcasing well-known features and regions of Mars (Map from http://planetarymapping.elte.hu/blank-map-of-mars/)

4.4 Sources of Errors and Assumptions

Our model made several assumptions that should be considered while discussing these results. Since perchlorates have been independently discovered at two landing sites (Phoenix and Curiosity) (Hecht et al., 2008 and Glavin et al., 2013), it is likely that the surface material at other locations on Mars also contains these oxidizing agents leading to further structural damage of organic compounds at these sites.

There is a remarkable discrepancy between the dust deposition calculated from MCD data and that from LOS-ext studies in the case of Gale crater. Upon normalizing the dust deposited globally, an approximate dust deposition of 8.1 μm was calculated for Gale's coordinates which is within order of magnitude agreement with the 3.54 μm value obtained from Moore (2019). However, there is no way to validate the actual dust deposition at other places on Mars unless more accurate climate models are devised or further global or local observations are made by instruments.

The UV flux considered for our modeling assumes that each point on the surface receives unobstructed UV radiation which is not the case in reality. Simply put, our model provides the same treatment to a point inside a crater rim and a point outside – it does not take into account the obstruction to solar radiation from cliff faces or other surface geometry features. Such features can further reduce the incident UV radiation in crevices, leading to more effective preservation of IDP organics.

Modeling results from Flynn (1996) which provided a detailed analysis of IDP particle sizes, fraction of unaltered and unmelted carbon, along side total predicted IDP flux were used in the IDP burial model calculations. Although detailed, Flynn (1996) relied on models created from terrestrial IDP fluxes. Flynn (1996) predicted a mass flux of 1.2×10^7 kg/year for the surface of Mars. How does this compare with observations and studies to constrain IDP fluxes on Mars undertaken since 1996? Modeling studies carried out from MAVEN observations of meteoritic layer consisting of Mg^{2+} ion in Mars' atmosphere report a flux of 2-3 tons of IDP material per sol (Crismani et al., 2017). Flynn's IDP fluxes translate to approximately 34 tons of IDP material per sol. Crismani et al. (2017) also mentions that the values obtained from MAVEN analysis of 3-2 tons per sol are a lower bound considering scaled measurements of IDP fluxes observed on Earth. Hence, Flynn's numbers which have been used to model organic burial in this thesis could very much be an upper bound for IDP fluxes and as an extension, IDP carbon reservoirs on Mars. However, if one were to consider the numbers reported in Crismani et al. (2017) as an absolute measure of IDP fluxes received on Mars, the organic carbon concentrations obtained in this work can be scaled down by a factor of 10 to take into account this change in IDP input flux.

Dust lifting was not considered in our model for two main reasons:

1. Dust lifting data for different Martian regions is not readily available in databases like the MCD. Dust lifting varies seasonally and hence the total dust deposited was taken into account for each Martian year
2. Dust lifting could be predicted from available data but that would require additional and extensive modeling which were out of scope for this project.

Chapter Five: LIF Spectroscopy of Tryptophan in JSC-1 Mars Matrix

In this section we explain the methodology, document the results and discuss implications of the findings from the experimental project on detectability of L-Tryptophan through UV LIF spectroscopy when it is mixed in a JSC-1 Mars simulant soil matrix.

5.1 Materials and Methods

5.1.1 Experimental Apparatus – 266 nm YU LIF Instrumentation

The experimental component of this thesis consists of using LIF spectroscopy. The experiments were conducted at the Planetary Exploration Instrumentation Laboratory (under Professor Michael Daly) at York University under the supervision of Elizabeth Lymer. The lab is equipped with a UV Raman instrument utilized a 266 nm laser (peak of Tryptophan excitation), a diffraction grating, and an iCCD camera (cooled to -35 C) to obtain the results presented. A schematic diagram of the same can be seen in Figure 5.1.

Specifically for our measurements, a slit opening of 30 μm and a diffraction grating of 600 lines/mm was used for the measurements.

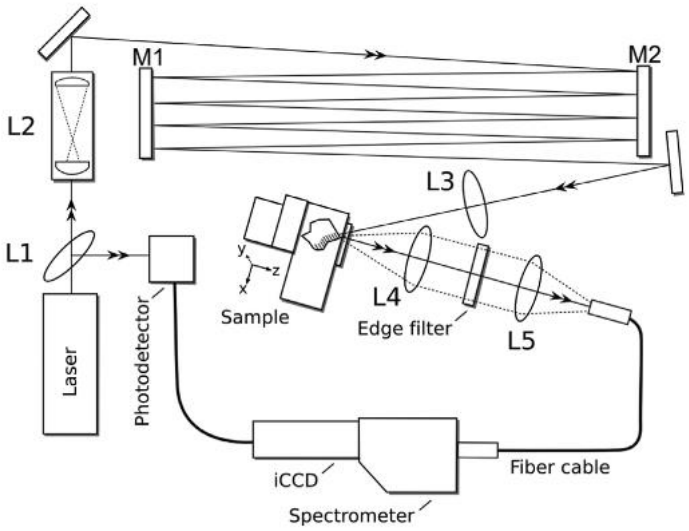

Figure 5.1: 266 nm Raman spectrometer instrument diagram (Source: Eshelman et al., 2014)

The light from the laser reaches L1 where a fraction of light triggers the photodetector. The rest of the laser beam is expanded in L2 and directed to the sample stage with the use of multiple mirrors (M1 and M2) and lenses (L3) arranged as shown in Figure 5.1. The scattered light after

interaction with the sample is collected with lens L4, L5 along with an edge filter and then later sent to the spectrometer through a fiber cable (also shown in Figure 5.1) for analysis. Spectral analysis was conducted using the Solis software (https://andor.oxinst.com/products/solis-software/). This combined instrument setup is henceforth referred to as YU LIF instrument.

The laser component of the instrument was first aligned to ensure the light path of the laser beam follows that of Figure 5.2. This is followed by calibrating the instrument with a Hg-Ar lamp which has a well-studied characteristic spectral signature. The x axis is calibrated according to standard specifications provided by the lamp manufacturer (example: https://www.newport.com/p/6035). Figure 5.2 below shows the calibration spectrum obtained on the day of data collection.

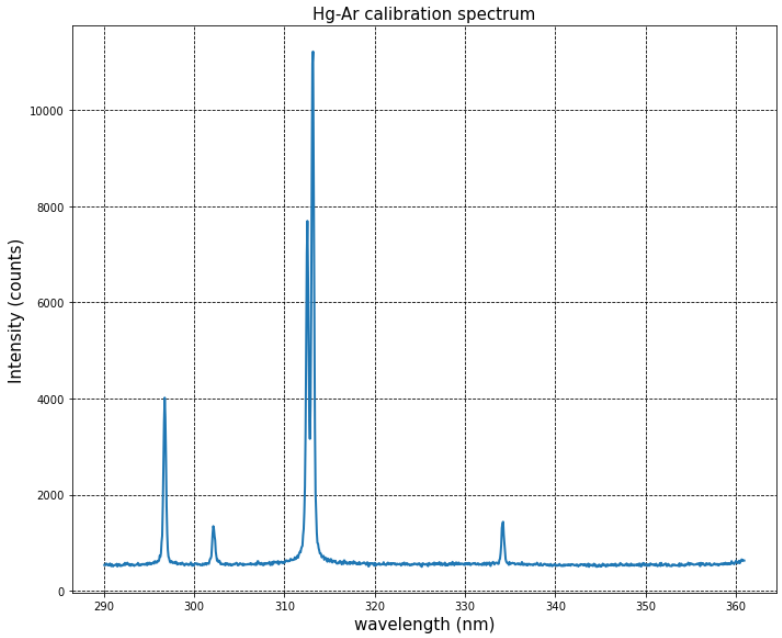

Figure 5.2: Calibration spectrum for Hg-Ar lamp

Instrument background noise was collected and was auto subtracted from subsequent measurements made. No separate background subtraction was necessary on the data files generated.

5.1.2 Experimental Matrix

The aim of this experiment was to investigate detectability of L-Tryptophan mixed with JSC-1 Mars simulant soil. The experimental matrix was designed to incorporate and eliminate potential

contamination sources. JSC-1 Mars simulant soil has a significant water and organic content. Martian soil and dust in contrast is thought to be sterile and severely lacking in water content - the Viking experiments reported only a 0.1% - 1% wt of water evolution when Martian soil was heated to 500 C). In order to ensure that our samples mimic that of the Martian environment as closely as possible (provided there are buried organics) and to ensure lucid interpretation of the results obtained, the following steps were undertaken for JSC-1 Mars:

1. JSC-1 Mars was crushed with a mortar and pestle and sieved to a particle size of <350 um to ensure homogeneity to a certain degree in addition to being compatible with the spot size of the laser being used
2. A part of the sieved JSC-1 Mars was baked at 400 C for four hours loosely wrapped (to ensure escape of water and CO_2) in aluminum foil to remove any organic and water content from the soil. This is done to further control our measurements and to ensure that no other organic fluorescence signal interferes with the Tryptophan signal we are trying to detect
3. A part of the crushed, un-sieved JSC-1 Mars was baked at 400 C for four hours, loosely wrapped in aluminum foil

In addition to this, the following protocols were followed throughout the experiment duration to ensure minimum contamination from external environments:

1. All surfaces were wiped down with alcohol to sterilize the surfaces we were working on
2. Aluminum spatulas were baked at 400 C for four hours along with the JSC-1 Mars
3. Glassware (rods and beakers) were ashed at 140 C for two hours
4. Aluminum foil weight boats were prepared by ashing pieces of folded aluminum foil at 400 C for 4 hours – this served as non-contaminated stations where samples were prepared and were covered and stored overnight

The oven used for baking the apparatus and JSC-1 Mars is a Paragon SC2 Sentry Xpress Oven operated at 120 volts and 20 Hz. The oven is equipped with a ceramic fiber firing chamber and the exterior consists of a steel casing. The oven can be programmed to fire at specific temperatures for set durations of time.

The experimental matrix was designed to have a combination of blanks consisting of JSC-1 Mars (crushed, non-crushed, sieved, non-sieved, baked, non-baked, with methanol, without methanol). Samples and blanks were placed in an aluminum cup after preparation. The samples consisted of:

a) Pure Tryptophan
b) 50 % Tryptophan: JSC-1 Mars
c) 50 ppm concentration of Tryptophan mixed with crushed, sieved, and baked JSC-1 Mars
d) 100 ppm concentration of Tryptophan mixed with crushed, sieved, and baked JSC-1 Mars

50 and 100 ppm were chosen values since they are the smallest attainable concentrations which can mimic possible IDP organic concentrations in sedimentary rhythmites. These are detailed in Table 5. An additional measurement of an empty aluminum cup was also made to test for aerosolized organic molecules which could contribute to contamination.

Table 5: Experimental Matrix showing sample space along with blanks

BLANK / SAMPLE	PICTURE	COMMENTS
JSC-1 Mars		JSC-1 Mars unaltered - contains organics and moisture content One can observe coarse grains in the sample
JSC-1 Mars (CNSNB)		JSC-1 Mars crushed with a mortar and pestle
JSC-1 Mars (CSNBM)		JSC-1 Mars crushed with mortar and pestle and sieved through a shaker
JSC-1 Mars (CSBNM)		JSC-1 Mars crushed, sieved, and baked at 400 C for 4 hours but not mixed with methanol
JSC-1 Mars (CSBM)		JSC-1 Mars crushed, sieved, and baked at 400 C for 4 hours, mixed with methanol - methanol might add an additional fluorescence signal
Tryptophan mixed with JSC-1 Mars (100 ppm concentration)		Tryptophan mixed with crushed, sieved, baked JSC-1 Mars at 100 ppm concentration with methanol
Tryptophan mixed with JSC-1 Mars (50 ppm concentration)		Tryptophan mixed with crushed, sieved, baked JSC-1 Mars at 50 ppm concentration with methanol
Tryptophan mixed with JSC-1 Mars (50% ratio)		Tryptophan mixed with crushed, sieved, baked JSC-1 Mars at 50% concentration with methanol
Tryptophan mixed with JSC-1 Mars (50%)		Tryptophan mixed with crushed, sieved, baked JSC-1 Mars at 50% concentration with methanol
Pure Tryptophan		Pure Tryptophan sample prepared with methanol

From Table 5, showing the experimental matrix, it can be noted that we have several blanks of JSC-1 Mars soil. The various parameters considered for the different blank preparations were crushing, sieving, and baking. Crushing and sieving were chosen since the particle size of the sample will interact differently with the 266 nm laser. Crushing will bring down the particle size – from Table 5, the unprocessed JSC-1 Mars has a coarse particle texture. Since the samples were prepared with methanol, some blanks were also prepared with methanol for ease of comparison between sample and blanks.

JSC-1 Mars Non-Crushed Non-Sieved Non-Baked (NCNSNB) – This is JSC-1 Mars that has not been altered by any procedures during sample preparation. The figure below shows the fluorescence spectra for this blank (NCNSNB or unprocessed JSC-1 Mars). The spikes visible in the spectra are possible instrument artifacts. The broad spectral curve faintly visible in Figure 5.3 is most likely due to organic content present in JSC-1 Mars and is observed to be very close to the noise level.

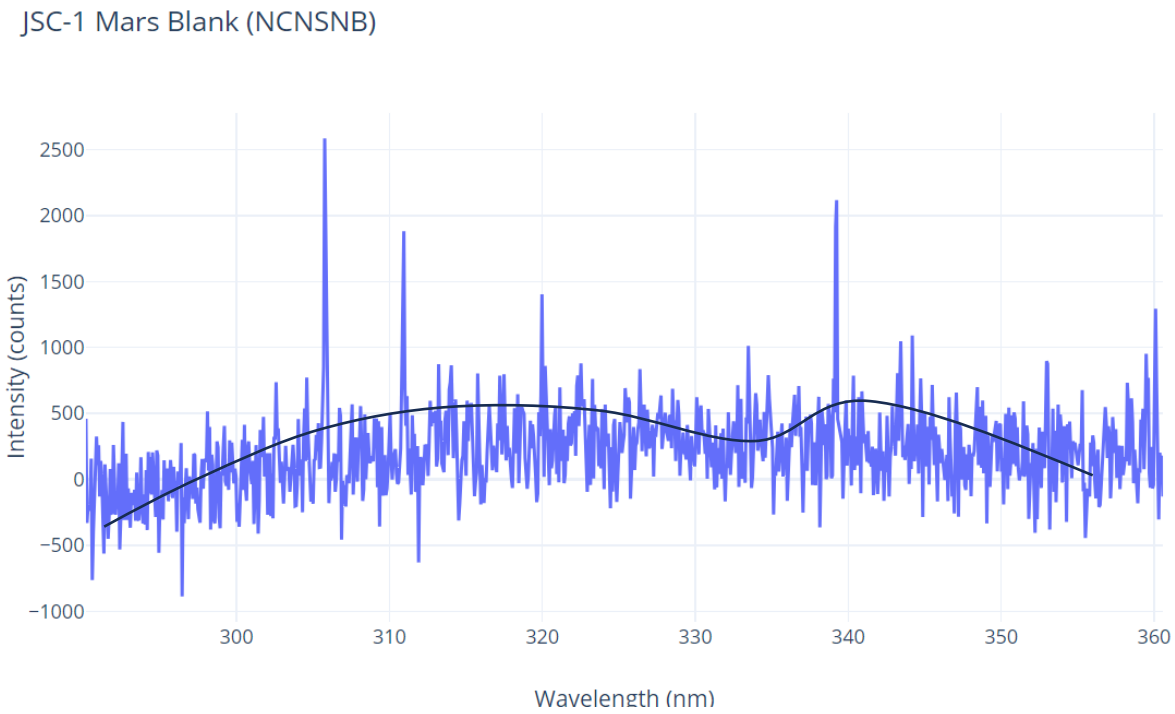

Figure 5.3: JSC-1 Mars unprocessed blank fluorescence spectra excited at 266 nm. The spikes visible are hot pixels or instrument artifacts. A broad spectral signature is faintly visible probably caused by organics present in JSC-1 Mars.

JSC-1 Mars Crushed Non-Sieved Non-Baked (CNSNB) – This blank was crushed with a mortar and pestle but no other procedures were conducted on the blank. The figure below shows the spectra obtained for this blank.

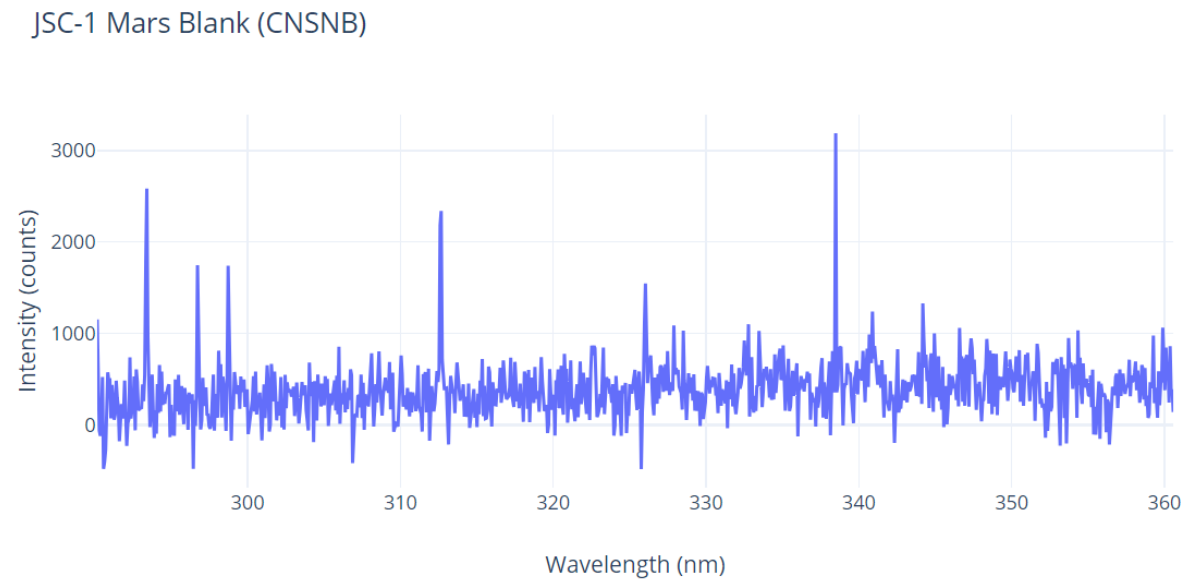

Figure 5.4: Crushed JSC-1 Mars measured using 266 nm YU LIF instrument set up. No characteristic organics detected here, only instrument artifacts. Intensity is roughly constant over wavelength. Indicating that spectra obtained in Figure 5.3 could be due to coarse particle sizes.

JSC-1 Mars Crushed Sieved Non-Baked with Methanol (CSNBM) – This blank was sieved to a particle size < 355 µm using a shaker after being crushed with a mortar and pestle. The sieved JSC-1 Mars was further mixed with methanol before measurement. The figure below shows the fluorescence measurement obtained for this blank.

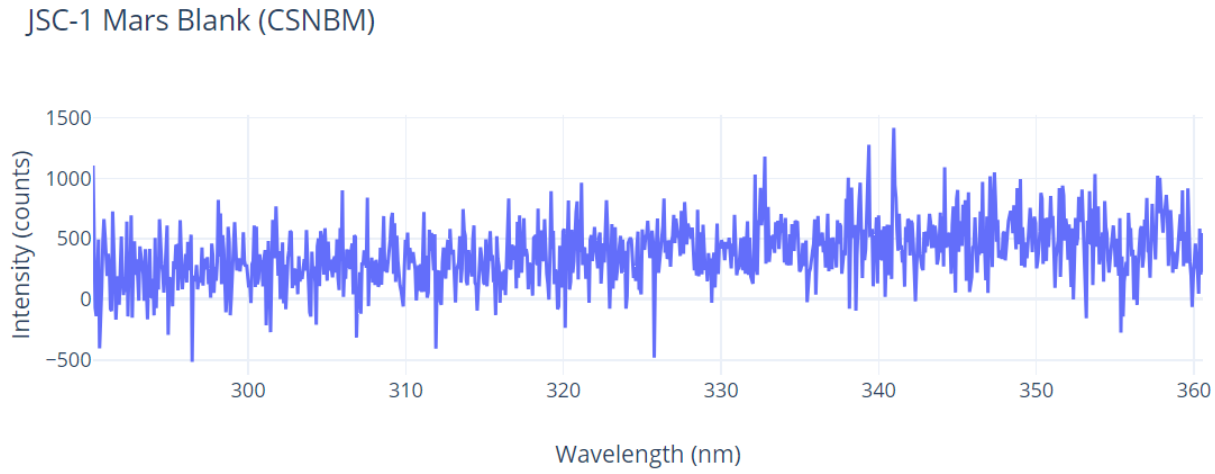

Figure 5.5: Crushed, Sieved, Non-baked JSC-1 Mars prepared with methanol

JSC-1 Mars Crushed Sieved Baked with Methanol (CSBM) – This blank was baked at 400 C for 6 hours to attain a blank that is not contaminated by any other organics. In addition to this, baking also removes any moisture present in JSC-1 Mars. This was then mixed with methanol and left to dry overnight before measurements were made. The figure below shows the fluorescence spectra of this blank. It should be noted that the spectra obtained for this blank is less noisy than the ones presented in Figures 5.4 and 5.5.

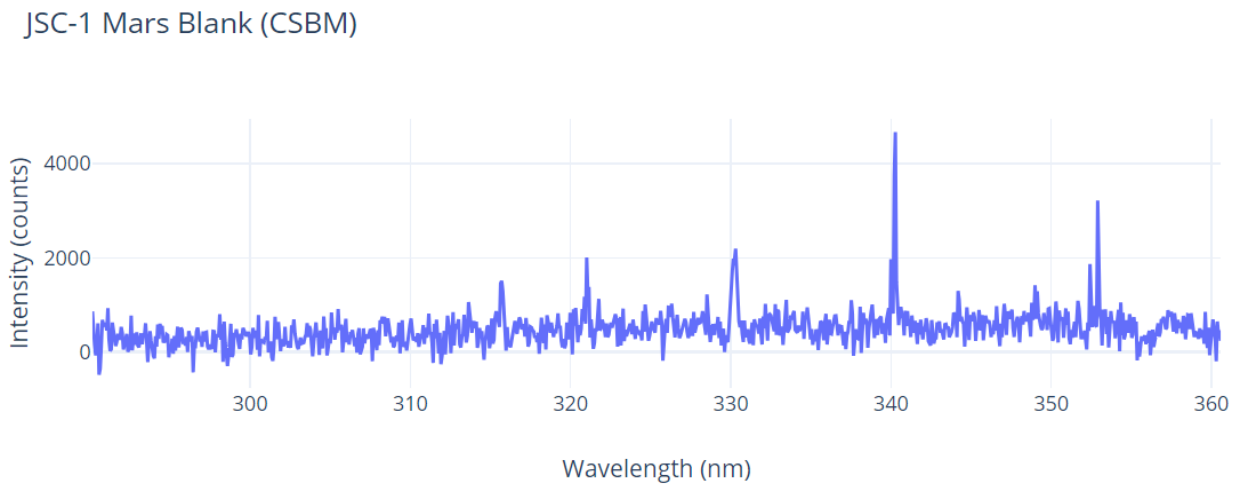

Figure 5.6: Crushed, Sieved, Baked JSC-1 Mars prepared with methanol. No characteristic organic or mineral component is visible. The spikes indicate instrument artifacts.

5.1.3 Sample Preparation Protocol (Manual Mixing)

L-Tryptophan used for this experiment was sourced from Sigma Aldrich (T0254). Samples of Tryptophan and Tryptophan mixed with crushed, sieved, and baked JSC-1 Mars were prepared by first weighing the quantities of Tryptophan and JSC-1 Mars to obtain the concentrations specified in the experimental matrix in Table 5. The following relationships were implemented to weigh out the substances for 50 ppm and 100 ppm samples:

10 g JSC-1 Mars ----------> 0.001 g Trp (100 ppm)

We weighed 30.03 +_ 0.01 g JSC-1 Mars and 0.0033 +_ 0.005 g Trp for our sample.

10 g JSC-1 Mars ----------->. 0.0005 g Trp (50 ppm)

We weighed 51.17 +_0.05 g JSC-1 Mars and 0.0027 g of Trp for our sample.

This was followed by first dissolving the measured Tryptophan with methanol (at least 20 ml) in a glass beaker, stirred manually with a glass rod. Once the Tryptophan is completely dissolved in the methanol, the measured JSC-1 Mars (CSB) is added to the beaker. Additional methanol is added to make the mixture that of a solution. A similar approach is taken with the pure Tryptophan sample. The glass beaker is then mixed thoroughly manually over a heating plate (at temperature 34 C). Once some of the methanol has evaporated due to the heat and the consistency of the sample reaches that of a slurry, the beaker is taken off the heat and left to dry overnight. To ensure homogeneity, before transferring the dried sample from the beaker to aluminum cups, the contents of the beaker is emptied into the mortar and pestle and crushed again.

Magnetic Stir-bar stirring

Ideally samples should be mixed with a magnetic stir-bar on a rotating plate to ensure more homogeneity. In the first half of our experiment, we decided to do an experimental tradeoff by opting for manual stirring – primarily due to the magnetic nature of JSC-1 Mars and the Martian soil which would have interfered with the magnetic stir-bar during mixing. Moreover, while removing the stir-bar from the sample, it can remove the magnetic particles, rendering our sample an inaccurate representation of the Martian environment. However, the magnetic particles also contribute to UV quenching making it harder for observations to be made. Because of this reason, the 50 ppm and 100 ppm samples were re-mixed with a magnetic stir-bar after one round of data collection.

Re-mixing was done by crushing the prepared samples in the mortar-pestle once again, followed by mixing the samples with methanol in a beaker and a magnetic stir-bar is added to the mix. The beaker is then placed on the same heating plate but this time it is automatically stirred at a rotational speed of 350 rpm (shown in Figure 5.7). The mixing was constantly monitored and the rotational speed was altered accordingly, the sample was not mixed at a rotational speed greater than 600 rpm at any given point. While stirring the 50 ppm sample using this method, we noticed that the magnetic particles were clumping in the beaker, resulting in inefficient mixing. Clumping was due to the 50 ppm sample being > 50 g in total mass. Mixing was continued for approximately 4 hours on the 50 ppm sample.

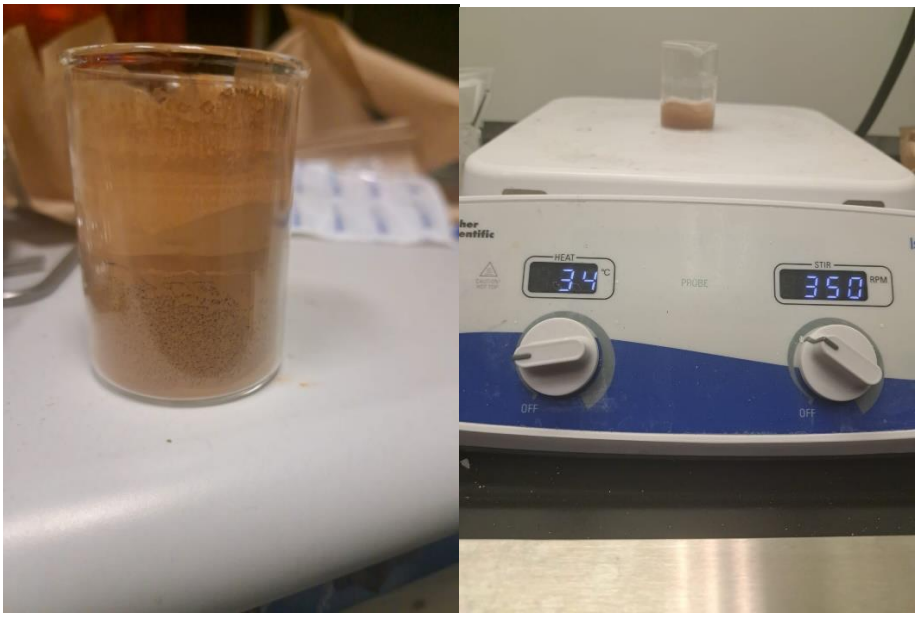

Figure 5.7: Mixed and dried 50 ppm sample (mixed with magnetic stir-bar) (left) and Mixing of 50 % Tryptophan: JSC-1 Mars sample on stirring and heating plate (right)

The 50% Tryptophan to JSC-1 Mars sample was prepared by only using this method. Similar to the previous procedure the samples were left to dry in the beaker overnight. The magnetic stir-bar was removed from the sample the following day after drying. In this instance, the sample was not re-crushed in the mortar-pestle, it was directly transferred to the aluminum cups and taken for LIF measurement.

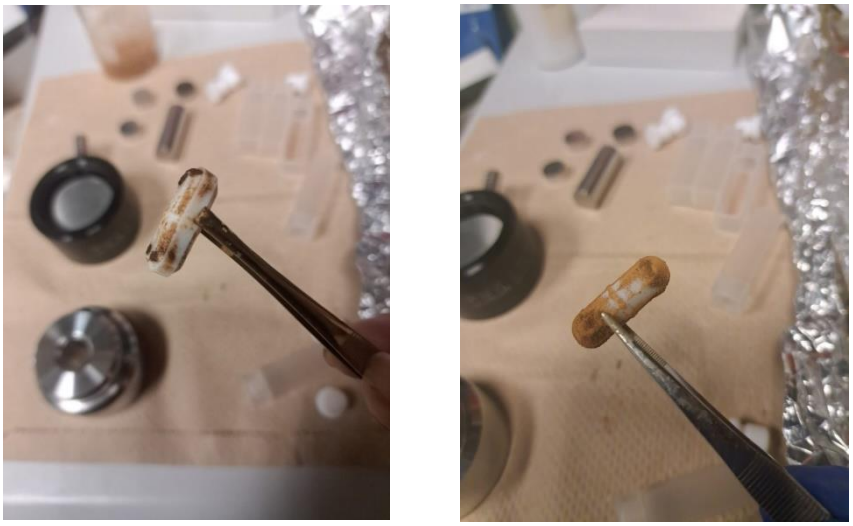

Figure 5.8: Images of magnetic stir-bar with magnetic particles from JSC-1 Mars - 100 ppm sample (left) and 50 ppm sample (right)

From Figure 5.8 above, one can notice the magnetic particles from JSC-1 Mars stuck on the stir-bar. However, not all magnetic particles were removed this way. Due to the large volume of JSC-1 Mars utilized to prepare samples in the ppm range, it was not possible to remove a significant fraction of magnetic particles from the sample. Although this does not offer much of an advantage over the manually mixed samples when it comes to potential UV quenching by the sample, mixing the sample using a magnetic stir-bar yields a more homogenously mixed sample.

5.1.4 Summary of Experiment

Figure 5.9 provides a flowchart summarizing the experiments conducted.

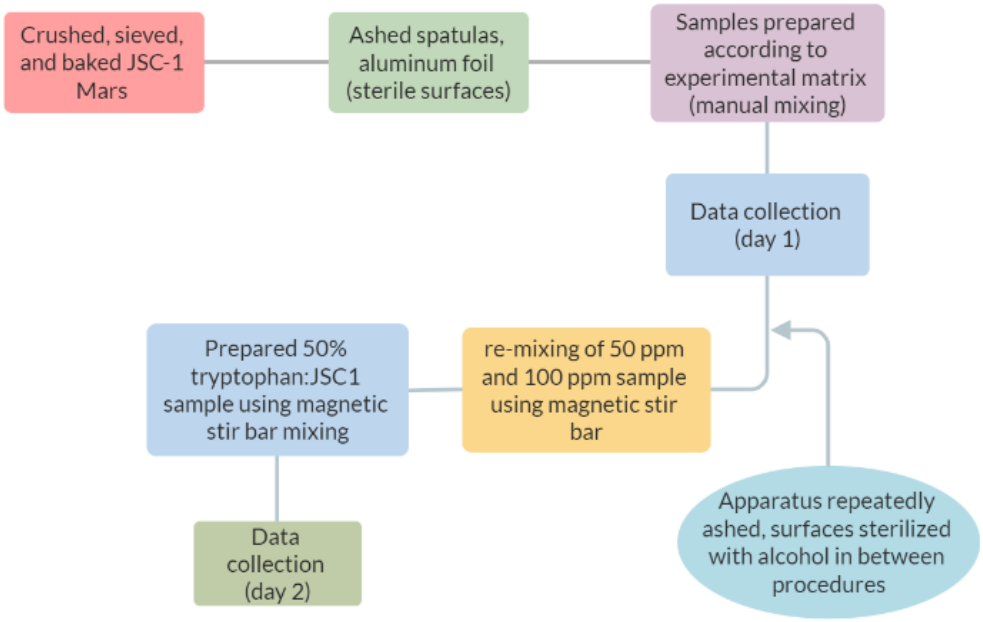

Figure 5.9: Flowchart summarizing the steps and procedures taken during the experiment starting from sample prep to data collection

5.1.5 LIF Spectroscopy Measurements – Specifications for Data Collection

The days of data collection were divided into two: one was on 16th May 2023 and the other took place on 30th May 2023. Table 6 summarizes the Raman instrument specifications during both experiments. These are henceforth referred to as experiment 1 and experiment 2. Data was collected following alignment, calibration, and background subtraction for both the experiments.

Table 6: UV LIF spectroscopy instrument specification

Specification	Value on data collection experiment 1 (manually mixed samples)	Value on data collection experiment 2 (Re-mixed samples – mixed with magnetic stir-bar)	Additional Comments
Spectra window	325 – 350 nm	325 – 350 nm	The window of wavelength we obtain a spectra for
Slit opening	30 µm	30 µm	
Diffraction Grating	600 lines/mm	600 lines/mm	
Accumulation	200 images	200 images	The spectra were taken 200 times for each sample measurement
Exposure Time	0.1 s	0.1 s	How long sample is exposed to 266 nm laser
Delay	47.5 ns	47.5 ns	Tells the instrument when to open the camera for each spectrum – depends on time taken for light to travel the path

Specification	Value on data collection experiment 1 (manually mixed samples)	Value on data collection experiment 2 (Re-mixed samples – mixed with magnetic stir-bar)	Additional Comments
Width	**5 ns**	**100 ns**	**How much time the camera is open for each accumulation**
Gain	**3000 (for pure Tryptophan), 4000 for the rest (samples + blank)**	**3000 (for pure Tryptophan), 4000 for the rest (samples + blank)**	

Figure 5.10 schematically explains some of the instrument specifications mentioned in Table 6. Since we operated the instrument at a frequency of 2 kHz, this gave us a repetition rate of 500 µs. The pulse width was different for the two experiments– 5 ns for experiment 1 and 100 ns for experiment 2 whereas the gate delay remained the same. Each scan had an exposure time of 0.1 s during which time the sample was exposed to the pulsed laser as depicted in the diagram. A total of 200 such scans or accumulations were taken for each sample.

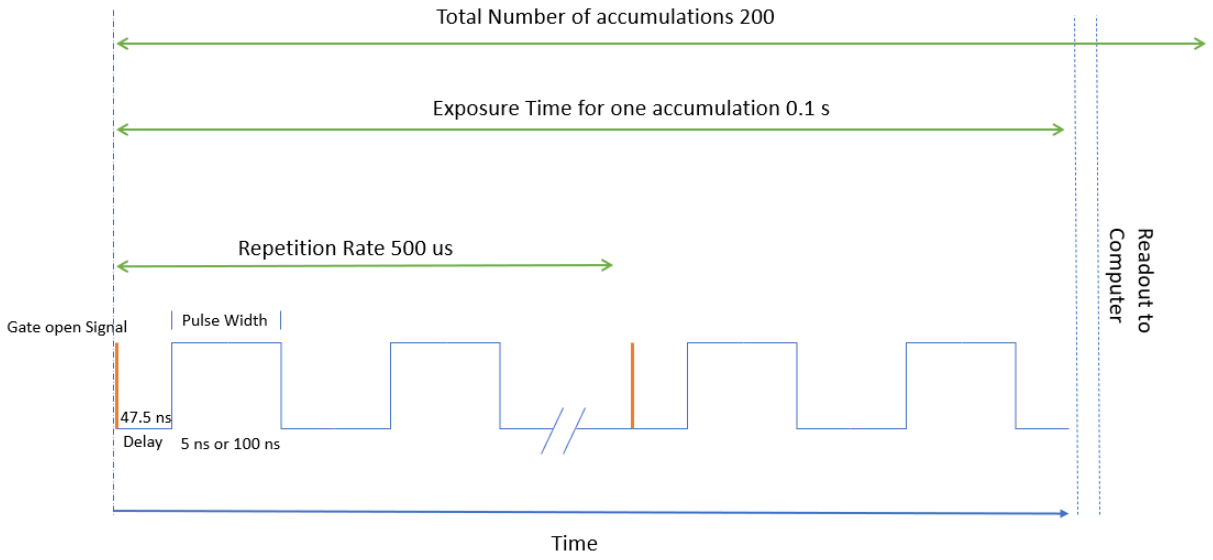

Figure 5.10: Sketch depicting various instrument specifications. The 266 nm laser enters the detector at a repetition rate of 500 us. An external trigger signal is sent to the detector when the pulse is emitted. The incoming pulse is allowed to enter the detector after a delay time (47.5 ns in our set up). The pulse width used in our measurements were 5 ns and 100 ns. The exposure time is the time instrument CCD is exposed to for one accumulation. We took 200 accumulations. The charge is read out from the detector after each exposure time (0.1 s) and the detector is prepared for the next accumulation. (Sketch adapted for our setup from Eshelman, 2016).

The data collected on 16th May consisted of samples which were mixed and prepared manually. Measurements were taken in the following order:

- Pure Tryptophan sample
- 100 ppm Tryptophan sample with JSC-1 Mars
- 50 ppm Tryptophan sample with JSC-1 Mars
- Blanks consisting JSC-1 Mars prepared in different ways (refer to Table 5)
- Pure Tryptophan sample sprinkled with 0.0261 g of crushed, sieved, baked JSC-1 Mars

The data collected during experiment 1 consisted of samples which were re-mixed using a magnetic stir-bar. In addition to this, a 50% Tryptophan to JSC-1 Mars sample was also prepared using this sample preparation method.

5.2. Results

The results from LIF spectroscopy of Tryptophan in a JSC-1 Mars matrix are presented in this section. Re-iterating from Methods and Materials section, there were two days of data collection (experiment 1 and experiment 2)– one where samples were prepared using manual mixing (experiment 1) while the second day of data collection looked at LIF spectroscopy of samples re-mixed using a magnetic stirrer (experiment 2) – which ideally achieves a more homogenous sample and could potentially remove magnetic particles which interferes with the data collection process.

5.2.1 Comparisons between Blanks

The blanks consisted of JSC-1 Mars prepared in different ways (refer to experimental matrix). These are compared to each other to ascertain what level of background organic contamination can we expect in the spectra of our samples. Figures 5.11 and 5.12 compare two blanks – one was baked and the other was not.

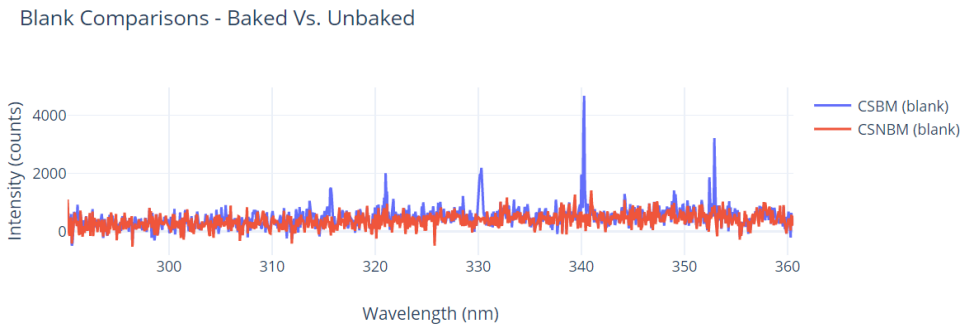

Figure 5.11: Fluorescence Spectra comparisons between two blanks (CSBM and CSNBM) excited at 266 nm. One is baked (purple) and the other is unbaked (red), both blanks were prepared with methanol. Both blanks were crushed and sieved and data was averaged over 5 points.

Figure 5.11 shows that the baked and unbaked JSC-1 Mars give a similar result on our instrument setup.

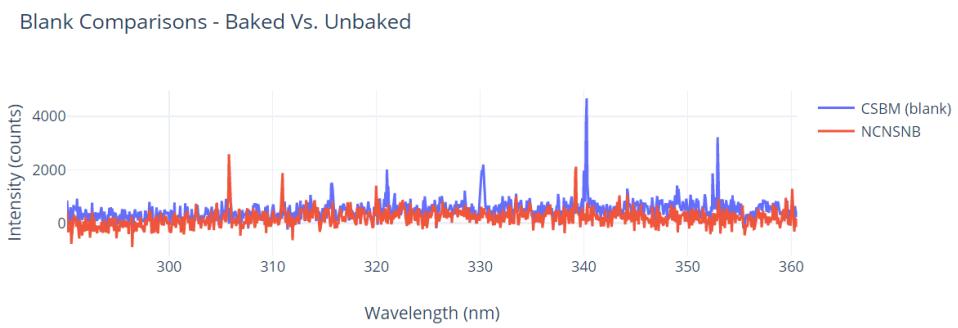

Figure 5.12: Fluorescence Spectra comparisons between two blanks (CSBM and NCNSNB) excited at 266 nm. One is baked (purple) and the other is unbaked (red), both blanks were prepared with methanol. One blank was not crushed and neither sieved (unaltered and unprocessed JSC-1 Mars). Both samples were averaged over 5 points. This comparison was made to show that the fluorescence spectra is not drastically different in this particular wavelength range between unprocessed JSC-1 Mars (NCNSNB) and Crushed, Sieved, Baked JSC-1 Mars prepared with Methanol. Although unprocessed JSC-1 Mars has a higher water and organic content in addition to having a coarse particle distribution compared to JSC-1 Mars (CSBM), the instrument gives very similar fluorescence results for both these measurements

JSC-1 Mars being sourced from Earth analogs, is high in organic content and thus can potentially interfere with our LIF measurements. Recalling Figure 5.3 which showed a low count level, broad organic signal for NCNSNB JSC-1 Mars blank, when this plot is compared to the CSBM blank, not much difference in spectra is observed. This is most likely due to the organic signature present in non-baked JSC-1 Mars being near noise level at 500 counts. The sharp peaks noticed in the spectra of the Crushed Sieved Baked with Methanol (CSBM) at 330 nm, 340 nm, and 355 nm and are most likely instrument artifacts. These peaks are too narrow to be classified as mineral peaks. Additionally, if they were mineral peaks, they would occur at same wavelength locations and not be shifted between measurements.

To verify if these peaks observed were indeed artifacts from the instrument and was not arising from sample properties, a spectra of an empty aluminum cup was taken at the same specifications.

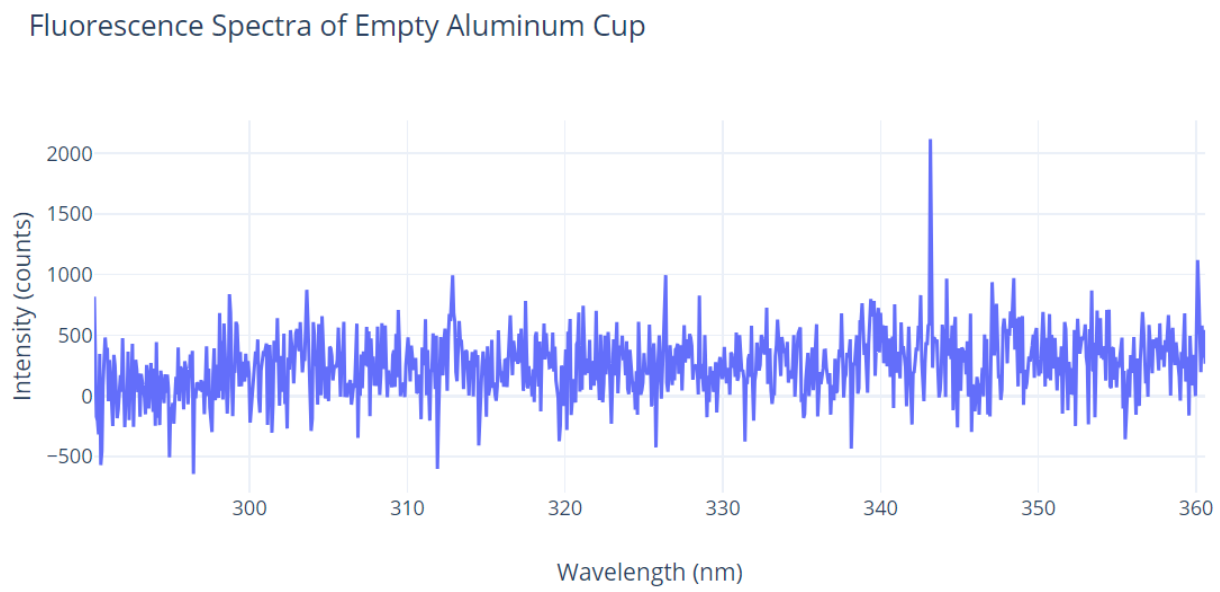

Figure 5.13: A fluorescence spectra of an empty aluminum cup taken (experiment 1). This spectrum shows a peak around > 340 nm – implying that the sharp peaks observed in the previous (5.11 and 5.12) and following results are in all likelihood instrument artifacts and are not indicative of neither minerals nor organics.

Another possible source for sharp peaks could be a resultant of automated background subtraction by the Solis software applied on all spectra presented thus far. Figure 5.14 shows the background spectra for the two experiments. Background was collected with a switched off laser. There are two visible peaks around wavelengths between 330 and 340 nm and one around 320 nm which align for both experiments. However, one peak around 315 nm is visible only for experiment 1.

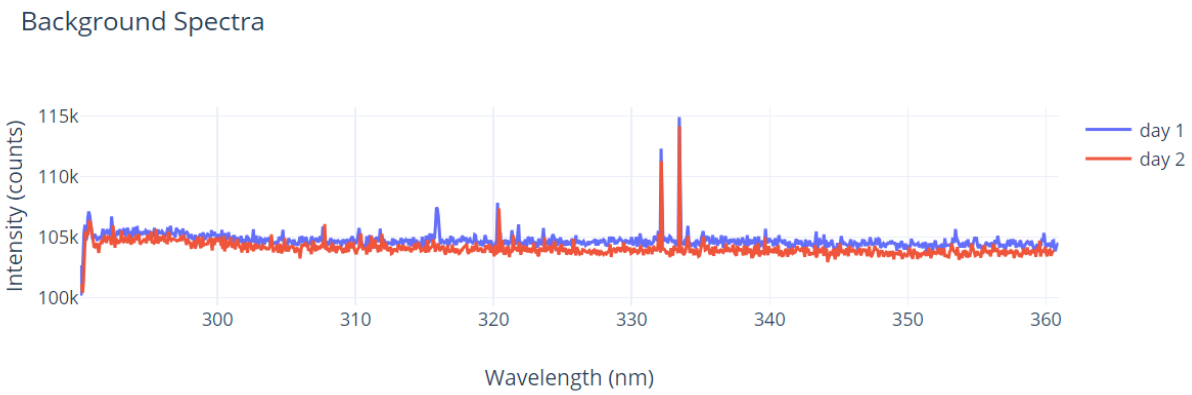

Figure 5.14: Background spectra automatically subtracted from spectra obtained

Given the unpredictable nature of peaks in the background spectra and spectra for the empty cup, it can be safely concluded that the sharp peaks observed in the JSC-1 blank spectra are due to the following:

A) Instrument artifacts
B) Cosmic rays
C) Changes in lab environment (presence/absence of room light)

5.2.2 LIF Results from Samples

The first sample analyzed during experiment 1 was the pure Tryptophan sample. The spectra obtained with gain = 3000 is presented in Figure 5.15.

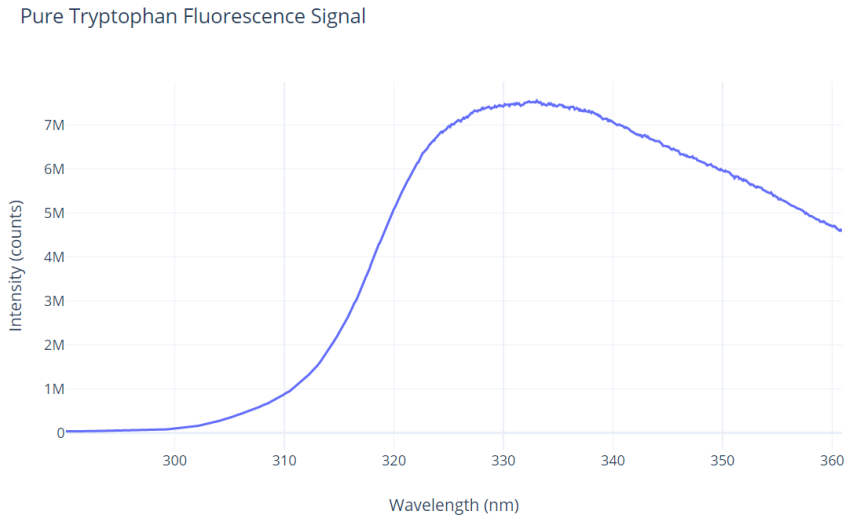

Figure 5.15: Fluorescence spectra of pure Tryptophan sample excited at 266 nm. Gain used was 3000 on the YU LIF instrument and averaged over 5 points

Spectrum obtained from pure Tryptophan sample is in agreement to the characteristic Tryptophan fluorescence, peaking at in the range of 320 - 340 nm – this was observed during experiment 1.

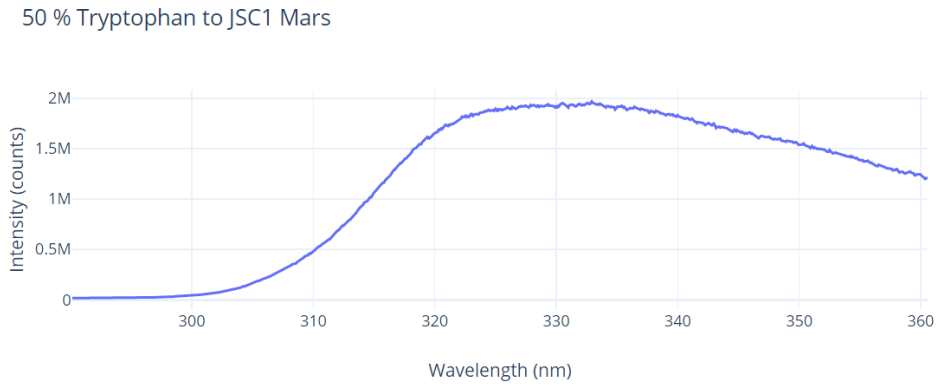

Figure 5.16: 50% Tryptophan to JSC-1 Mars concentration sample excited at 266 nm during experiment 2 (averaged over 5 points). This observation was made at a higher pulse width (100 ns) than conditions for experiment 1 (pulse width of 5 ns) – here the sample was exposed to a higher number of photons per accumulation.

50 % Tryptophan to JSC-1 Mars gives us a spectrum similar to that of the pure Tryptophan sample but with lower intensity. The result shown in Figure 5.16 was obtained during experiment 2. A direct comparison of the intensities cannot be drawn since the data were taken during two

different experiments with two different width values during data acquisition. The main takeaway from Figure 5.16 is a 50% Tryptophan to JSC-1 Mars concentration is detectable through YU LIF at 266 nm excitation. The 50% concentration is an exaggerated concentration and any realistic IDP organic to Martian dust concentration would be significantly lower than this value.

Fluorescence spectra for 100 ppm and 50 ppm concentrations are presented in Figure 5.17. The spectra in Figure 5.17 were taken during experiment 1. No detectable fluorescence originating from Tryptophan was observed in the 100 ppm and 50 ppm spectra collected during experiment 1 (samples were manually mixed). The lack of Tryptophan signature in the 100 and 50 ppm spectra is attributed to UV quenching caused ferric bearing minerals present in JSC-1 Mars.

After the null result of Tryptophan signal from 100 and 50 ppm spectra, we decided to make an additional measurement of pure Tryptophan layered with Crushed Sieved Baked with Methanol (CSBM) JSC-1 Blank sample. The intention behind this exercise was to see how much a thin layer of baked JSC-1 Mars can attenuate a pure Tryptophan signal. The result of the same is represented in Figure 5.17 with the other spectra. A spectra of JSC-1 (CSBM) blank is also plotted for comparison.

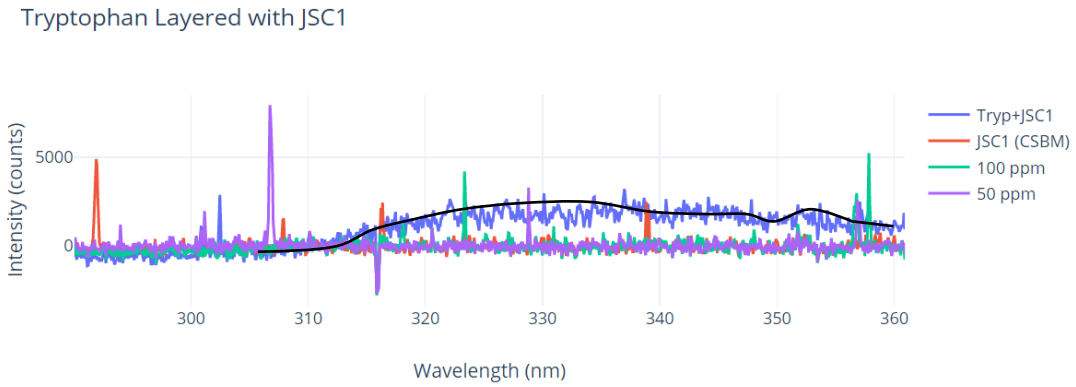

Figure 5.17: Fluorescence signal of pure Tryptophan sample sprinkled with CSB JSC-1 Mars – compared to JSC-1 Blank, 100 ppm and 50 ppm Tryptophan: JSC-1 Mars (excited at 266 nm)

Figure 5.17 shows very weak Tryptophan curve noticeable while comparing with blank JSC-1 Mars, 100 ppm, and 50 ppm sample. The layer of JSC-1 Mars manually sprinkled on top was

equal to a mass of 0.0261 g of crushed, sieved, and baked JSC-1 Mars. The Tryp+JSC1 curve is an average over 10 points. An average was taken since the layer was sprinkled manually which could have resulted in uneven layering of JSC-1 Mars. The quantity to be sprinkled was calculated assuming the bulk density of JSC-1 Mars to be 79% of 0.87 +_ 0.02 g/cm^3 (79% since larger particles were sieved out – calculation in Appendix. The corresponding depth for this mass of JSC-1 Mars layer was calculated to be 0.03 cm. This approximately the accumulated depth of airfall dust sediment computed at Gale after 100 years of dust deposition.

Comparing Figure 5.17 and Figure 5.15, the intensity of the pure Tryptophan peak exceeds 7 million counts whereas layered Tryptophan with JSC-1 Mars has an approximate intensity of 2200 counts. Layered Tryptophan with JSC-1 Mars peak is almost 3.4 x 10^{-4} times intensity of pure Tryptophan peak. This indicates the highly UV absorptive nature of JSC-1 Mars – a layer of 0.03 cm of JSC-1 Mars at particle size < 350 nm is enough to attenuate a UV signal to a large extent. Additional analysis is conducted in the discussion section.

5.2.3 Spectrum after Magnetic Stir-bar Mixing

The lack of a Tryptophan signal in 100 ppm and 50 ppm manually mixed sample was attributed to two possible causes:

1. Mineralogic components of JSC-1 Mars – magnetic and ferric bearing centers which quench the UV signal, hindering the LIF process to detect organic signals like that of Tryptophan
2. Lack of homegeneity in the sample – this could be caused by opting for manually mixing our samples resulting in the Tryptophan not evenly mixing with the rest of JSC-1 Mars

To obtain better results we opted to remix these samples with a magnetic stirrer. We had hoped this would serve the purpose of removing some of the magnetic particles causing an interference in the organic LIF signal and would also ensure that the Tryptophan is evenly mixed with the JSC-1 Mars. Thus when a small portion of the prepared sample is transferred into the aluminum cup for measurement, it accurately represents a 100 ppm and 50 ppm concentration of Tryptophan to JSC-1 Mars.

The results of this exercise and necessary comparisons are presented in Figures 5.18 – 5.19.

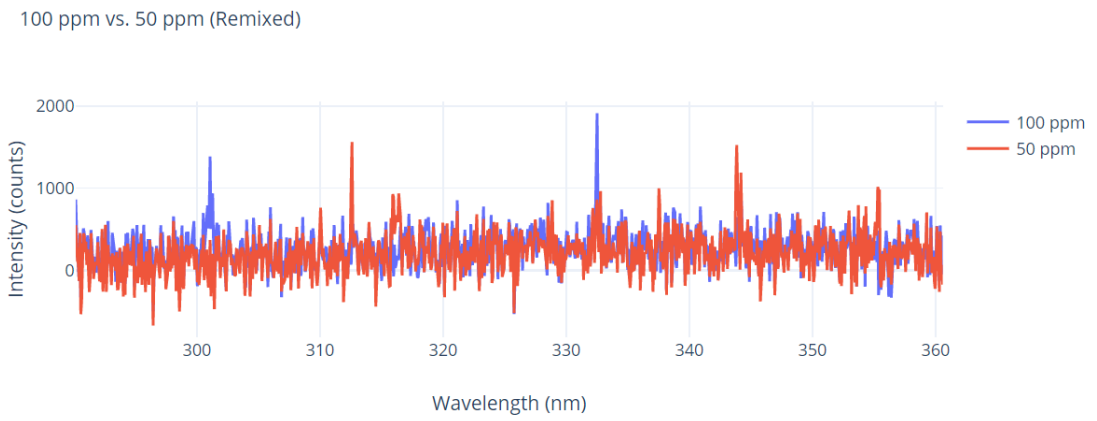

Figure 5.18: Fluorescence signal of re-mixed 100 ppm and 50 ppm sample – no organic signature detected (excited at 266 nm)

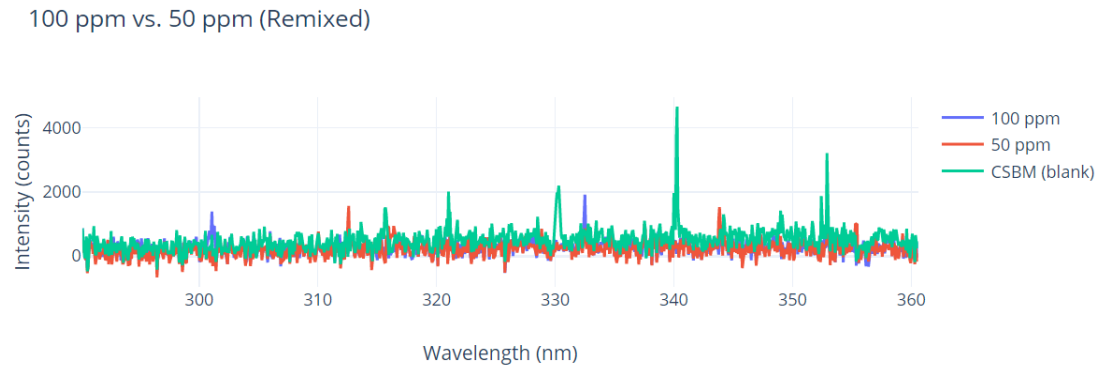

Figure 5.19: Fluorescence signal of re-mixed 100 ppm and 50 ppm sample compared to blank JSC-1 Mars (excited at 266 nm)

Figures 5.18 and 5.19 depict the LIF spectra results of the remixed samples. Despite re-mixing the samples, no fluorescence signal of Tryptophan is observed in these plots.

5.2.4 Manual vs. Magnetic Mixing

The spectra obtained from manually mixed and magnetic stirrer re-mixed samples are compared in Figures 5.20 and 5.21. The width specified in the instrument settings for manually mixed samples and magnetic stirrer re-mixed samples are different and no concrete conclusions can be drawn from these plots.

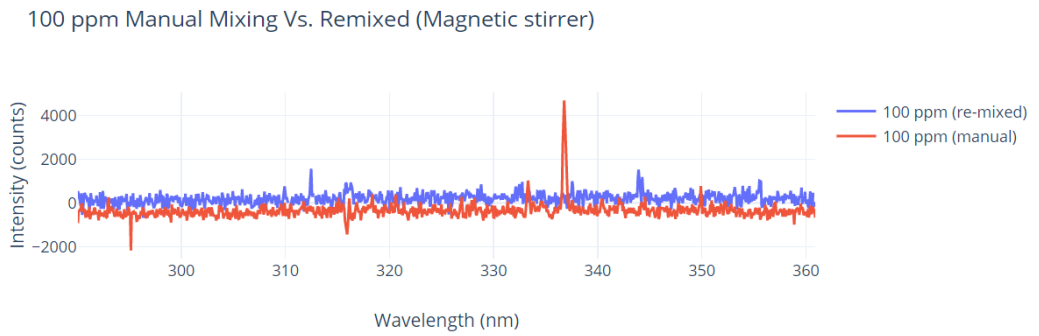

Figure 5.20: Fluorescence spectra of two 100 ppm samples (excited at 266 nm) - A

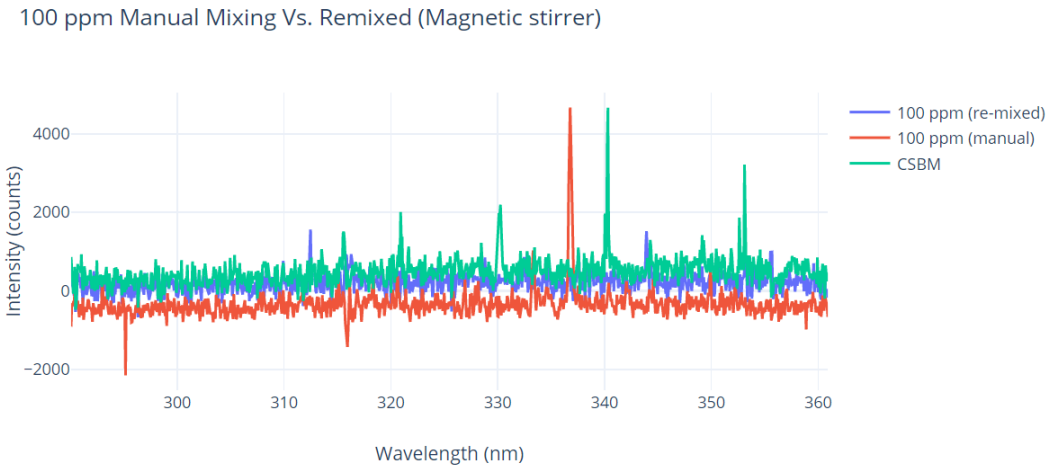

Figure 5.21: Fluorescence spectra of two 100 ppm samples (excited at 266 nm) - B

The data from Figure 5.20 and 5.21 are mostly inconclusive. The pulse width for manual mixing was 5 ns whereas the acquisitions for magnetic stir-bar mixing data was taken at a significantly larger pulse width of 100 ns. This is also reflected in the number of counts for the re-mixed sample being at a higher value than that of the manually mixed sample.

5.3 Discussion

Summarizing the results, spectral analysis of pure Tryptophan sample and 50% Tryptophan to JSC-1 sample shows a Tryptophan peak. Our measurements of 100 ppm and 50 ppm did not yield any Tryptophan peak primarily due to UV quenching arising from the magnetic component and iron rich component of JSC-1 Mars. JSC-1 Mars simulant soil is sourced from a cinder cone in Hawaii and has been cited by several studies as an analog for Martian soil due to its similar

spectral and magnetic properties to Martian soil (Allen et al., 1998). JSC-1 has a mineralogical composition of Ca-feldspar, Ti-magnetite (15 – 22 wt % TiO2), olivine, pyroxene and glass (Morris et al., 1993). The iron bearing minerals and magnetic components of JSC-1 Mars a significant fraction of which are amorphous in nature results in quenching of UV light. Since this study uses a laser operating in the UV domain, JSC-1 Mars presents a serious challenge in detecting organics in the ppm range. In-situ studies (Mossbauer spectroscopy) carried out by Spirit (MER-A) and Opportunity (MER-B) have confirmed the magnetic properties of Martian dust (Morris et al., 2004). Our current understanding of Martian dust indicates that a large fraction of atmospheric dust on Mars which is homogenized due to global dust storms are basaltic and magnetic in nature (Goetz et al., 2005). These studies indicate that JSC-1 Mars is a reasonable analog for the spectral properties of Martian dust.

We look at similar studies conducted both in-situ by the SHERLOC instrument on the Perseverance rover and laboratory studies done with SHERLOC like laser (MOBIUS) to compare and evaluate the validity of our results. Carrier et al. (2019) carried out LIF spectroscopy measurements on Phenanthrene and Phenylalanine under a layer of Mojave Mars Simulant (MMS) to determine detection limit for the laser (only preliminary results are available at the time of writing). Additionally, findings from the SHERLOC instrument which landed on Mars along with the Perseverance rover in 2021 are now being made available.

In order to draw reasonable comparisons between the results obtained by SHERLOC, MOBIUS, and our YU LIF (266 nm) setup, we need to look at how different the soil matrix is for all these three studies. Additionally, instrument specifications of these three instrumental setups are vastly different, implying that results may vary between these three instruments even if they are using the same technique of organic detection – LIF spectroscopy. Table 7 shows the mineralogical composition of MMS stimulant (Carrier et al., 2019; Clark et al., 2020).

Table 7: Mineralogical composition of MMS simulant used in Carrier et al. (2019) (Data from Clark et al., 2020)

Mineral	MMS (measured at JSC) (Wt%)
Plagioclase	60.4
Olivine	n.d.
Pyroxene	12.3
Magnetite	n.d.
Anhydrite	n.d.
Hematite	1.1
Quartz	0.6
Calcite	1
Ilmenite	2.2
K-feldspar	2.2
Analcime	1.3
Goethite	n.d.
Pyrite	n.d.
Ferric sulfate	n.d.
Amorphous	3.1
Amorphous + smectite	18.7

Similar to JSC-1 Mars, MMS also consists of weathered volcanic ash and hence has a similar makeup of minerals. JSC-1 Mars is more suited to represent global dust composition of Mars as both contain a high concentration of ferric oxide and fine-grained basaltic minerals and glass.

MMS on the other hand is a good mineralogical analog for igneous rocks found on Mars and their weathered products. Both Martian rocks and MMS are dominated by the presence of plagioclase feldspar, pyroxene with lesser quantities of olivine and magnetite. It should also be noted that neither JSC-1 Mars nor MMS are a good analog for the sulfate component in Martian material (Peters et al., 2008) Additionally, both these simulant soils lack in clay particles. Studies from the Perseverance rover has shown that the surface material composition at Jezero crater is also dominated by basaltic minerals (Corpolongo et al., 2023). Given the similar basaltic dust environments all these three studies take place, we can compare the results obtained by SHERLOC, Carrier et al., 2019, and this study.

Table 8: Instrument comparisons between three instruments – SHERLOC, MOBIUS, and YU LIF instrument (266 nm)

Instrument Setup	MOBIUS	SHERLOC	YU LIF (266 nm)
Wavelength (nm)	248.7	248.7	266
Spot Size (mm^2)	3.54E-03	7.54E-03	1.00E+00
Pulse Energy (uJ)	2.8	8	1.6
Energy Density (uJ/mm^2)	791.0	1061.0	1.6
Pulse Width (us)	40	40	0.1
Number of Pulses	100	100	677966.1
Exposure Time for one accumulation (ms)	4	4	67.8
Number of Accumulation	25	25	200
Total Exposure to laser (s)	0.1	0.1	13.6
Energy Density ($uJ/mm^2/s$)	7.9E+03	1.1E+04	1.2E-01
Photons (mm^2/s)	1.1E+19	1.3E+19	1.6E+14

Table 8 details the instrument comparisons between the three instruments mentioned. One can note that the YU LIF instrument has a significantly lower energy density compared to SHERLOC and MOBIUS. While comparing, one can note that the spot-size of YU LIF instrument being larger than that of MOBIUS and SHERLOC reduces its energy density to an

extent. The data presented in these columns were obtained from a bunch of SHERLOC and MOBIUS papers (Razzel Hollis et al., 2021; Bhartia et al., 2021; Beegle et al., 2020; Razzel Hollis et al., 2020; Eshelman et al., 2015). Both SHERLOC and MOBIUS have various operational modes and hence singling out the number of pulses and number of accumulations for each instrument from existing and rapidly evolving literature was a challenge. Razzel Hollis et al. (2021) reports the MOBIUS instrument taking 25 accumulations for each observation. We have used this value for SHERLOC as well in the calculations presented in Table 8. Our final column indicates the number of photons a sample is exposed to per area per second by these instruments. It can be seen that the SHERLOC instrument has a much higher photon density (mm^2/s) (approximately 10^5 times higher) than our LIF setup. This implies that a sample exposed to the SHERLOC laser would be subjected to almost 10^5 times more photons than a sample exposed to the YU LIF (266 nm) laser.

Preliminary results from Carrier et al., (2019) indicate a positive fluorescence spectra detection of Phenylalanine under a layer of 0.168 cm of MMS simulant. However, it can be noted from Figure 5.21 (from Carrier et al. (2019) that there is a drastic drop in intensity when the sample is measured under MMS.

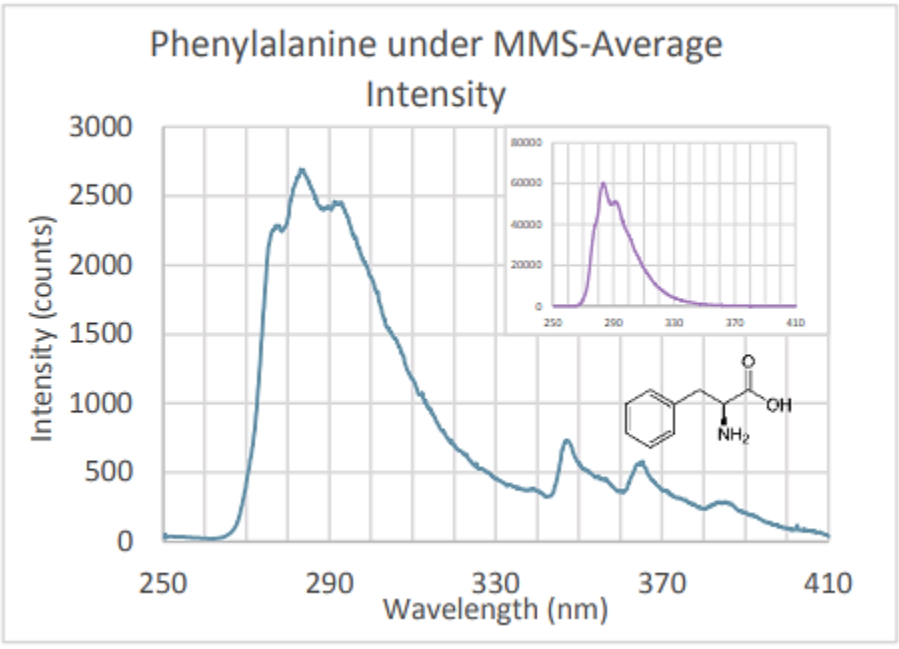

Figure 5.22: Preliminary results from Carrier et al (2019) studying fluorescence spectroscopy of Phenylalanine under MMS simulant (0.168 cm) The peak in the pure

Phenylalanine sample is read to be 60000 counts and that of the sample under MMS is read to be 2700

Figure 5.22 in accordance to results presented in this thesis (Figure 5.17) goes to show that basaltic dust and soil matrix severely hamper fluorescence detection of organic molecules through UV detection methods. Figure 5.23 shows the laser interactions with the samples in this thesis (using YU LIF instrument) and that presented in Carrier et al. (2019).

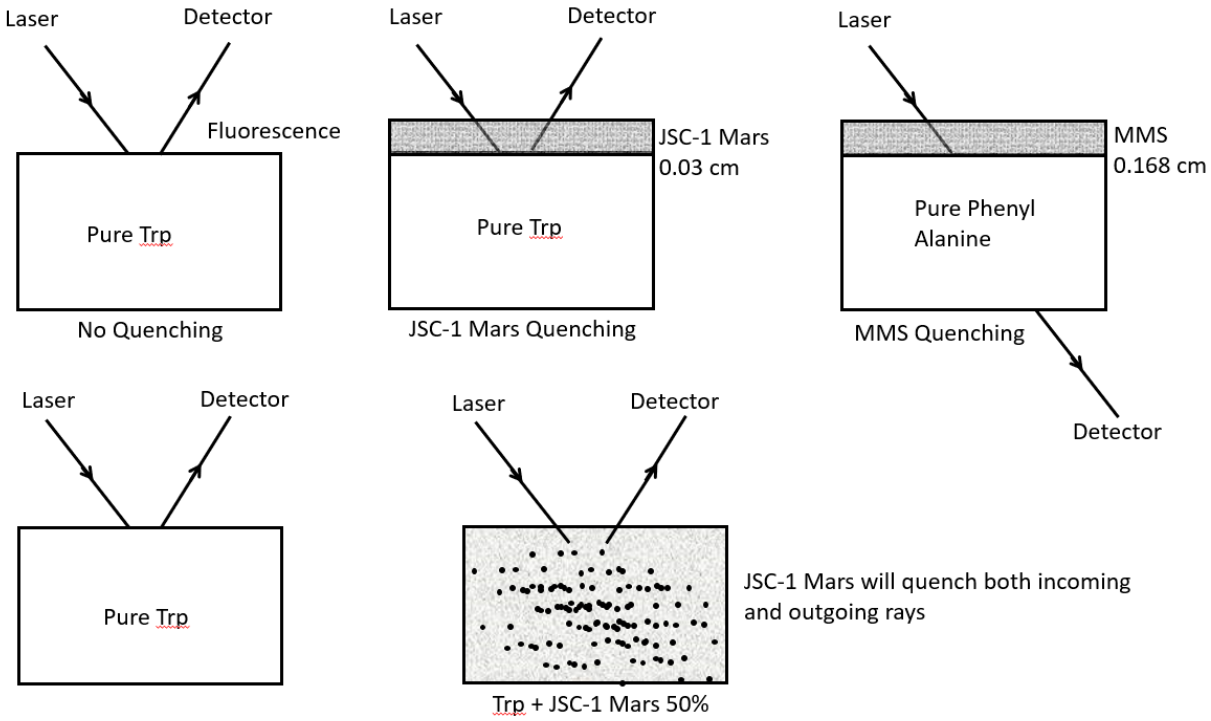

Figure 5.23: Schematic depiction of laser interactions with samples for YU LIF instrument (266 nm) (this work) and work presented in Carrier et al. (2019) The top panel shows (left to right) a) 266 nm laser interacting with pure Tryptophan sample using YU LIF instrument, b) 266 nm interacting with Tryptophan sample layered with JSC-1 Mars (CSB) where UV laser experiences quenching on its journey through the JSC-1 layer to the sample and the emitted fluorescence signal which is also in UV experiences additional quenching before reaching the detector, c) laser-sample interactions of work presented in Carrier et al. (2019) which uses transmittance, Phenyl alanine as fluorescing organic material, and MMS simulant soil. Bottom panel shows 266 nm laser interaction with pure Tryptophan sample compared to Tryptophan sample doped with 50% JSC-1 Mars

These schematics show that quenching happens both when the laser interacts with the sample but also when the fluoresced light is emitted by the Tryptophan in the dust matrix and has to travel, interact with JSC-1 Mars particles – which further quenches the signal.

Table 9: Summary of Quenching in various samples tested in this work using YU LIF instrument (266 nm)

Sample	Counts Observed	Counts Expected without quenching	% Absorbed Calculated	Counts Expected with quenching
Pure Tryptophan	7000000	N/A	N/A	N/A
50% Tryptophan	2000000	70000000	97.1	N/A
100 ppm	Below Detection	14000	N/A	400
50 ppm	Below Detection	4000	N/A	114.3

Table 9 provides the summary of quenching in different samples. The pure Tryptophan sample measured showed fluorescence peaking at 7 million counts. The 50% Tryptophan measured showed a peak at 2 million counts. Considering the pulse widths and relative concentration of Tryptophan in these two measurements, we calculate that we should have detected 70 million counts for the 50 % tryptophan sample at a 100 ns pulse width but we only detect 2 million counts. Similarly, expected counts for 100 ppm and 50 ppm are below detection limits. The percentage absorbed in the 50% Tryptophan sample as a result of quenching was calculated to be around 97%. Thus, the number of counts expected from the 100 ppm and 50 ppm with quenching will be around 3 % of the counts expected without quenching. This amounts to 400 counts and 114 counts for 100 ppm and 50 ppm respectively which is below the detection limit and agrees with what was observed during the experiment.

Table 10: Quenching of Tryptophan sample layered with 0.03 cm of JSC-1 Mars – Compared with results presented in Carrier et al. (2019)

Sample	Counts Observed at peak for pure sample	Layering	Layering (cm)	Counts Observed at peak for layered sample	% Reduction	Absorption Coefficient (mm-1)
Tryptophan (this thesis)	7000000	JSC-1 Mars	0.03	2200	0.031	13.44
Phenylalanine (Carrier et al., 2019)	60000	MMS	0.17	2700	4.5	2.17

Table 10 provides a comparison of quenching of Tryptophan sample with that of Phenylalanine, published by Carrier et al. (2019).

In order to arrive at the absorption coefficient, Beer-Lambert's law was invoked and the following calculations were carried out:

The final intensity of a beam of light passing through a medium can be given by the expression: $I = I_o \exp(-\tau)$ where τ is optical depth and is wavelength dependent.

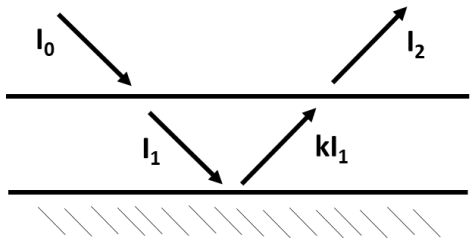

Figure 5.24: Incident intensity Io interacts with JSC-1 layer resulting in intensity I1 to interact with pure Tryptophan (shaded region). A fluorescence signal which is kI_1 in intensity is emitted. This beam undergoes absorption by the JSC-1 layer and a final intensity of I_2 is detected by the detector.

The incident wavelength is the wavelength of the laser, λ_1 = 266 nm and the emitted wavelength from fluorescence is λ_2 = 330 nm

$\tau_1 = \tau(\lambda_1)$ and $\tau_2 = \tau(\lambda_2)$ since optical depth is wavelength dependent. We can write the following expressions:

$I_1 = I_o \exp(-\tau_1)$ ----------(1)

$I_2 = I_o \exp(-\tau_2)$ ----------(2)

$I_2 = k I_0 \exp(-\tau_1) \exp(-\tau_2)$ ----------(3)

$I_2 = k I_0 \exp(-(\tau_1 + \tau_2))$) ----------(4)

Recalling UV extinction by 350-micron sized JSC-1 Mars layer (Godin et al., 2023) in Figure 4.2, we can assume τ_1 approximately equal to τ_2. The above expressions can then be modified to:

$I_2 = k I_0 \exp(-2\tau)$

$= 7 \times 10^6 \exp(-2\tau)$

Without JSC-1 layer (0.03 cm), $I_2 = k I_0 = 7 \times 10^6$ (observed counts from Tryptophan fluorescence without dust layer, absorption of fluorescence signal)

With JSC-1 layer (0.03 cm), $I_2 = 2200 = 7 \times 10^6 \exp(-2\tau)$

$-2\tau = \ln(2200 / (7 \times 10^6)) = -8.06$

$\tau = 4.03$

Absorption coefficient = $(\tau / d) = 4.03 / 0.3\text{mm} =$ **$13.43\ \text{mm}^{-1}$** (where d = depth = 0.03 cm = 0.3 mm)

The absorption coefficient calculated for tryptophan layered with JSC-1 Mars above aligns with value in Godin et al. (2023) for 350 μm JSC-1 (16 mm^{-1}). In our experiment, a mass of JSC-1 Mars (0.026 g) was sprinkled manually on top of the pure Tryptophan sample and gently tapped on the table to obtain the results presented. Given the density of JSC-1 Mars, a mass of 0.026 g in the aluminum cup holder corresponds to 0.03 cm of dust layer. Errors could have arisen from two sources: 1) un-even layering of JSC-1 Mars b) errors from mass to depth conversion (we never measured depth of the layer, only the mass of material sprinkled). To counter un-evenness of the JSC-1 layer, observations were made over 10 points and averaged. Hence, the absorption coefficient obtained in this analysis for 0.3 mm layer of JSC-1 Mars of 350 μm particle size is a lower bound.

The absorption coefficient calculated for data presented in Carrier et al. (2019) is not in agreement with the absorption coefficient calculated from the YU LIF instrument observations

we made. A possible explanation for this could be varying grain sizes, and the use of pellets in work presented in Carrier et al. (2019).

Analysis performed by the SHERLOC instrument located at Jezero crater on Mars have reported fluorescence spectra consistent with several aromatic organic molecules. Although this could very well mean organic detection in a basaltic-dust rich place on Mars, the study also states that Cerium 3+ in phosphates can emit luminescence similar to the organics being detected (Scheller et al., 2022). Furthermore, Scheller et al. (2022) also notes that strongest fluorescence signatures were detected in materials associated with sulfate and carbonate bearing minerals (resultant of aqueous processes). Hence, this requires further investigation.

The YU LIF instrument's inability to detect organics at 100 ppm and 50 ppm concentrations are primarily due to quenching resulting from iron bearing minerals in JSC-1. However, YU LIF instrument operates on a significantly lower energy density compared to MOBIUS and SHERLOC. In order to make successful detections using the present YU LIF instrument setup, we need to optimize the photon density at the sample and also ensuring the sample isn't subjected to photo-bleaching.

YU LIF instrument and SHERLOC are differently equipped. SHERLOC has a suite of tools which can remove dust layers from the surface and Raman and Fluorescence spectroscopy can be conducted on rock surfaces. This is in contrast to the study we conducted where we used loose soil (non-lithified) to layer our fluorescing organic.

5.4 Sources of Error and Possible Explanations for Observed Results

Potential sources of error in our experiment include errors while weighing out our samples – wherein since the JSC-1 Mars was very finely crushed (<355 μm), a miniscule fraction of the JSC-1 Mars was lost while transferring the weighed-out simulant soil to the beaker. Although, our apparatus (spatulas, glass rods, and beakers) were ashed in between most procedures, a completely organic contamination free environment was difficult to reproduce. The results for 100 ppm and 50 ppm Tryptophan to JSC-1 Mars samples yielded a null result which could be due to the large fraction of magnetic particles present in JSC-1 Mars or it could also be attributed to insufficient mixing despite employing the use of a magnetic stirrer. Additionally, it is possible that the Tryptophan in these samples were lost during the re-crushing of dried manually prepared

sample while using mortar and pestle. Hence, when the samples were re-mixed using magnetic stirrers, our measurements still yielded a null result.

The measuring scale used to measure out the samples provided measurements up to 0.0001 g. However, during sample preparation an uncertainty of up to 0.0005 was noted. This could have led to errors in sample measurement which were neglected.

Several sharp spikes were observed in our spectra for almost all observations made except that presented in Figure 5.6. The wavelengths the spikes appeared at were not consistent and the spikes were narrow – of nm in width. Due to the narrow width of the spike, we couldn't attribute this to any mineral peak. The spikes were 1000 counts – 5000 counts in intensity and the frequency (along with intensity) of the spikes varied in each measurement. We couldn't successfully identify an exact explanation for this observation due to its unpredictability. However, possible explanations include instrument artifacts, aggressive background subtraction, and possible light contamination in the observation room. Since the background subtraction for the data presented was performed automatically by the Solis software which used curve fitting and approximations, this could have led to the observed spikes. In order to check if this was indeed the case, follow-up experiments could be performed with the manual background subtraction option while data acquisition. The light present in the room was not controlled during the experiment duration with the light being turned off for some observations. Although unlikely, it could be possible that the light contamination present in the data collection room could have affected the spikes since the light was not controlled during the different data acquisitions. For follow-up experiments, keeping the light in the room a constant could be a suggestion. Other possible explanations include calibration errors. Repeating the experiment at least three more times will give us a better perspective on the results and could potentially help us identify the source of these spikes.

5.5 Summary - How both projects are related

This project consisted of two parts: one assessing the preservability of IDP organics in layered sedimentary deposits (consisting of Martian dust) through modeling studies and the other studying the detectability of the same through relevant organic detection methods such as fluorescence spectroscopy. A common reoccurring theme in this thesis is the highly-absorptive (in UV regime) nature of Martian soil and by extension, Martian simulant soils as well. While our modeling studies

in the first half of the thesis show how this material can effectively shield IDP organics on the surface of Mars from UV photolysis, the same material becomes a barrier when it comes to experimentally detecting organic matter embedded or mixed with Martian soil/dust (work presented in the latter half of this thesis).

Our modeling studies indicated it is possible to preserve organic carbon (originating from IDPs) in $10^2 – 10^3$ ppb concentrations embedded within sedimentary rhythmites over several regions on Mars. However, our experimental studies which attempted at detecting strongly fluorescing organic material such as Tryptophan struggled to detect a signal in an organic: Mars simulant soil dust matrix of 100 ppm and 50 ppm concentrations (10^5 ppb and 5 x 10^4 ppb). The YU LIF instrument was able to detect a faint Tryptophan signal when layered with JSC-1 soil (0.03 cm deep). However, drawing observations from the work in the IDP burial section, it is highly unlikely that such a pure layer of Tryptophan would exist on the Martian surface – given IDP and dust are most likely mixed by wind processes on Mars. The scenario tested in that particular LIF data acquisition is an ideal scenario at best. The LIF results obtained for this particular exercise demonstrates that a thin layer of Martian simulant soil is capable of reducing the emitted fluorescence by a great degree. Furthermore, one must be reminded that Tryptophan is one of the strongest fluorescing molecules, if the YU LIF instrument in its current setting is struggling to detect ppm concentrations of Tryptophan in a dust matrix, it has a reduced possibility of detecting fluorescent signals from any other organic molecule.

Thus, a balance must be struck between these two opposing implications of the UV-absorptive Martian soil. The lower concentration limit at which the YU LIF instrument (in its current setting) can detect an organic molecule such as Tryptophan in a dust matrix could indicate locations on Mars where similar investigations on IDP organics buried in rhythmites could yield favorable results.

Figures 4.12 and 4.13 from the modeling section of this thesis indicate that regions of Medusae Fossae, Arabia Terra, Sytris Major, among other mid-latitudinal regions are favorable for IDP organics preservation in sedimentary rhythmites. However, keeping in mind from the experimental results where we found that due to the UV quenching property of iron bearing minerals in JSC-1 Mars, there was a great reduction in UV fluorescence of Tryptophan under a thin layer of JSC-1 Mars. Thus, the organic preservation potential of a region becomes inconsequential if the local

mineralogy prevents the detection of said organics through methods like LIF. Hence, both preservation potential and local mineralogy go hand in hand when it comes to being able to detect IDP organics using the methods discussed. From this we could argue that regions with high mineral diversity will favor both preservation (absorption of UV by basaltic components) and would also favor detection - sulfate rich minerals corresponded to higher fluorescence detection at Jezero crater using SHERLOC instrument (Scheller et al., 2022). Regional mineralogies reported from orbital data tend to be inaccurate. However, from the results presented here combined with existing literature indicate that Gale crater checks all the requirements:

1. There is existing literature reporting presence of sedimentary rhythmites at Gale crater
2. According to our IDP organics burial model, Gale crater favors organics preservation
3. Diverse mineralogies (clays) have been reported by the Curiosity which will also favor organics detection through methods like LIF.

Chapter Six: Conclusions

From the modeling work presented, it can be concluded that the organic content present in IDPs gets rapidly preserved in sedimentary structures forming from gradual dust settling at several regions on Mars. This sequestration happens over a relatively short timescale of about 50 Martian years depending on the exact location being investigated. Since organic burial happens so rapidly, these particles are not a notable contributor to the methane budget on Mars. Our investigations have shown that the concentration of organics embedded within sedimentary rhythmites are of ppb concentration and can hence be further investigated by future spacecraft missions. Global dust deposition on Mars was also explored using data from MCD and inferences on regions of dust excess were drawn – some regions near the southern pole were the richest in dust and many equatorial to mid-latitude regions were sites where significant dust accumulated during the year. These regions are good candidates to further explore organic burial within sedimentary rhythmites. Finally, comments on the validity of MCD were made and further observations on potential dust sources on Mars were pointed at.

The experimental project presented in this thesis investigated the detectability of strong fluorescing organic molecules like Tryptophan in a Martian dust matrix composed of simulated Martian soil. JSC-1 Mars was chosen to simulate a dust matrix due to its closeness to the spectral and magnetic properties of Martian dust reported by several in-situ investigations carried out by spacecraft. UV LIF measurements were made of various samples of Tryptophan mixed with JSC-1 Mars. This method was unsuccessful in detecting Tryptophan at low concentrations (100 ppm and 50 ppm) mixed with JSC-1 Mars which is closer to expected IDP organic concentrations in sedimentary rhythmites. However, the YU LIF instrument was successful in detecting Tryptophan layered with 0.03 cm of JSC-1 Mars and this is consistent with other research done with similar fluorescing organics and other Martian simulant soil.

Chapter Seven: Future Work

This research on buried organics on Mars can be extended further in several ways both computationally and experimentally. Some of these are discussed here.

1. Updating existing IDP burial model – Our current model considers IDPs to be evenly distributed over Mars along with assuming a "flat" surface for UV flux reaching the surface. Thus, shielding from cliff faces and crevices would enhance the preservation of IDP organics. Codes can be developed taking into account Moores et al., (2017) which explores UV flux in specific geometries. The specific environments suggested by Tomkins et al. (2019) favorable for having a higher IDP concentration can be also incorporated within such modeling studies. This will help us further constrain IDP concentrations preserved in niche environments and can aid in future in-situ investigations

2. LIF studies should be carried out using other simulant soils which are richer in clay minerals instead of basaltic minerals. Scheller et al. (2022) pointed out the presence of sulfate-rich minerals which correlated with higher fluorescence signal detected by the SHERLOC instrument. Tryptophan mixed with other classes of simulant soil having a more clay-rich mineralogy could be studied through the YU LIF instrument and conclusions could be drawn on the effect of these minerals to organic fluorescence detection in a laboratory setting.

3. We measured the fluorescence spectra of Tryptophan mixed with JSC-1 Mars at three different concentrations – 50%, 100 ppm, and 50 ppm. A detectable fluorescence signal of 2 million counts was obtained for the 50% sample. However, no detection was made for the ppm level concentrations. Further experiments are required to constrain the lower limit of detectability of Tryptophan in a JSC-1 Mars soil matrix using the YU LIF instrument. Furthermore, the results detailed in this thesis must be independently verified with future experiments done at the same LIF setting

4. Optimizing the YU LIF instrument detectability – From the comparisons drawn between YU LIF instrument, MOBIUS, and SHERLOC, one can recall that the amount of photons/area/time for the latter two instruments are significantly higher than the photon flux produced at sample for the YU LIF instrument. This is attributed to be one of the possible reasons as to why MOBIUS and SHERLOC might be better at detecting low concentration organics. The specifications at

which the YU LIF instrument was used at could be tweaked to increase the photon count received at sample. However, one must keep in mind to not over-expose the organic sample which might cause damage and photobleaching.

References

Allen, C. C., Jager, K. M., Morris, R. V., Lindstrom, D. J., Lindstrom, M. M., & Lockwood, J. P. (1998). JSC Mars-1: a Martian soil simulant. In *Space 98* (pp. 469-476). https://doi.org/10.1061/40339(206)54

Allen, C. C., Morris, R. V., Jager, K. M., Golden, D. C., Lindstrom, D. J., Lindstrom, M. M., & Lockwood, J. P. (1998b, March). Martian regolith simulant JSC Mars-1. In *Lunar and Planetary Science Conference* (No. 1690, p. 1690).

Anderson, R., Bridges, J. C., Williams, A., Edgar, L., Ollila, A., Williams, J., ... & Vaniman, D. (2015). ChemCam results from the Shaler outcrop in Gale crater, Mars. *Icarus*, *249*, 2-21. https://doi.org/10.1016/j.icarus.2014.07.025

Atreya, S. K., Mahaffy, P. R., & Wong, A. S. (2007). Methane and related trace species on Mars: Origin, loss, implications for life, and habitability. *Planetary and Space Science*, *55*(3), 358-369. https://doi.org/10.1016/j.pss.2006.02.005

Banfield, D., Conrath, B. J., Smith, M. D., Christensen, P. R., & Wilson, R. J. (2003). Forced waves in the Martian atmosphere from MGS TES nadir data. *Icarus*, 161(2), 319-345. https://doi.org/10.1016/S0019-1035(02)00044-1

Baumstark-Khan, C., & Facius, R. (2002). Life under conditions of ionizing radiation. In Astrobiology: the quest for the conditions of life (pp. 261-284). Berlin, Heidelberg: Springer Berlin Heidelberg.

Beegle, L., Bhartia, R., White, M., DeFlores, L., Abbey, W., Wu, Y. H., ... & Sobron, P. (2015, March). SHERLOC: Scanning habitable environments with Raman & luminescence for organics & chemicals. In 2015 IEEE aerospace conference (pp. 1-11). IEEE. https://doi.org/10.1109/AERO.2015.7119105

Beegle, L., & Bhartia, R. (2016, April). SHERLOC: an investigation for Mars 2020. In EGU General Assembly Conference Abstracts (pp. EPSC2016-11215).

Bhartia, R., Beegle, L. W., DeFlores, L., Abbey, W., Razzell Hollis, J., Uckert, K., ... & Zan, J. (2021). Perseverance's scanning habitable environments with Raman and luminescence for organics and chemicals (SHERLOC) investigation. *Space Science Reviews*, *217*(4), 58. https://doi.org/10.1007/s11214-021-00812-z

Bhartia, R., Hug, W. F., Salas, E. C., Reid, R. D., Sijapati, K. K., Tsapin, A., ... & Conrad, P. G. (2008). Classification of organic and biological materials with deep ultraviolet excitation. *Applied Spectroscopy*, 62(10), 1070-1077. https://doi.org/10.1366/000370208786049123

Bhartia, R., Salas, E. C., Hug, W. F., Reid, R. D., Lane, A. L., Edwards, K. J., & Nealson, K. H. (2010). Label-free bacterial imaging with deep-UV-laser-induced native fluorescence. *Applied and Environmental Microbiology*, 76(21), 7231-7237. https://doi.org/10.1128/AEM.00943-10

Biemann, K., Oro, J., Toulmin III, P., Orgel, L. E., Nier, A. O., Anderson, D. M., ... & Biller, J. A. (1976). Search for organic and volatile inorganic compounds in two surface samples from the Chryse Planitia region of Mars. *Science*, 194(4260), 72-76. https://doi.org/10.1126/science.194.4260.72

Bradley, B. A., Sakimoto, S. E., Frey, H., & Zimbelman, J. R. (2002). Medusae Fossae formation: New perspectives from Mars global surveyor. *Journal of Geophysical Research: Planets*, *107*(E8), 2-1. https://doi.org/10.1029/2001JE001537

Bradley, P. M. (2003). History and ecology of chloroethene biodegradation: a review. *Bioremediation Journal*, 7(2), 81-109. https://doi.org/10.1080/713607980

Brownlee, D. E., Joswiak, D. J., Schlutter, D. J., Pepin, R. O., Bradley, J. P., & Love, S. G. (1995, March). Identification of individual cometary IDP's by thermally stepped He release. In Abstracts of the Lunar and Planetary Science Conference, volume 26, page 183, (1995) (Vol. 26). https://adsabs.harvard.edu/full/1995LPI.... 26..183B

Brownlee, D. E. (1985). Cosmic dust: Collection and research. *Annual Review of Earth and Planetary Sciences*, 13(1), 147-173. https://doi.org/10.1146/annurev.ea.13.050185.001051

Busemann, H., Nguyen, A. N., Cody, G. D., Hoppe, P., Kilcoyne, A. D., Stroud, R. M., ... & Nittler, L. R. (2009). Ultra-primitive interplanetary dust particles from the comet

26P/Grigg–Skjellerup dust stream collection. *Earth and Planetary Science Letters*, 288(1-2), 44-57. https://doi.org/10.1016/j.epsl.2009.09.007

Carr, M. H., & Head III, J. W. (2010). Geologic history of Mars. *Earth and Planetary Science Letters*, *294*(3-4), 185-203. https://doi.org/10.1016/j.epsl.2009.06.042

Carrier, B. L., Beegle, L. W., Bhartia, R., & Abbey, W. J. (2016, March). Measurement of uv fluorescence and raman signatures of organic compounds in the subsurface of mars relevant minerals to constrain detection depth for the sherloc mars 2020 instrument. In *47th Annual Lunar and Planetary Science Conference* (No. 1903, p. 2660).

Carrier, B. L., Abbey, W. J., Beegle, L. W., Bhartia, R., & Liu, Y. (2019). Attenuation of ultraviolet radiation in rocks and minerals: implications for Mars science. Journal of Geophysical Research: Planets, 124(10), 2599-2612. https://doi.org/10.1029/2018JE005758

Carter, J., Poulet, F., Bibring, J. P., Mangold, N., & Murchie, S. (2013). Hydrous minerals on Mars as seen by the CRISM and OMEGA imaging spectrometers: Updated global view. *Journal of Geophysical Research: Planets*, *118*(4), 831-858. https://doi.org/10.1029/2012JE004145

Chan, Q. H. S., Stroud, R., Martins, Z., & Yabuta, H. (2020). Concerns of organic contamination for sample return space missions. *Space Science Reviews*, 216, 1-40. https://doi.org/10.1007/s11214-020-00678-7

Clark, J. V., Archer, P. D., Gruener, J. E., Ming, D. W., Tu, V. M., Niles, P. B., & Mertzman, S. A. (2020). JSC-Rocknest: A large-scale Mojave Mars Simulant (MMS) based soil simulant for in-situ resource utilization water-extraction studies. *Icarus*, *351*, 113936. https://doi.org/10.1016/j.icarus.2020.113936

Clemett, S. J., Maechling, C. R., Zare, R. N., Swan, P. D., & Walker, R. M. (1993). Identification of complex aromatic molecules in individual interplanetary dust particles. *Science*, 262(5134), 721-725. https://doi.org/10.1126/science.262.5134.721

Cockell, C. S., Catling, D. C., Davis, W. L., Snook, K., Kepner, R. L., Lee, P., & McKay, C. P. (2000). The ultraviolet environment of Mars: biological implications past, present, and future. *Icarus*, 146(2), 343-359. https://doi.org/10.1006/icar.2000.6393

Cockell, C. S., Schuerger, A. C., Billi, D., Friedmann, E. I., & Panitz, C. (2005). Effects of a Simulated Martian UV Flux on the Cyanobacterium, Chroococcidiopsis sp. 029. *Astrobiology*, *5*(2), 127–140. https://doi.org/10.1089/ast.2005.5.127

Corpolongo, A., Jakubek, R. S., Burton, A. S., Brown, A. J., Yanchilina, A., Czaja, A. D., ... & Abbey, W. (2023). SHERLOC Raman mineral class detections of the Mars 2020 Crater Floor Campaign. *Journal of Geophysical Research: Planets*, *128*(3). https://doi.org/10.1029/2022JE007455

Crismani, M. M. J., Schneider, N. M., Plane, J. M. C., Evans, J. S., Jain, S. K., Chaffin, M. S., … Jakosky, B. M. (2017). Detection of a persistent meteoric metal layer in the Martian atmosphere. Nature Geoscience, 10(6), 401–404. https://doi.org/10.1038/ngeo2958

Dartnell, L. R. (2011). Ionizing radiation and life. *Astrobiology*, 11(6), 551-582. https://doi.org/10.1089/ast.2010.0528

Dartnell, L. R., Desorgher, L., Ward, J. M., & Coates, A. J. (2007). Martian sub-surface ionising radiation: biosignatures and geology. *Biogeosciences*, 4(4), 545-558. https://doi.org/10.5194/bg-4-545-2007

Ehlmann, B. L., & Edwards, C. S. (2014). Mineralogy of the Martian surface. *Annual Review of Earth and Planetary Sciences*, 42, 291-315. https://doi.org/10.1146/annurev-earth-060313-055024

Ehlmann, B. L., Mustard, J. F., Murchie, S. L., Bibring, J. P., Meunier, A., Fraeman, A. A., & Langevin, Y. (2011). Subsurface water and clay mineral formation during the early history of Mars. *Nature*, *479*(7371), 53-60. https://doi.org/10.1038/nature10582

Eigenbrode, J. L., Summons, R. E., Steele, A., Freissinet, C., Millan, M., Navarro-González, R., ... & Coll, P. (2018). Organic matter preserved in 3-billion-year-old mudstones at Gale crater, Mars. *Science*, 360(6393), 1096-1101. https://doi.org/10.1126/science.aas9185

Ehrenfreund, P., Bernstein, M. P., Dworkin, J. P., Sandford, S. A., & Allamandola, L. J. (2001). The Photostability of Amino Acids in Space. *The Astrophysical Journal*, *550*, 95–99. https://doi.org/10.1086/319491

Eshelman, E., Daly, M. G., Slater, G., & Cloutis, E. (2015). Time-resolved detection of aromatic compounds on planetary surfaces by ultraviolet laser induced fluorescence and Raman spectroscopy. *Planetary and Space Science*, 119, 200–207. https://doi.org/10.1016/j.pss.2015.09.021

Eshelman, E. J. (2016). Stand-Off Detection of Organic Compounds on Mars Using Ultraviolet Raman Spectroscopy and Time-Resolved Laser-Induced Fluorescence. http://hdl.handle.net/10315/32346

Flynn, G. J. (1996). The Delivery of Organic Matter from Asteroids and Comets to the Early Surface of Mars. *Earth Moon Planets*, *72*, 469–474.

Flynn, G. J., Rivers, M., Sutton, S. R., Eng, P., & Klock, W. (2000). X-ray computed microtomography (CMT): a noninvasive screening tool for characterization of returned rock cores from mars and other solar system bodies. Lunar and Planetary Science XXXI. LP1# 1893. https://www.lpi.usra.edu/meetings/lpsc2000/pdf/1893.pdf

Flynn, G. J., Keller, L. P., Jacobsen, C., & Wirick, S. (2004). An assessment of the amount and types of organic matter contributed to the Earth by interplanetary dust. *Advances in Space Research*, 33(1), 57-66. https://doi.org/10.1016/j.asr.2003.09.036

Flynn, G. J. (2020). *Interplanetary Dust Particles*. https://doi.org/10.1093/acrefore/9780190647926.013.143

Forget, F., Hourdin, F., Fournier, R., Hourdin, C., Talagrand, O., Collins, M., … Huot, J.-P. (1999). Improved general circulation models of the Martian atmosphere from the surface to above 80 km. Journal of Geophysical Research, 104, 24155–24176. https://doi.org/10.1029/1999JE001025

Fraundorf, P., Brownlee, D. E., & Walker, R. M. (1982). Laboratory studies of interplanetary dust (pp. 383-409). Tucson: University of Arizona Press.

Freissinet, C., Glavin, D. P., Mahaffy, P. R., Miller, K. E., Eigenbrode, J. L., Summons, R. E., ... & MSL Science Team. (2015). Organic molecules in the sheepbed mudstone, gale crater, mars. *Journal of Geophysical Research: Planets*, 120(3), 495-514. https://doi.org/10.1002/2014JE004737

Geminale, A., Formisano, V., & Sindoni, G. (2011). Mapping methane in Martian atmosphere with PFS-MEX data. *Planetary and Space Science*, 59(2-3), 137-148. https://doi.org/10.1016/j.pss.2010.07.011

Glavin, D. P., Freissinet, C., Miller, K. E., Eigenbrode, J. L., Brunner, A. E., Buch, A., ... & Mahaffy, P. R. (2013). Evidence for perchlorates and the origin of chlorinated hydrocarbons detected by SAM at the Rocknest aeolian deposit in Gale Crater. *Journal of Geophysical Research: Planets*, 118(10), 1955-1973. https://doi.org/10.1002/jgre.20144

Goetz, W., Bertelsen, P., Binau, C. S., Gunnlaugsson, H. P., Hviid, S. F., Kinch, K. M., ... & Yen, A. (2005). Indication of drier periods on Mars from the chemistry and mineralogy of atmospheric dust. *Nature*, *436*(7047), 62-65. https://doi.org/10.1038/nature03807

Gómez-Elvira, J., Armiens, C., Carrasco, I., Genzer, M., Gómez, F., Haberle, R., ... & Zorzano, M. P. (2014). Curiosity's rover environmental monitoring station: Overview of the first 100 sols. *Journal of Geophysical Research: Planets*, 119(7), 1680-1688. https://doi.org/10.1002/2013JE004576

Griffith, C. A., Doose, L., Tomasko, M. G., Penteado, P. F., & See, C. (2012). Radiative transfer analyses of Titan's tropical atmosphere. *Icarus*, *218*(2), 975–988. https://doi.org/10.1016/j.icarus.2011.11.034

Grotzinger, J. P., & Milliken, R. E. (2012). The Sedimentary Rock Record of Mars: Distribution, Origins, and Global Stratigraphy. In SEPM (Society for Sedimentary Geology) eBooks (pp. 1–48). https://doi.org/10.2110/pec.12.102.0001.

Hamilton, V. E., & Christensen, P. R. (2005). Evidence for extensive, olivine-rich bedrock on Mars. *Geology*, 33(6), 433-436. https://doi.org/10.1130/G21258.1

Hansen, J. E., & Travis, L. D. (1974). Light scattering in planetary atmospheres. *Space Science Reviews*, 16(4), 527-610. https://doi.org/10.1007/BF00168069

Hartmann, W. K., & Neukum, G. (2001). Cratering chronology and the evolution of Mars. In Chronology and evolution of Mars: Proceedings of an ISSI Workshop, 10–14 April 2000, Bern, Switzerland (pp. 165-194). Springer Netherlands. https://doi.org/10.1007/978-94-017-1035-0_6

Hecht, M. H., Kounaves, S. P., West, S. J., Morookian, J. M., Young, S. M. M., Quinn, R., Grunthaner, P., Wen, X., Weilert, M., Cable, C. A., Fisher, A., Gospodinova, K., Kapit, J., Stroble, S., Hsu, P. C., Clark, B. C., Ming, D. W., & Smith, P. H. (2009). The MECA wet chemistry laboratory on the 2007 Phoenix Mars Scout Lander. *Journal of Geophysical Research E: Planets*, *114*(3). https://doi.org/10.1029/2008JE003084

Iglesias-Groth, S. (2023). A search for tryptophan in the gas of the IC 348 star cluster of the Perseus molecular cloud. Monthly Notices of the Royal Astronomical Society, 523(2), 2876–2886. https://doi.org/10.1093/mnras/stad1535

Kerber, L., & Head, J. W. (2010). The age of the Medusae Fossae Formation: Evidence of Hesperian emplacement from crater morphology, stratigraphy, and ancient lava contacts. *Icarus*, *206*(2), 669-684. https://doi.org/10.1016/j.icarus.2009.10.001

Kerridge, J. F. (1999). Formation and processing of organics in the early solar system. *Space Science Reviews*, 90(1-2), 275-288. https://doi.org/10.1023/A:1005222804192

Kite, E. S., Sneed, J., Mayer, D. P., Lewis, K. W., Michaels, T. I., Hore, A., & Rafkin, S. C. R. (2016). Evolution of major sedimentary mounds on Mars: Buildup via anticompensational stacking modulated by climate change. *Journal of Geophysical Research: Planets*, *121*(11), 2282–2324. https://doi.org/10.1002/2016JE005135

Krot, A. N., Keil, K., Scott, E. R. D., Goodrich, C. A., & Weisberg, M. K. (2014). Classification of meteorites and their genetic relationships. *Meteorites and Cosmochemical Processes*, 1, 1-63. https://ui.adsabs.harvard.edu/abs/2014mcp..book....1K/abstract

Kuhn, W. R., & Atreya, S. K. (1979). Solar radiation incident on the Martian surface. *Journal of Molecular Evolution*, *14*, 57-64. https://doi.org/10.1007/BF01732367

Lakowicz, J. R. (2006). *Principles of Fluorescence Spectroscopy*. Boston, MA: Springer US.

Laskar, J. (2004). A comment on "Accurate spin axes and solar system dynamics: Climatic variations for the Earth and Mars." *Astronomy and Astrophysics*, *416*(2), 799–800. https://doi.org/10.1051/0004-6361:20035710

Lemmon, M. T., Guzewich, S. D., McConnochie, T., Vicente-Retortillo, A., Martínez, G., Smith, M. D., … Jacob, S. (2019). Large Dust Aerosol Sizes Seen During the 2018 Martian Global

Dust Event by the Curiosity Rover. Geophysical Research Letters, 46(16), 9448–9456. https://doi.org/10.1029/2019gl084407

Lewis, K. W., & Aharonson, O. (2014). Occurrence and origin of rhythmic sedimentary rocks on Mars. *Journal of Geophysical Research E: Planets*, *119*(6), 1432–1457. https://doi.org/10.1002/2013JE004404

Mackinnon, I. D., & Rietmeijer, F. J. (1987). Mineralogy of chondritic interplanetary dust particles. *Reviews of Geophysics*, 25(7), 1527-1553. https://doi.org/10.1029/RG025i007p01527

Mandt, K. E., de Silva, S. L., Zimbelman, J. R., & Crown, D. A. (2008). Origin of the Medusae Fossae Formation, Mars: Insights from a synoptic approach. *Journal of Geophysical Research: Planets*, *113*(E12). https://doi.org/10.1029/2008JE003076

Malin, M. C., & Edgett, K. S. (2000). Sedimentary rocks of early Mars. Science, 290(5498), 1927-1937. https://doi.org/10.1126/science.290.5498.1927

Matrajt, G., Borg, J., Raynal, P. I., Djouadi, Z., d'Hendecourt, L., Flynn, G., & Deboffle, D. (2004). FTIR and Raman analyses of the Tagish Lake meteorite: Relationship with the aliphatic hydrocarbons observed in the diffuse interstellar medium. Astronomy & Astrophysics, 416(3), 983-990. https://doi.org/10.1051/0004-6361:20034526

Millour, E., Forget, F., Spiga, A., Vals, M., Zakharov, V., Montabone, L., … González-Galindo, F. (n.d.). THE MARS CLIMATE DATABASE (VERSION 5.3). Retrieved from https://www.cosmos.esa.int/documents/1499429/1583871/Millour_E.pdf

Montmessin, F., & Lefèvre, F. (2013). Transport-driven formation of a polar ozone layer on Mars. *Nature Geoscience*, *6*(11), 930–933. https://doi.org/10.1038/ngeo1957

Moore, C. A. (2019). *Radiative Transfer in the Martian Environment: In-situ Results from the MSL Curiosity Rover and Laboratory Experimentation on Martian Regolith and Crystalline Rock Analogs* (Doctoral Dissertation, York University, Toronto). https://yorkspace.library.yorku.ca/items/0e942cb8-c3c7-4c43-9ac0-e209a3c1bc4e

Moores, J. E., & Schuerger, A. C. (2012). UV degradation of accreted organics on Mars: IDP longevity, surface reservoir of organics, and relevance to the detection of methane in the

atmosphere. *Journal of Geophysical Research E: Planets*, *117*(E8). https://doi.org/10.1029/2012JE004060

Moores, J. E., Smith, P. H., Tanner, R., Schuerger, A. C., & Venkateswaran, K. J. (2007). The shielding effect of small-scale Martian surface geometry on ultraviolet flux. *Icarus*, 192(2), 417-433. https://doi.org/10.1016/j.icarus.2007.07.003

Moores, J. E., Smith, C. L., & Schuerger, A. C. (2017). UV production of methane from surface and sedimenting IDPs on Mars in light of REMS data and with insights for TGO. *Planetary and Space Science*, *147*, 48–60. https://doi.org/10.1016/j.pss.2017.09.008

Morris, R. V., Golden, D. C., Bell III, J. F., Shelfer, T. D., Scheinost, A. C., Hinman, N. W., ... & Britt, D. T. (2000). Mineralogy, composition, and alteration of Mars Pathfinder rocks and soils: Evidence from multispectral, elemental, and magnetic data on terrestrial analogue, SNC meteorite, and Pathfinder samples. *Journal of Geophysical Research: Planets*, 105(E1), 1757-1817. https://doi.org/10.1029/1999JE001059

Morris, R. V., Klingelhofer, G., Bernhardt, B., Schroder, C., Rodionov, D. S., de Souza Jr, P. A., ... & Arvidson, R. E. (2004). Mineralogy at Gusev crater from the Mossbauer spectrometer on the Spirit rover. *Science*, *305*(5685), 833-836. https://doi.org/10.1126/science.1100020

Morris, R. V., Klingelhoefer, G., Schröder, C., Rodionov, D. S., Yen, A., Ming, D. W., ... & Arvidson, R. E. (2006). Mössbauer mineralogy of rock, soil, and dust at Meridiani Planum, Mars: Opportunity's journey across sulfate-rich outcrop, basaltic sand and dust, and hematite lag deposits. *Journal of Geophysical Research: Planets*, 111(E12). https://doi.org/10.1029/2006JE002791

Navarro-González, R., Vargas, E., de La Rosa, J., Raga, A. C., & McKay, C. P. (2010). Reanalysis of the Viking results suggests perchlorate and organics at midlatitudes on Mars. *Journal of Geophysical Research: Planets*, 115(E12). https://doi.org/10.1029/2010JE003599

Ojha, L., Lewis, K., Karunatillake, S., & Schmidt, M. (2018). The Medusae Fossae Formation as the single largest source of dust on Mars. *Nature Communications*, 9(1), 2867. https://doi.org/10.1038/s41467-018-05291-5

Oravec, H. A., Asnani, V. M., Creage, C. M., & Moreland, S. (2021). Geotechnical Review of Existing Mars Soil Simulants for Surface Mobility. *17th Biennial International Conference on Engineering, Science, Construction, and Operations in Challenging Environments*. American Society of Civil Engineers. https://doi.org/10.1061/9780784483374.016

Patel, M. R., Zarnecki, J. C., & Catling, D. C. (2002). Ultraviolet radiation on the surface of Mars and the Beagle 2 UV sensor. *Planetary and Space Science*, 50(9), 915-927. https://doi.org/10.1016/S0032-0633(02)00067-3

Pavlov, A. A., Vasilyev, G., Ostryakov, V. M., Pavlov, A. K., & Mahaffy, P. (2012). Degradation of the organic molecules in the shallow subsurface of Mars due to irradiation by cosmic rays. *Geophysical Research Letters*, *39*(13). https://doi.org/10.1029/2012GL052166

Pereira, W. E., Summons, R. E., Rindfleisch, T. C., Duffield, A. M., Zeitman, B., & Lawless, J. G. (1975). Stable isotope mass fragmentography: Identification and hydrogen-deuterium exchange studies of eight Murchison meteorite amino acids. *Geochimica et Cosmochimica Acta*, *39*(2), 163-172. https://doi.org/10.1016/0016-7037(75)90168-4

Pollack, J. B., Colburn, D. S., Flasar, F. M., Kahn, R., Carlston, C. E., & Pidek, D. (1979). Properties and effects of dust particles suspended in the Martian atmosphere. *Journal of Geophysical Research: Solid Earth*, 84(B6), 2929-2945. https://doi.org/10.1029/JB084iB06p02929

Quinn, R. C., Martucci, H. F. H., Miller, S. R., Bryson, C. E., Grunthaner, F. J., & Grunthaner, P. J. (2013). Perchlorate radiolysis on mars and the origin of martian soil reactivity. *Astrobiology*, *13*(6), 515–520. https://doi.org/10.1089/ast.2013.0999

Razzell Hollis, J., Fornaro, T., Rapin, W., Wade, J., Vicente-Retortillo, Á., Steele, A., ... & Beegle, L. W. (2021). Detection and degradation of adenosine monophosphate in perchlorate-spiked Martian regolith analog, by deep-ultraviolet spectroscopy. *Astrobiology*, *21*(5), 511-525. https://doi.org/10.1089/ast.2020.2362

Rietmeijer, F. J., & Warren, J. L. (1994, July). Windows of opportunity in the NASA Johnson Space Center cosmic dust collection. In AIP Conference Proceedings (Vol. 310, No. 1, pp. 255-276). American Institute of Physics. https://doi.org/10.1063/1.46515

Scappini, F., Casadei, F., Zamboni, R., Franchi, M., Gallori, E., & Monti, S. (2004). Protective effect of clay minerals on adsorbed nucleic acid against UV radiation: possible role in the origin of life. *International Journal of Astrobiology*, 3(1), 17-19. https://doi.org/10.1017/S147355040400179X

Scheller, E. L., Razzell Hollis, J., Cardarelli, E. L., Steele, A., Beegle, L. W., Bhartia, R., ... & Zorzano, M. P. (2022). Aqueous alteration processes in Jezero crater, Mars—implications for organic geochemistry. *Science*, 378(6624), 1105-1110. https://doi.org/10.1126/science.abo5204

Schuerger, A. C., Moores, J. E., Clausen, C. A., Barlow, N. G., & Britt, D. T. (2012). Methane from UV-irradiated carbonaceous chondrites under simulated Martian conditions. *Journal of Geophysical Research: Planets*, *117*(E8), n/a-n/a https://doi.org/10.1029/2011je004023

Sephton, M. A. (2002). Organic compounds in carbonaceous meteorites. *Natural Product Reports*, 19(3), 292-311. https://doi.org/10.1039/B103775G

Sharma, S., Roppel, R. D., Murphy, A. E., Beegle, L. W., Bhartia, R., Steele, A., ... & Yanchilina, A. (2023). Diverse organic-mineral associations in Jezero crater, Mars. *Nature*, 619, 724–732. https://doi.org/10.1038/s41586-023-06143-z

Smith, C. L., & Moores, J. E. (2020). Modelled small-scale crack orientations in Martian surface clasts caused by differential insolation-mobilized water. *Icarus*, *338*, 113497. https://doi.org/10.1016/j.icarus.2019.113497

Smith, M. D., Zorzano, M. P., Lemmon, M., Martín-Torres, J., & Mendaza de Cal, T. (2016). Aerosol optical depth as observed by the Mars Science Laboratory REMS UV photodiodes. *Icarus*, *280*, 234–248. https://doi.org/10.1016/j.icarus.2016.07.012

Stoker, C. R., & Bullock, M. A. (1997). Organic degradation under simulated Martian conditions. *Journal of Geophysical Research: Planets*, 102(E5), 10881-10888. https://doi.org/10.1029/97JE00667

Tanaka, K. L. (1986). The stratigraphy of Mars. *Journal of Geophysical Research: Solid Earth*, 91(B13), E139-E158. https://doi.org/10.1029/JB091iB13p0E139

Vicente-Retortillo, Á., Valero, F., Vázquez, L., & Martínez, G. M. (2015). A model to calculate solar radiation fluxes on the Martian surface. *Journal of Space Weather and Space Climate*, 5, A33. https://doi.org/10.1051/swsc/2015035

Westall, F., Foucher, F., Bost, N., Bertrand, M., Loizeau, D., Vago, J. L., ... & Cockell, C. S. (2015). Biosignatures on Mars: what, where, and how? Implications for the search for martian life. *Astrobiology*, 15(11), 998-1029. https://doi.org/10.1089/ast.2015.1374

Yang, H., Xiao, X., Zhao, X., & Wu, Y. (2017). Intrinsic fluorescence spectra of tryptophan, tyrosine and phenyloalanine. *SPIE Proceedings*, *10255*. https://doi.org/10.1117/12.2268397

Yen, A. S., Kim, S. S., Hecht, M. H., Frant, M. S., & Murray, B. (2000). Evidence that the reactivity of the Martian soil is due to superoxide ions. *Science*, 289(5486), 1909-1912. https://doi.org/10.1126/science.289.5486.1909

Yen, A. S., Gellert, R., Schröder, C., Morris, R. V., Bell III, J. F., Knudson, A. T., ... & Zipfel, J. (2005). An integrated view of the chemistry and mineralogy of Martian soils. *Nature*, 436(7047), 49-54. https://doi.org/10.1038/nature03637

Appendices

Appendix A: Source Code Base for IDP Burial Model

The up-to-date source code files are maintained in GitHub repository: https://github.com/ankitadas99/IDP. Access can be provided on request. The latest version of code listing is provided below.

```
import numpy as np
import matplotlib
import matplotlib.colors as colors
import matplotlib.pyplot as plt
import matplotlib.cm as cm
from scipy.interpolate import griddata
import csv
import seaborn as sns
from numpy import loadtxt
import pandas as pd
import sys
sys.path.append("C://Users/arind/Downloads")
import os
from subprocess import call
from mpl_toolkits.mplot3d import Axes3D
from itertools import product, combinations
import math as mt
from numpy import trapz
import time
plt.rcParams.update({'font.size': 10})
dustdensity = 800 #kg/m3
FlynnIN = [2.595*10**-11, 2.725*10**-10, 9.343*10**-10, 8.954*10**-10, 5.840*10**-10, 2.336*10**-10, 9.084*10**-11, 7.786*10**-12, 2.595*10**-12, 1.168*10**-12, 3.893*10**-13, 7.786*10**-14]
```

```
Aparticle = [6.50388*10**-7, 1.41863*10**-7, 2.98648*10**-8, 6.36173*10**-9, 1.48617*10**-9,
2.98648*10**-10, 6.36173*10**-11, 1.59043*10**-11, 3.14159*10**-12, 5.02655*10**-13,
1.59043*10**-13, 3.14159*10**-14 ]

Mparticle = [3.94569*10**-7, 4.01944*10**-8, 3.88242*10**-9, 3.81704*10**-10, 4.30989*10**-11,
3.88242*10**-12, 3.81704*10**-13, 4.77129*10**-14, 4.18879*10**-15, 2.68083*10**-16,
4.77129*10**-17, 4.18879*10**-18 ]

IDPdiam1 = np.array([910, 425, 195, 90, 43.5, 19.5, 9, 4.5, 2, 0.8, 0.45, 0.2])

IDPdiam = IDPdiam1/(1000000)

Surfload = [None]*len(IDPdiam)

IDPunalt = np.array([0.01, 0.07, 0.24, 0.46, 0.75, 0.88, 0.95, 1, 1, 1, 1, 1])

IDPunmelt = np.array([0.5, 0.7, 0.9, 0.98, 1, 1, 1, 1, 1, 1, 1, 1])

Areasum = 0

total_load = 0

dfc = pd.DataFrame(np.loadtxt('uvcdata.txt'), columns=['long', 'lat', 'energyc'])

dfb = pd.DataFrame(np.loadtxt('uvbdata.txt'), columns=['long', 'lat', 'energyb'])

dfa = pd.DataFrame(np.loadtxt('uvadata.txt'), columns=['long', 'lat', 'energya'])

temp = pd.DataFrame(np.loadtxt('daytemp_arabiaterra.txt'))

dfd = pd.DataFrame(np.loadtxt('arabiaterra.txt'))

dep = np.array(dfd[1])

ls = np.array(dfd[0])

daytemp = np.array(temp[1])



fig = plt.figure()

fig.set_size_inches(11.5, 9.5)

a =plt.plot(ls,dep, color='tab:brown')

plt.xlabel('Solar Longitude $(L_s)$',size=15)

plt.ylabel('Deposition $(kg/m^2/sol)$',size=15)

plt.title('Dust Deposition at Arabia Terra',size=15)

#plt.xticks([150,175,200,225,250,275,300,325,350,375,400,425,450,475,500,525,550,575,600],
['150','175','200','225','250','275','300','325','350','375','400','425','450','475','500','525','550','575','600']
)
```

```
plt.tight_layout
plt.grid(color='black', linestyle='--', )
plt.show()


rate = (trapz(dep,dx=5))/dustdensity
print(rate)
rate = 4.2*(10**-5)
energy_c = np.array(dfc['energyc'])
energy_b = np.array(dfb['energyb'])
energy_a = np.array(dfa['energya'])
lat = np.array(dfc['lat'])
long = np.array(dfc['long'])
e_new_c = [None]*36
e_totalc = 0
e_new_b = [None]*36
e_totalb = 0
e_new_a = [None]*36
e_totala = 0
j = 0
for i in range(len(energy_c)):
    if lat[i] == 20:
        x = [lat[i],lat[i+1]]
        y = [energy_c[i],energy_c[i+1]]
        e_new_c[j] = np.interp(21,x,y)
        e_totalc = e_totalc + e_new_c[j]
        j = j+1
j = 0
for i in range(len(energy_b)):
    if lat[i] == 20:
        x = [lat[i],lat[i+1]]
```

```
        y = [energy_b[i],energy_b[i+1]]
        e_new_b[j] = np.interp(21,x,y)
        e_totalb = e_totalb + e_new_b[j]
        j = j+1
j = 0
for i in range(len(energy_a)):
    if lat[i] == 20:
        x = [lat[i],lat[i+1]]
        y = [energy_a[i],energy_a[i+1]]
        e_new_a[j] = np.interp(21,x,y)
        e_totala = e_totala + e_new_a[j]
        j = j+1
Ls = np.array(list(range(0,360,10)))
years = np.array(np.linspace(1,10,num=10))
energy_a = e_new_a
energy_b = e_new_b
energy_c = e_new_c
energy_time_c = np.array(np.zeros((len(years),len(Ls))))
energy_time_b = np.array(np.zeros((len(years),len(Ls))))
energy_time_a = np.array(np.zeros((len(years),len(Ls))))
IDPlife = np.array(np.zeros((len(years),len(IDPdiam))))
etotal_Ls = np.array(np.zeros((len(years),len(Ls))))
ec = np.array([0]*len(years))
eb = np.array([0]*len(years))
ea = np.array([0]*len(years))
ec[0] = sum(energy_c)
eb[0] = sum(energy_b)
ea[0] = sum(energy_a)
energy_time_c[0,:] = energy_c
energy_time_b[0,:] = energy_b
```

```
energy_time_a[0,:] = energy_a
for i in range(len(years)):
    for j in range(len(Ls)):
        if i>=0:
            energy_time_c[i,j] = energy_c[j]/(2.71**(i*30.49*1000*rate))
            ec[i] = ec[i] + energy_time_c[i,j]
            energy_time_b[i,j] = energy_c[j]/(2.71**(i*29.54*1000*rate))
            eb[i] = eb[i] + energy_time_b[i,j]
            energy_time_a[i,j] = energy_c[j]/(2.71**(i*29.35*1000*rate))
            ea[i] = ea[i] + energy_time_a[i,j]
QE = np.array([None]*len(Ls))
FQEdaily = np.array(np.zeros((len(years),len(Ls))))
totalfqe = np.array([None]*len(years))
totaluv = np.array(np.zeros((len(years))))
IDPlife = np.array(np.zeros((len(years),len(IDPdiam))))
for i in range(len(Ls)):
    QE[i] = (daytemp[i]*((2.76*10**-15))-(1.54*10**-13))
for i in range(len(years)):
    for j in range(len(Ls)):
        totaluv[i] = (energy_time_c[i,j]+energy_time_b[i,j]+energy_time_a[i,j])
        FQEdaily[i,j] = QE[j]*(energy_time_c[i,j]+energy_time_b[i,j]+energy_time_a[i,j])
for i in range(len(years)):
    totalfqe[i] = 0
    for j in range(len(Ls)):
        totalfqe[i] = totalfqe[i]+FQEdaily[i,j]
totaluv = totaluv/88775*36
totalfqe = (totalfqe/(88775*36))*(59354500)
for i in range(len(years)):
    for j in range(len(IDPdiam)):
        IDPlife[i,j] = (2*0.1*IDPunalt[j]*1000*IDPunmelt[j]*IDPdiam[j])/(3*totalfqe[i]*0.012)
```

```
#print(IDPlife/(88775*36*59354500))
IDPlife = IDPlife
carbon = np.array(np.zeros((len(years),len(IDPdiam))))
carbon[0,:] = (np.array(FlynnIN))/2
carbon[0,:] = carbon[0,:]
sumcarbon = np.array([None]*len(years))
layermass = np.zeros(len(years))
ppb = np.zeros(len(years))
for i in range(len(years)):
   layermass[i] = rate*800

for i in range(len(years)):
   for j in range(len(IDPdiam)):
      if i>=1:
         carbon[i,j] = (carbon[i-1,j] - carbon[i-1,j]/(IDPlife[i-1,j]))
for i in range(len(years)):
   sumcarbon[i] = sum(carbon[i,:])
   ppb[i] = (sumcarbon[i]/layermass[i])*10**9
print(ppb[0])
print(ppb[9])
print(ppb[0]-ppb[9])
#sumcarbon = sumcarbon*(10**9)
print(sumcarbon)
fig = plt.figure()
fig.set_size_inches(11.5, 9.5)
a =plt.plot(years,ppb,marker='o',color='tab:orange')
#fig.set_edgecolor('black')
plt.xlabel('Martian Years',size=15)
plt.ylabel('Organic Carbon remaining (ppb)',size=15)
plt.title('Destruction of organics at Arabia Terra',size=15)
```

```
#plt.xticks([1,5,10], ['1','5','10'])
#plt.yticks([3.0486,3.0475,3.0470,3.0465,3.0461],['3.0486','3.0475','3.0470','3.0465','3.0461'])
plt.grid(color='black', linestyle='--')
plt.tight_layout
plt.show()
```

Appendix B: Calculation for Depth used in Layered JSC-1 Mars on Tryptophan Measurement

Density of JSC-1 Mars = (0.79 x 0.87) ± 0.02 g/cm^3 [m (g) / V (cm^3)]

δ = 0.69 ± 0.02 g/cm^3

Diameter of aluminum cup sample holder= 12.7 ± 0.25 mm

r = 6.35 ± 0.12 mm

Area of sample holder = πr^2 = π(6.35 ± 0.12)^2

A = 1.26 ± 0.04 cm^2

V = A x h

3 µm in 1 year ---------- Deposition of Martian Dust at Gale Crater in one year

100 years → 3 x 10^{-4} m = 0.03 cm = 3 mm ---------- Deposition of Martian Dust at Gale in 100 years

m = V x δ

m = (1.26 ± 0.04) x 0.03 x (0.69 ± 0.02) g

= 0.0261 ± 0.0016 g

≈ 0.0261 g

A mass of 0.0261 g was sprinkled on top of our pure tryptophan sample to take our LIF measurements